InnoVationinfo
eBooks

Double Circulation Solar Thermal Installation with Thermosiphon Circulation

Yedilkhan Amirgaliyev
Murat Kunelbayev

Double Circuit Solar Thermal Installation With Thermosiphon Circulation

Authors

Amirgaliyev Y.N, Kunelbayev M, Kalizhanova A.U, Kozbakova A. Kh, Daulbayev S.M, Auelbekov O. A, Kataev N.S, Yedilkhan D, Merembayev T, Ormanov T. A, Sundetov T.

Ministry of Education and Science of the Republic of Kazakhstan Committee of Science Republican State Enterprise Institute of Information and Computational Technologies.

ISBN: 978-1-63278-898-6

Published: July 2020

Printed: July 2020

Published by Innovationinfoebooks

Hearthrow Stockley Park,

Heathrow UB11BD, UK

Contents

Preface

This book describes the methods and methodological foundations of the mathematical analysis of two loop solar thermal installations with thermosyphon circulation, the hydrodynamic regime of thermal processes in this installation, the methods of automatic control theory, as well as experimental and mathematical modeling methods using the MatLab (Simulink) software package and computer simulation using Neural Networks to analyze this system. The main research methodology is modeling of technological processes using an application package and planning experiments with programs.

Acknowledgment

This work was supported by a grant from the MES RK BR05236693, carried out at the Institute of Information and Computational Technologies of the CN of the MES RK, under Contract No. 318 dated 03.30.2018.

Notice

Statements and opinions expressed in the book are these of the individual contributors and not necessarily those of the editors or publisher. No responsibility is accepted for the accuracy of information contained in the published chapters. The publisher assumes no responsibility for any damage or injury to persons or property arising out of the use of any materials, instructions, methods or ideas contained in the book.

Additional hard copies can be obtained by orders

@https://www.innovationinfobooks.com/

Abstract

Object of study. Combined by pass solar solar collectors with thermosiphon circulation, a system of controllers and a computer model of solar collector control. The subject of research is the use of mathematical modeling, discrete optimization, operations research, thermal physics, mathematical physics, technical thermodynamics, software engineering technology.

The purpose of this study is to develop mathematical and computer models, software and hardware tools and conduct experimental work on the creation of a network of combined efficient bypass solar collectors with thermosyphon circulation to supply buildings with energy and heat, as well as monitoring their functioning.

Research methods. The methodological basis of the research will be a systematic approach, methods of mathematical analysis, mathematical physics used in describing the dynamic mode of thermal processes, methods of the theory of automatic control, as well as methods of experimental and mathematical modeling using an application package. The research methodology is the modeling of technological processes using an application package and planning experiments with programs.

Scientific novelties are:

- Development of a new approach to the design of solar power plants with thermosiphon circulation and a multi-level heat pump for the production of thermal energy.
- Development of a new type of solar collector design with thermosiphon circulation.
- Development of new principles for solving problems of the mathematical model of a two-loop solar heating system with thermosiphon circulation together with a heat pump.
- New method of studying the temperature and thermal conditions of flat solar collectors, which allows to obtain high efficiency solar power.
- A new method for solving the problem of forming a thermosiphon flow in a solar heating system.
- Development of a method for determining the thermal performance of solar collectors with double-glazed windows, including a computational-experimental method for determining pressure.
- Development of a simulation model of a double-circuit solar collector.

Performing work under this program will allow the development of new controlled systems for the autonomous power supply of small settlements, which will create an alternative to traditional energy sources.

The socio-economic effect of the research results is to provide the population and industrial buildings, objects of the agro-industrial and livestock complexes with autonomous heating systems with low performance characteristics. Applicability of research results. The results of scientific research in the form of recommendations and methods of creation and application will find their application in organizations that specialize in the development and implementation of energy-saving building structures, renewable energy sources, enterprises of the housing and utilities sector.

Target consumers can be housing and communal services, public and private enterprises, private farms in remote areas, agricultural enterprises, livestock and private homeowners. This work was supported by a grant from the MES RK BR05236693, carried out at the Institute of Information and Computational Technologies of the CN of the MES RK, under Contract No. 318 dated 03.30.2018. Thus, we can conclude that all the tasks envisaged in the calendar plan for 2018 have been completed. Relevant scientific papers have been published, both in rating foreign publications and in domestic ones. The main results were reported and discussed at international conferences held in Turkey (Ankara), Kazakhstan (Almaty) and in institute seminars. Applied for security documents.

Introduction

Currently in the Republic much attention is paid to the development of autonomous systems based on the use of renewable energy sources, mainly solar energy. Fundamental state programs on motivating the development and introduction of green energy have been adopted: the Strategy "Kazakhstan-2050". Messages from the Head of State "The Third Modernization of Kazakhstan: Global Competitiveness" dated January 31, 2017, the State Program for the Industrial and Innovative Development of the Republic of Kazakhstan for 2015-2019. The State Program for the Development of Education and Science of the Republic of Kazakhstan for 2016-2019 and other strategic and program documents and tasks set by the President of the Republic of Kazakhstan in connection with the preparation for the Republic's entry into the WTO - on the need for technical re-equipment. The Law of the Republic of Kazakhstan "On Energy Saving", where a special place is given to measures to involve the energy balance of renewable energy sources (RES). Kyoto Protocol on Clean Development. Johannesburg World Summit 2002, which dictate to reduce emissions of combustion products into the atmosphere.

The goal of the program. Development of mathematical and computer models, software and hardware tools and conducting experimental work on the creation of a network of effective combined two-circuit solar collectors with thermosyphon circulation to supply buildings with energy and heat, as well as monitoring their functioning.

To achieve the goal of the Program it is supposed to solve the following tasks:

- Review, analytical analysis based on the study of existing experience in the design and use of various types of solar power plants.
- Conducting research and development work on the selection of a constructive model and the development of a methodology for calculating the effectiveness of the proposed type of solar collector with thermosyphon circulation and a new type of multi-level heat pump.
- Mathematical and computer modeling of the features of the thermal calculation, including the choice of the main dimensions, the calculation of solar radiation, the substantiation of the main parameters of the solar collector with thermosyphon circulation, and the calculation of the output characteristics of the solar system.
- Computer models of the computational scheme of a solar collector with a thermosiphon circulation with a multi-level heat pump, used to build a generalized model of solar power plants.

- Development of mathematical and computer modeling of joint operation of a solar collector with a heat pump.
- Computer simulation of thermal conditions and convective heat exchange in flat solar collectors.
- Study of the thermosiphon circulation and the finding of the thermosiphon flow.
- Justification of the basic parameters of a new.

Naturally, for the reporting year, research work was performed according to the schedule for 2018. The scientifically based methods for creating new types of solar collectors have been generalized, the corresponding scientific works have been published in rating foreign publications and Kazakhstan. Work continues on the preparation of applications for security documents on this subject of work.

In general, the specified tasks are accomplished by the Program executors on time. Preliminary executors created a certain scientific and technical background, received patents for the construction of solar collectors, which will be used in the framework of the Program.

The project executors have a brief overview of foreign scientific publications; they analyzed the experience on the use of renewable energy systems. Solar power plants are widely used in the EU countries: Spain, Italy, Greece, Germany, France and others, where national programs and laws of their development are adopted. For example, in Israel, hot solar water supply of 80% of residential buildings saves more than 5% of the electricity produced in the country, and in the US more than 60% of the pools are heated by solar collectors. The total area of solar collectors in the world already exceeds 50 million m^2, and this process continues upwards.

Abroad, such systems are welcome, the state helps the population with grants and grants, knowing that one-time investments will pay off the energy security of small towns and settlements. In addition, the problem of fuel supply, especially in the winter period, will decrease by an order of magnitude.

Yi-Mei Liu, Kung-Ming Chung, Keh-Chin Chang and Tsong-Sheng Lee [**1**] from National University of Taiwan developed and calculated the performance of Taiwanese solar collectors with thermosyphon circulation. Myeong Jin Ko [**2**] from Incheon National University of the Republic of Korea designed a multi-purpose optimization for indirectly forced circulation of hot water using a solar system. Figure 1 shows a diagram of an indirect SWH system of forced circulation. The SWH system consists mainly of flat solar collectors, an external heat exchanger, a storage tank, auxiliary heaters, circulation pumps and a differential temperature controller (DTC). This SWH system has two circulation circuits: a primary circuit that collects solar energy and transfers it to the storage

tank through an external heat exchanger and a secondary circuit that transfers heat stored in the tank to the load. Two circulation pumps in the primary circuit are controlled by DTC.

Auxiliary heaters are added according to the energy needs of the hot water when the temperature in the tank does not reach the desired temperature.

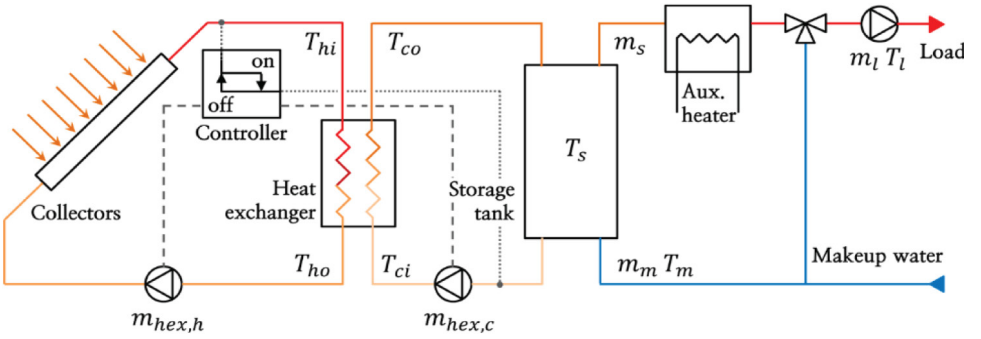

Figure 1: A schematic diagram of the indirect solar heat supply system of forced circulation used in this study

Xu Ji, Ming Li, Weidong Lin, Tufeng Zheng, and Yunfeng Wang [**3**] calculated the effect of a solar collector installation on performance.

Lacour Ayompe, Aidan Duffy [**4**] developed an analysis of the thermal efficiency of a solar water heating system with a tubular collector. Ruchi Shukla, K.Sumathy, Phillip Erickson, Jiawei Gong [**5**] provides a detailed overview of aspects of the design of solar water heating systems and discusses alternative refrigerant technologies and technological advances in improving performance, as well as the economic efficiency of the system.

The study M.U.Siddiqui, S.A.M.Said [**6**] provides an overview of work in the field of solar energy absorption systems that use working fluid vapors. The focus of this study is on solar energy absorption cooling systems, diffusion absorption systems, ejector-based absorption systems, compression absorption systems, and cogeneration / trigeneration absorption systems. This study examined the thermodynamic properties of most common working fluids, as well as the use of ternary mixtures in solar energy absorption systems.

Soteris A.Kalogirou [**7**] calculated optical, thermal and thermodynamic analysis of solar collectors and a description of the methods used to assess their effectiveness. T.T.Chow, K.F.Fong, A.L.S.Chan, Z.Lin [**8**] developed a numerical study of a centralized solar water heating system in a high-rise residential area. S.R.Park, A.K.Pandey, V.V.Tyagi, S.K.Tyag [**9**] developed an energy and energy analysis of typical renewable energy sources.

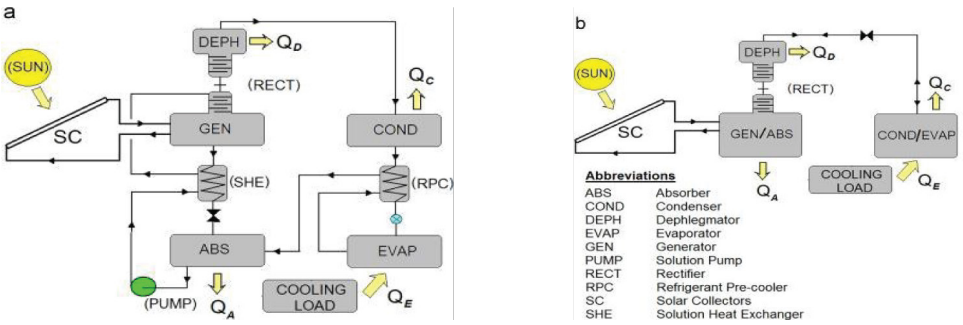

a) Continuous operation based on solar energy.

b) Absorption system based on a solar battery, based on intermittent operation.

Figure 2: Absorption system.

Hussein, H.M.S. [**10**] theoretically investigated a natural circulating two-phase closed thermosiphon flat plate solar water heater. The article S.M. Khairnasov, A.M. Naumova [**11**] presents an analysis of the current state and prospects for the use of heat pipes in solar energy systems.

Maldonadoa, E. Huertab, J. E. Coronab, O. Cehb, A. I. Leóne, I. Henandeza [**12**] investigated the design and the instantaneous efficiency of a solar water heater. The geometry and dimension of the reservoir were determined from the results of thermal analysis and the thermal properties of materials. Carlos Eduardo Camargo Nogueira, Magno Luiz Vidotto, Fernando Toniazzo, Gilson Debastiani

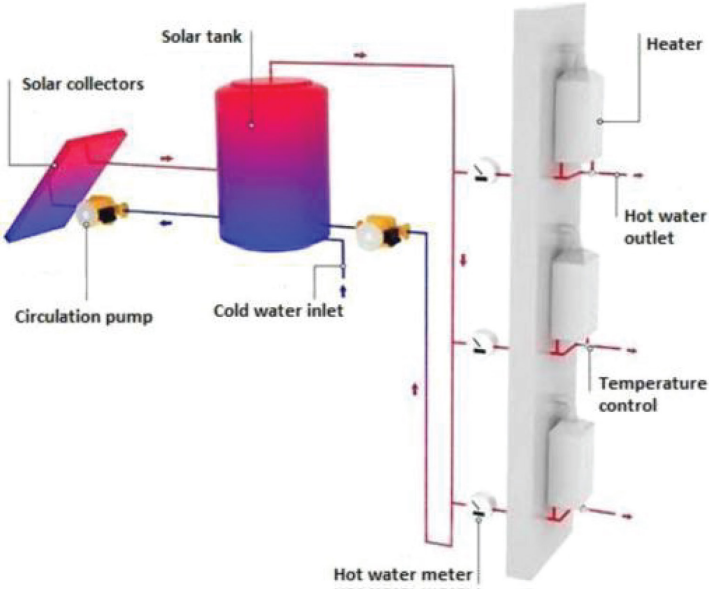

Figure 3: Solar system with gas heaters.

[**13**] presented a complete software development using the MATLAB platform, and its algorithm for calibrating small solar water heating systems. Figure 2 (a, b) shows the layout and operation of the solar system with support from continuous heaters using liquefied petroleum gas (LGP).

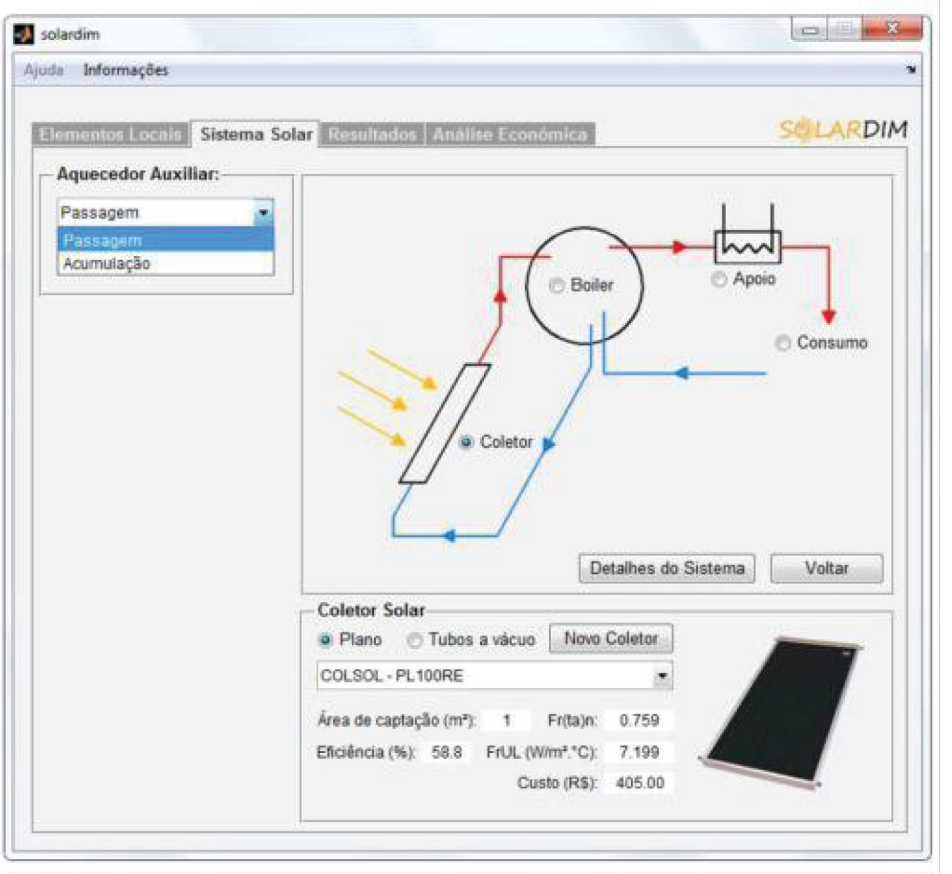

Figure 4: Solar system window in MatLab.

In the Solar Collector module (**Figure 3**), the user can select a collector type (flat or vacuum) for later access to the list with various collector models available on the market. When you select a model, the application automatically displays the specific characteristics of this collector, such as the catchment area, average energy efficiency, thermal resistance and optical characteristics. There is even the option "new collector", which allows the user to insert a new collector, if he does not find the necessary equipment.

Shiv Kumar, Aseem Dubey, G.N.Tiwari [**14**] developed a thermal model of an integrated system system for predicting solar activity under climatic conditions in New Delhi. Direct flow through the evacuated solar tube to the water heater in combination with a simple solar tube shown in (**Figure 5**).

Figure 5: Direct flow through an evacuated tubular solar collector in combination with a simple solar.

The vast territory of Kazakhstan and sufficient solar radiation favor the use of solar systems to generate energy and heat. Existing solar solar power plants did not find wide use due to the fact that the design was not perfect, or the cost of used foreign analogues of geocollectors is rather high, as a result of which they are mostly not available to autonomous consumers. In addition, there are no and not imposed service. The solution to this problem is a lot of vector, consisting in finding a new fundamental approach to energy, the development of new hybrid energy complexes using mathematical methods and computer modeling, software and hardware tools and information and communication technologies. One of the ways of rational use of energy resources is the involvement in the fuel and energy complex of the Republic of new sources of small energy, constantly renewable and environmentally friendly. Therefore, the development of an energy complex based on a double-circuit solar power plant with a heat pump is a pressing and urgent problem for an autonomous power supply.

This scientific report consists of 4 sections. In the first section, an analytical analysis was conducted on the basis of a study of the existing experience in the design and use of various types of solar power plants and the use of solar energy resources in Kazakhstan.

In the second section, mathematical and computer simulations of a two-circuit solar system with a thermosiphon circulation are considered. A mathematical model of a heat pump with a solar collector is presented. A simulation model of a double-circuit solar system with thermosiphon circulation has been developed. Computer simulation of thermal conditions and convective heat exchange in flat solar collectors.

The third section substantiates the main parameters of the new types of solar collector design. The substantiation of the angle of incidence of the solar collector is carried out. The process of thermosiphon circulation and heat flux is investigated.

In the fourth section, experimental design work was carried out on the choice of a constructive model and the development of a calculation method. Calculated experimental testing of a solar power plant based on flat solar collectors was carried out. The results of the experimental tests of the solar system and the technical characteristics of the solar collector are analyzed. Presents photo reports of artists on the design work of assembling different types of solar collectors.

Currently, much attention is paid in the republic to the development of solar power plants, the cost of which is quite high, as a result of which they are not available to autonomous consumers. The solution to this problem is multi-vector, consisting in finding a new fundamental approach to energy, developing new hybrid energy complexes using mathematical methods and computer modeling, software and hardware tools and information and communication technologies. One of the ways of rational use of energy resources is the involvement of new sources of small energy, constantly renewable and environmentally friendly, in the fuel and energy complex of the republic. Therefore, the development of an energy complex based on a dual-circuit solar installation with a heat pump is an urgent and urgent problem for autonomous energy supply.

Unlike solar collectors, heat pumps do not convert direct solar radiation into usable heat; on the contrary, they draw it where solar heat has accumulated for a long time - in the deep layers of the earth, in groundwater and in the surrounding air. The use of these natural batteries allows most heat pump systems, even on particularly cold winter nights, to do without the support of a boiler. Approximately 60 thousand homeowners in Germany are gradually switching to appliances that are environmentally friendly. At one time, the Germans, who recognized the oil crisis, acquired about 30 thousand units in one year. I must say that then in the hype that gripped everyone, not one heat pump changed hands, not justifying the great expectations of the previous owner. The technical flaws of the plants have caused great damage to the pump's reputation. But be that as it may, failures and overlays provoked a natural process of purification. Several manufacturers of those times had already turned their backs on, and only eminent ones remained, such as, for example, Siemens (Siemens), Dimplex or Stiebel Eltron. “Who is developing heat pump technology today,” says Gerd Dietmar Kolrush, commercial director of the Kulmbach air conditioning plant (KKW), “is really taking this seriously.” In terms of sales, engineer Michael Birke (Stiebel Eltron) notes a tendency towards smaller installations. Being integrated into an existing heating system, the heat pump takes over the actual production of heat.

Abroad, such systems are welcomed, the state helps the population with subsidies and non-repayable loans, knowing that one-time investments will pay off with the energy security of small towns and settlements. In addition, the problem of providing fuel, especially in winter, will decrease by an order of magnitude.

The purpose of the program. Development of mathematical and computer models, software and hardware tools and experimental work on the creation of a network of combined effective dual-circuit solar collectors with thermosiphon circulation for supplying buildings with hot water and heat, as well as monitoring their functioning.

To achieve the goal of the Program, it is supposed to solve the following tasks:

- Review, analytical analysis based on a study of existing experience in the design and use of various types of solar systems.
- Carrying out research and development work on the selection of a constructive model and development of a methodology for calculating the effectiveness of the proposed type of solar collector with thermosiphon circulation.
- Mathematical and computer modeling of thermal calculation features, including the selection of the main dimensions, calculation of solar radiation, substantiation of the main parameters of the solar collector with thermosiphon circulation, as well as the calculation of the output characteristics of the solar installation.
- Computer models of the design scheme of a solar collector with thermosiphon circulation with a multilevel heat pump, used to build a generalized model of solar installations.
- Study of thermosiphon circulation and finding the thermosiphon flow.
- Justification of the main parameters of a new type of design of a solar collector with a heat pump in the solar system.

In general, the indicated tasks of the calendar plan were completed by the program executors on time. A brief review of foreign scientific publications, an analysis of experience in the use of renewable energy systems was carried out. As you know, solar systems have found wide application in the EU countries: Spain, Italy, Greece, Germany, France, etc., where national programs and laws for their development are adopted. For example, in Israel, hot solar water supply to 80% of residential buildings saves more than 5% of the electricity produced in the country, while in the United States more than 60% of pools are heated by solar collectors. The total area of solar collectors in the world exceeds already 50 million m^2, and this process continues to increase.

Abroad, such systems are welcomed, the state helps the population with subsidies and non-repayable loans, knowing that one-time investments will pay off with the energy security of small towns and settlements. In addition, the problem of providing fuel, especially in winter, will decrease by an order of magnitude.

The vast territory of Kazakhstan and sufficient solar radiation favor the use of solar systems to produce hot water and heat. Due to the incomplete design of the widespread use, the existing solar solar energy installations were not found or the cost of the used foreign analogues of solar collectors is quite high, as a result of which they are mainly not available to autonomous consumers. In addition, there are no maintenance services. The solution to this problem is a lot of vector, consisting in finding a new fundamental approach to energy, the development of new hybrid energy systems using mathematical methods and computer modeling, software and hardware tools and information and communication technologies. One of the ways of rational use of energy resources is the involvement of new sources of small energy, constantly renewable and environmentally friendly, in the fuel and energy complex of the republic. Therefore, the development of an energy complex based on a dual-circuit solar installation with a heat pump is an urgent and urgent problem for autonomous energy supply.

Chapter 1

Analytical Analysis of Solar Energy Resources of the Republic of Kazakhstan about the Possibility of Using Different Types of Solar Heating Systems

Authors
Amirgaliyev Y.N, Kunelbayev M, Kalizhanova A.U, Kozbakova A. Kh, Daulbayev S.M, Auelbekov O. A, Kataev N.S, Yedilkhan D, Merembayev T, Ormanov T. A, Sundetov T.

*__Corresponding author:__ Ministry of Education and Science of the Republic of Kazakhstan Committee of Science Republican State Enterprise Institute of Information and Computational Technologies, E-mail: murat7508@yandex.kz

The present project considers the solar-driven resources of the Republic of Kazakhstan. To assess the solar energy potential, falling onto the territory in any region, it is necessary to have data on the solar energy potential. Based on actual observations and theoretical calculations generalizing, there exists the data: annual and latitudinal motion of possible monthly and annual sums of the direct solar irradiation falling onto the perpendicular surface under the conditions of clear sky, data on sunshine duration, daily motion of solar radiation for typical days of the year, maps of distributing the average monthly radiation sums for June and December on the territory as well as the maps of distributing «technically applicable and economically profitable solar capacity», developed criteria of defining the notion thereof. All solar systems estimates upon assessing the solar-driven resources on Kazakhstan territory are based on quantitative characteristics of the direct solar radiation onto the horizontal surface from which there might be done recalculation from

the horizontal to inclined plane of any orientation. Proceeding from the results of average values of the direct, total irradiation and duration of the sunshine statistical treatment there have been differentiated five zones and compiled a histogram characterizing the possibility of introducing the solar plants onto Kazakhstan territory.

Analytical Analysis of Solar Energy Resources of the Republic of Kazakhstan

Upon specifying the solar plants usage feasibility at any location there conducted preliminary calculations, taking into account the average annual, average monthly total amount of solar radiation, number of clear and dull days, duration of frostless period, cost of solar plant, their efficiency factor, etc.

At that, there was used reference data and passport data of solar stations with their technical specifications.

To assess the solar energy potential falling onto the territory in any region it is necessary to have the data on the solar energy potential.

In the article [**15**] there is analyzed the current energetic situation in Kazakhstan, including fossil energy sources and renewable energy sources and have been studied political factors in the energetic sector. The main aim of the article [16] is studying the prospects of the energy renewable sources development. It has been proved, that about 18% of the world energy consumption has been received from the renewable energy sources. In the article herein [**17**] there were presented some offers for developing the solar industry in Kazakhstan, based on the analysis of the global solar energetic model. In the document [**18**] the principal attention was paid to discussing the new technological components, which might be used for developing the system of renewable sources monitoring. There are being discussed the principles and architectural technologies which can be applied to such system implementation. As well, there were considered several examples of monitoring systems and engineering aspects behind such system. The article [**19**] considers different potential local resources, unrelated to fossil fuels, water power, solar power, wind, biomass and uranium, and there is being installed the structure of those resources' priority evaluation.

To use the solar power effectively in combination with other climate components for the needs of the solar heating, the criteria for zoning are the solar intensity, climate meteorological parameters (outside air temperature, wind regime and other atmospheric phenomena). As the base of all solar system factors calculations while assessing solar power resources on the territory of Kazakhstan there were accepted quantitative characteristics of direct solar radiation on the horizontal surface, from which it is possible to perform recalculation from the horizontal to inclined plane of any orientation (**Table 1.1**).

Proceeding from the results of statistical treatment of the direct, total radiation and sunshine duration average values in compliance with the (**Figures 1.1** and

20) there were differentiated five zones and drawn up a histogram, characterizing the possibilities of introducing the solar stations along the territory of Kazakhstan. Zone 1 occupies forest-steppe zones, located in the Northern Kazakhstan with an average June totals of the direct and global radiation of 11-14 and 20-22 MJ /v^2, i.e. 350-400 and 600-700 MJ /m^2 a month. According to the main features the solar power usage in this region is possible for practical aims of CCTC systems, but it is limited with a climatic, meteorological factor, wind and frequent sharp decrease in temperature in spring-autumn period. Sunshine duration in the year fluctuates from 1900 to 2200 hours.

Zone 2 is on the territory of Turgai valley, southern suburbs of Western-Siberian lowlands. Daily there is 22-24 MJ /m^2 of global radiation, but the most part of it is in the form of direct one, 13-15 MJ /m^2. Monthly amount is 600-700 and 400-500 MJ /m^2. The region thereof is characterized with sufficient amount of sunshine hours, i.e. 2200-2500 approximately, comparing to the Zone 1. But meteorological factors are not favorable either. In spring-autumn period there is stable cold air in Turgai lowlands, conditioning frequent, lasting ground frost.

Zone 3 is moderately- favorable for the solar power usage, which includes Precaspian lowland, Mugodzhary upland, Kazakh hummocky topography, Altai mountain uplift. Daily amount of average total radiation here is in July 23-26 MJ /m^2, whereof 15-18 MJ /m^2 is in the form of the direct radiation, monthly total amounts - to 700-800 and 400-550 MJ/m^2. Annual sunshine duration fluctuates within 2500-2700 hours.

Zone 4 includes Kyzyl Kum, Turan lowland, plain of Balkhash-Alakol basin, Tarbagata, Junggar and Zailiisky Ala Tau mountain ranges. Daily average total solar radiation here is 23-26 MJ /m^2, at that, the big amount is in the form of direct one, 15-18 MJ /m^2. Thus, correspondingly the monthly solar power amount is 700-800 and 500-600 MJ /m^2. Annual sum of direct radiation is higher here, especially in the mountains. Sunshine duration is 2700-2900 hours and the region is characterized as favorable for the solar power usage. Zone 5 is the deserts Ak-Kum, Betpak-Dala with an average daily solar power intensity totals of correspondingly 18-22 and 25-28 MJ / m^2, and monthly sums 550-700 MJ /m^2 and 750-900 MJ /m^2. The region is also favorable for using the solar power, and as we can see, in general, grasps the south of the republic. Sunshine duration in summer is about 390 hours, annual - 2900-3200 hours at minimal amount of dull days.

As it is shown with analysis a wide range of quantitative characteristics, reflecting the solar radiation regime peculiarities, sunshine duration and cloudiness confirms that the separating having been done.

Structural temporary features of the supposed days of “sunny” and "electric" solar plants heating are given for all the zones. The greatest interest from the energy point of view is the amount of days with the sun and electric water

heating in the solar plants within a year. It is typical for the 1st zone to use the solar power during 180 days, the rest 180 days there is the electric heating. For the 2nd, 3rd and 4th zones the number of days when the solar energy is used grows up to 270, and amount of days while using electric water heating decreases to 94. In the 5th zone it is possible to use the solar power more efficiently within a year. Criterion for such evaluation is an average time period, when the radiation amounts to minimum 0,4 kW/m^2 and exceeds 6 hours per day.

Radiation regime characteristics definition has been conducted as exemplified by Almaty hydro-meteorological station (HMS). The solar radiation is the main source for the heat conductor process in the solar station. For that purpose, firstly, it is necessary to get an average background mode of the solar radiation according to available data, many years of observation for Almaty city.

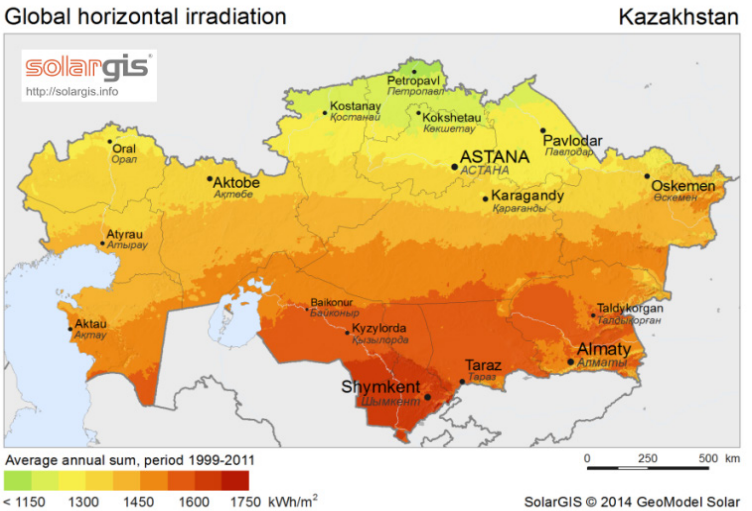

	Zone 1. The conditions, in whole, meet the requirements of using the solar stations
	Zone 2. Conditions of more or less effective use of the solar statioms
	Zone 3. Conditions secure sustainable operation
	Zone 4. Conditions for more effective use of the solar station
	Zone 5. Conditions of the most effective use of the solar station

Figure 1.1: Solar power resource of the Republic of Kazakhstan.

Region appropriate for practical usage	Total direct irradiation onto the horizontal surface (S'), MJ/m²									Total of global irradiation on the horizontal surface, (Q), MJ/m²								
	days		min max		winter	spring	summer	fall	year	days		min max		winter	spring	summer	fall	year
	1	7	1	7	12,1,2	3,4,5	6,7,8	9,10,11						12,1,2	3,4,5	6,7,8	9,10,11	
1.Conditions, in whole, meet the requirements of the solar plants usage Kostanai, Astana)	1,2 1,4	11,2 13,5	37,7 41,9	347,7 419,0	138 276	842 771	1064 1185	322 339	2367 2509	3,6 4,5	20,1 22	113,2 138,3	624 683	389 473	1520 1529	1839 1935	662 733	4412 4671
2.Conditions more or less effective for the solar plants usage Dzhanybek, Semipalatinsk)	1,2 2,3	13,9 14,5	37,7 71,2	431,6 448,4	150 243	880 1018	1252 1315	440 490	2723 3067	4,0 5,3	22,6 22,8	125,7 163,4	699 708	414 817	1525 1730	2002 2065	775 863	4717 5191
3.Conditions secure sustainable operation of the solar plants (Atyrau,Aktobe Aktau)	1,9 1,75 1,6	17,4 15,8 15,8	58,7 54,5 50,3	540,5 490,2 490,2	230 197 192	1127 934 1009	1596 1446 1454	662 553 636	3616 3129 3293	5,1 5 4,19	25,5 24,5 23	159,3 155 129,9	792 758 716	469 532 452	1780 1634 1646	2300 2191 2099	1047 905 997	5664 5262 5195
4. Conditions for more effective usage of the solar stations (Aralsk Sea, Zhezkazgan, Buran)	2,7 3,1 2,9	17,9 15,9 17,0	83,8 96,4 92,2	557,3 494,4 528	276 297 293	1156 1043 1152	1650 1462 1546	708 632 662	3791 3435 3653	6,0 6,0 5,9	25,4 23,7 24,5	188,5 188,5 184,4	787 737 762	624 607 607	1872 1726 1784	2317 2149 2208	1076 993 1013	5891 5476 5614
5. Conditions for the most effective usage of the solar plants (Barsa-Kelmes, Ak-Kum, Kuigan)	2,9 4,19 3,6	17,4 21,3 19,7	92,2 129,8 113,1	540,5 662,0 611,7	272 360 347	1169 1210 1122	1713 1965 1751	699 972 825	3854 4508 4047	5,9 7,3 7,3	24,6 27,9 26,7	184,4 226,3 226,3	762 867 829	578 695 720	1822 1851 1826	2312 2543 2384	1030 1324 1206	5744 6414 6138

Table 1.1: Solar power and meteorological zonal characteristics of Kazakhstan's territory.

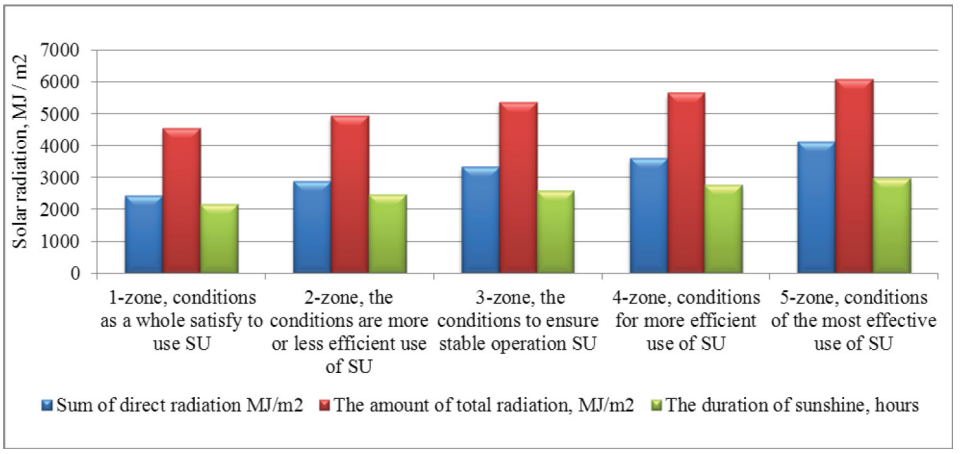

Figure 1.2: Histogram of the solar stations usage dependence from average values of direct, total radiation and duration of the sunshine.

The big city's radiation regime has Almaty HMS, situated at Zailiisky Ala Tau foothills. Along with the area's height increase the solar radiation grows at the expense of atmosphere's transparentizing. Usually in the summer time's first part the atmosphere is more clear, than in the second part, which is connected with the atmosphere dust content increase, and convective clouds.otal irradiation and duration of the sunshine statistical treatment there have been differentiated five zones and compiled a histogram characterizing the possibility of introducing the solar plants onto Kazakhstan territory.

We have studied actinometric and climatic characteristics, used in the methodology of the solar energy usage assessment for the following hydrometeorological stations, located on the territory of Kazakhstan:

Araljsk Sea (Kyzyl-Orda region).

Barsa-Kelmes (Kyzyl-Orda region).

Ak-Kum (Kyzyl-Orda region).

Almaty, GMO (Almaty region).

Cloudiness increase decreases the direct and increases the diffused radiation. Diffused radiation flow, though partially, compensates the direct solar radiation weakening in the atmosphere but the compensation is not complete. Therefore the total radiation flow under cloudiness conditions, if the sun is not covered with clouds, will be bigger comparing to the clear sky conditions.

Apart from transparency and cloudiness the big influence at diffused radiation is exerted with the nature of underlying surface. Upon the snow cover there is increased the reflection of the direct solar radiation, secondary diffusion of which in the atmosphere brings to the diffused radiation growth.

Along with the elevation increase the direct solar radiation flow is growing, which is explained by lessening the optical width of the atmosphere. Hereupon the solar radiation flow maximum values in mountainous regions are bigger, than on the flat topography. Value of the diffused radiation flow with elevation over sea level decreases at clear sky, as the thickness of atmosphere's scattering layers decreases. Upon cloudiness the diffused radiation flow in the layers lower than the clouds increases according to the elevation. Appearance of direct and global radiation decreases in the areas, located in the floors of valleys or pits due to the closed horizon. Direct, diffused and total solar radiation has well defined annual motion, which is distinctly seen on the (**Figures 1** and **2**).

Criterion 1

Average time duration. When radiation is no lower than 0,4 kW /m^2 and exceeds 6 hours per day. The (**Table 1.2**) demonstrates averaged long-term data of total daily accumulated radiation.

Criterion 2

Average number of clear days shall be no less than a half of an average number of dull days. With account of that the provision of daily totals of accumulated radiation is 4,6 kWh/m^2 and higher and according to long-term data of Almaty station amounts to (%):

Month	1	2	3	4	5	6	7	8	9	10	11	12
	-	8	20	50	72	83	79	60	55	40	15	-

Table 1.2: Averaged daily global radiation.

The most favorable period to use the solar energy in Almaty is from March to November, according to provision of daily totals of global radiation from April to September (**Table 1.3**).

According to the data on long term observations of the sunshine duration in compliance with the sunshine recorder we differentiate the periods of the solar continuous shining 5,6,7, etc. At that, we exclude the time during one hour after and till the sun up. Results in Almaty city are given in the tabular form.

	2	3	4	5	6	7	8	9	10	11	12
Almaty	4	4,8	7	8,2	8,4	8,3	8	6	5	4,8	4

Table 1.3: Solar station operational capacity (hour) depending on the solar continuous shining (for 10 years period).

Analysis of (**Table 1.3**) demonstrates, that it is inappropriate to use the solar plants in Almaty city in March and November, much more successfully they will operate from April to October.

Chapter 2

Mathematical and Computer Simulation of Double-Circuit Solar Heating Systems with Thermosifon Circulation

Authors
Amirgaliyev Y.N, Kunelbayev M, Kalizhanova A.U, Kozbakova A. Kh, Daulbayev S.M, Auelbekov O. A, Kataev N.S, Yedilkhan D, Merembayev T, Ormanov T. A, Sundetov T.

*__Corresponding author:__ Ministry of Education and Science of the Republic of Kazakhstan Committee of Science Republican State Enterprise Institute of Information and Computational Technologies, E-mail: murat7508@yandex.kz

The article herein considers the theoretical and mathematical analysis of double-circuit solar station with a thermo siphon circulation. To implement the work herein there has been offered a new solar collector with a thermo siphon circulation where being increased the thermal transmission performance factor through exclusion of additional divider walls between a panel and heat insulation, which simplifies the collector construction. The solar collector is convenient in operation and quickly has been heated up at the expense of thermo siphon insulation, as well there is a thermal pump having been made in the form of spirals, which put up one upon another, and it increases the square and intensity of heat exchange. Conducted theoretical and mathematical analysis of non-stationary thermal regime of flat plate solar collectors allows optimizing the construction elements, predicting the thermal mode and selecting the alternative solution.

In the article [**20**] there has been noted, that virtual prototyping of the solar collector helps predict collector's performance until operation. The work herein admits, that in order to ground the solar collector project at physical state space it should be drove to a state of modeling to research collector's dimensions, which gives the air outlet low temperature. Upon studying the design and operation models there is also taken into account the performance parameters. Duffie and Beckman in the work [**21**] have constructed the solar collectors, which are applied to the models. In the current research there are several novelty aspects in the model-based approach. Duffie and Beckman [**22**] in the previous literature have told about the solar collectors modeling, being limited to using the analytic expressions and approximants. With numerical models the restrictions of the approach thereof can be alleviated. Duffie and Beckman mention, that for the heat loss overall coefficient calculation to define the spatial average temperature of the absorbing plate is difficult. In the spatially distributed model as presented here, this is not a problem. Moreover, the solar collectors are often characterized by the heat which shall be defined experimentally.

Koyunsu in the work [**23**] concerning the solar collector has noted that the special attention is paid to the heat increase from the solar power radiation factor and heat output. Kicsiny [**24**] has experimentally simulated the solar collector where the temperature output does not help design the solar collector's dimensions, particularly the solar collectors being operated under different conditions. Kicsiny, [**25**] Gao et al., [**26**] Alvarez et al. [**27**] have given the information on the solar collector's parameters calculation.

Mathematical Model of a Heat Pump with a Solar Collector

The scheme of interfacing the elements of the operation of a heat pump with a solar collector is shown in (**Figure 2.1**).

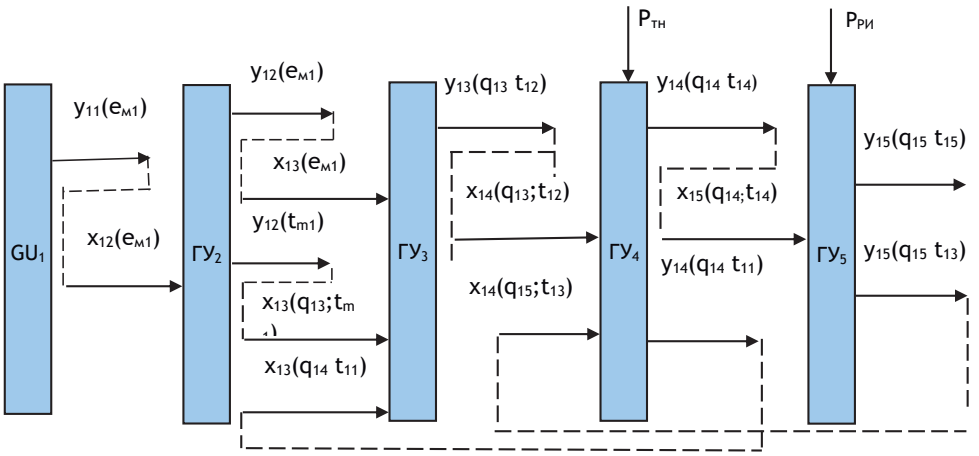

Figure 2.1: Model and scheme of interface elements of the solar sub system.

Where GU_1 - is solar energy, GU_2 - is the heat of atmospheric air, GU_3 - is a solar collector, GU_4 -is a heat pump, and GU_5 - is a heat energy accumulator.

When formalizing the model, the analogies with the real object are observed. The input and output signals are indicated by x_{1i} and y_{1i}, where the symbol i - indicates the number of the element to which the signal belongs, and the number 1, according to the adopted notation (Figure 2.1), belongs to the parameters of this subsystem. Accordingly: q_{1i} - is the heat flux, t_{1i} - is the temperature of the heat flux. Assumptions are made for the quasi-stationarity of bonds between elements and the independence of the flow of solar energy and heat of the atmosphere.

$$y_{11}(e_{m_1}) = x_{12}(e_{m_1}) = y_{12}(e_{m_1}) = x_{13}(e_{m_1});\ y_{12}(t_{m_1}) = x_{13}(t_{m_1});$$

$$y_{13}(q_{13}; t_{12}) = x_{14}(q_{13}; t_{12});\quad y_{14}(q_{14}; t_{14}) = x_{15}(q_{14}; t_{14});$$

$$y_{14}(q'_{14}; t_{11}) = x_{13}(q_{14}; t_{11});\quad y_{14}(q'_{15}; t_{13}) = x_{13}(q_{14}; t_{11})$$

The model has special input contacts, which receive control signals, two of which are the power of the heat pump compressor ($p_{mн}$)) and the power of the backup source (p_{pu}). Feedbacks from GU_4 to GU_3 and from GU_5 to GU_4 show the circulation of coolant from the evaporator outlet of the heat pump to the solar collector inlet and y_{14} $(q_{14}; t_{11})$ and from the battery outlet to the condenser inlet of the heat pump y_{15} $(q_{15}; t_{13})$.

The variable intensity of solar radiation, in the heating months, is modeled by the output signal from PG_1 and can be represented by a polynomial:

$$\acute{o}_1\ (\mathring{a}_{\grave{o}\,1}) = \mathring{a}_{\grave{o}} = \sum_{\ddot{\imath}=1}^{\ddot{\imath}} \grave{a}_{1\ddot{\imath}} \cdot \grave{o}^{\ \ddot{\imath}-1}$$

The variable temperature of the atmospheric air, in the heating months, is modeled by the output signal from PG_2 and can also be represented by a polynomial:

$$\acute{o}_2\ (t_{\grave{o}\,1}) = t_{\grave{o}\,1} = \sum_{\ddot{\imath}=1}^{\ddot{\imath}} b_{1\ddot{\imath}} \cdot \grave{o}^{\ \ddot{\imath}-1}$$

where a_{1n}; b_{1n} - constants of polynomials; m is the ordinal number of the current month.

Justification of the design-technological scheme. Taking into account the requirements for improving the performance of the device, a schematic diagram of a double-circuit solar system with a heat pump has been developed (**Figure 1**), where the studied diesel-hydraulic generators are formed by four main nodes: thermosyphon 1, solar collector 2, heat pump 3, storage tank (BA) 4.

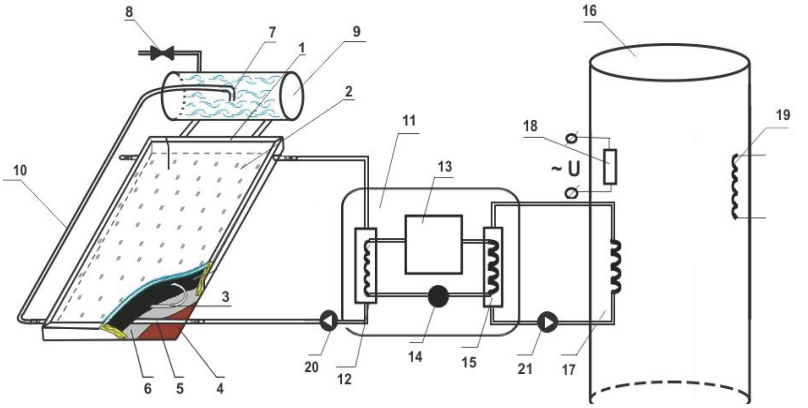

Figure 2.2: Schematic diagram of a dual-circuit solar system with thermosiphon circulation.

The work of the proposed installation is as follows. Solar energy E is absorbed by the solar collector 1, heating the flow of solar energy passes through a translucent insulating transparent glass unit 2. The heat received from the solar flow heats the fluid in the coils, which is removed from the collector, and in its place cold liquid flows from the siphon 9 and there is a constant circulation. The evaporator 10, absorbing the heat transfer fluid, lowers its temperature below the temperature of atmospheric air, thereby contributing to additional heat absorption from the atmospheric air (Q_2). The diagram also shows solar radiation reflected from the translucent coating (Q_0) and the surface of the absorbing panel (Q_1). In heat pump the transfer of energy of the coolant (Q_3), with a relatively low temperature, to the heat carrier of the heat exchanger of the condenser 13 with a higher temperature.

For the implementation of such a cycle is used compressor 11, with electric drive 15 (WEL). Further, by means of the heat exchanger 14, heat from the heat pump (Q_6) is transferred to the BA, where the water temperature is brought to the required technological level and heating. In parallel with the main flow, heat losses occur from the surface of the compressor (Q_4) and the surface of the heat exchanger of the condenser (Q_5). Taking into account the aforesaid in the thermal model of the system, the following areas can be distinguished: - solar energy receivers; - tank sections; - pipelines; - elements of the collector. We formulate the law of energy conservation for each region of the thermal model (**Figure 2.3**).

Area The heat flux absorbed by the receiver from the sun is spent on the change in enthalpy, $C_n \frac{dt_c}{d\theta} + C_T \frac{dt_f}{d\tau} + G_0 C_p (t_3 - t_5)$, the receiver and the liquid in it, the heat transfer to the elements $\sum_m U_p (t_p - t_a)$ and the environment $U_c (t_m - t_a)$.

Scope nuk. Heat flow $G_0 C_p (t_3 - t_5)$ obtained by the liquid goes to change its enthalpy $C_\delta \frac{dt_f}{d\theta} + C_p \frac{dt_n}{d\theta}$ heat emission to the environment $U_T (t_n - t_a)$.

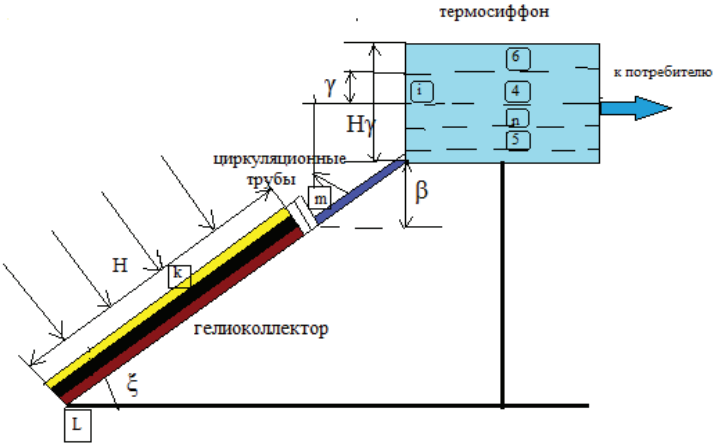

Figure 2.3: Model of a solar collector with a thermosiffon.

According to the law of energy conservation for each region of the thermal model, we can write:

$$G_0 C_p (t_3 - t_5) = \eta_n [E(\tau\alpha) - U_c (t_m - t_a)] - C_n \frac{dt_c}{d\theta} - C_T \frac{dt_f}{d\theta} - U_p (t_p - t_a) \qquad (2.1)$$

$$G_0 C_p (t_3 - t_5) = U_m (t_n - t_a) + C_\delta \frac{dt_\tau}{d\theta} + C_p \frac{dt_n}{d\theta} \qquad (2.2)$$

According to the accepted assumptions, it can be assumed that the temperatures of the solar receiver and the tank are equal to the temperatures of the corresponding water. Thus, given that $t_c = t_m, t_0 = t_n, t_f = t_p$ equations take the form

$$G_0 C_p (t_3 - t_5) = \eta_n F_k [E(\tau\alpha) - \eta_c U_c (t_m - t_a)] + U_p (t_p - t_a) - C_n \frac{dt_m}{d\theta} - C_T \frac{dt_p}{d\theta}$$

$$G_0 C_p (t_3 - t_5) = (C_p + C_\delta) \frac{dt_n}{d\theta} + U_T (t_n - t_a)$$

Based on experimental studies, the average temperature of the water in the storage tank is the same as in the solar collector during the day, which is also true for the temperature of the pipes, if we consider the average temperature of both pipes. So, taking that $t_m = t_n = t_p$ and eliminating from equations (2.1) and (2.2), we obtain the equation for the average temperature of the system:

$$W \frac{dt_n}{d\theta} + U (t_n - t_a) = \eta_n F_k E(\tau\alpha)$$

where $W = C_n + C_T + C_\delta + C_p$

$$U = \eta_n F_k U_c + U_T + U_p$$

Movement through natural convection formed as a result of heating water in the solar collector caused by a thermosiphon effect, to determine the flow rate of a liquid, it is necessary to consider at any time, the density at various points of 1-6 flow circles. It is assumed that the density distribution in the solar collector and the tank is linear and the energy losses in the pipe are insignificant compared with the heating in the receiver. Assuming the quadratic density-temperature dependence.

$$D_w = At^2 + Bt + C$$

It can be shown that the thermal pressure formed by solar heating is determined by the equation:

$$\hbar_1 = \frac{(t_5 - t_3)}{2}\left[2\mathrm{At_n} + B\right] f(s)$$

where $f(s)$ - is the function of the system depending on many parameters: the geometry of the solar receiver, the location of the pipes (β, γ, ξ), the height of the water in the tank (H_t), the length of the solar receiver, and its inclination (l_0, ε). We write these dependencies

$$f(s) = l_0 \sin\varepsilon + 2\beta(H_t - \gamma) \tag{2.3}$$

$$t_n = \frac{t_5 + t_3}{2} \tag{2.4}$$

Eliminating $(t_5 - t_3)$ from (2.3) and (2.4), we obtain

$$h_1 = \frac{\left[\left(W_{\omega t} + W_s\right)\right]\frac{dt_n}{d\theta} + U_T\left(t_n - t_a\right)}{2G_0 C_p}\left[2At_n + B\right] + f(s) \tag{2.5}$$

The speed of the thermosyphon flow will be such that at any time the pressure of the thermal pressure is balanced by frictional pressure loss $(h_{ä})$ in the cycle of the circulation flow. Based on the Darcy equation, the value of the functional head loss can be represented as follows: $h_f = \frac{flU^2}{2gdp}$, where f equal to 0.035 for normal flows in such systems, which are possibly laminar flows. Applying speed (U) as a function of mass flow rate (G_0) we will receive: $h_f = \frac{DG_0^2}{dp^2}l$ where D is the known constant: l is the effective cycle length of the circulating flow with an internal diameter dp depending on the configuration of the receiver and the location of the pipe. For a receiver having parallel tubes between the water tank (collectors) and the location of the pipe, as shown in (**Figure 2.3**).

$$l = \{\frac{Sl_T}{l_k}(\frac{dp}{dc})^5 + l_k(\frac{dp}{dh})^5\} + \{l_T + H_t - \gamma + \beta\chi(1 - \cos ec\varepsilon)\} + l_c + L_0 \tag{2.6}$$

Having solved (2.5) and (2.6), we obtain the equation of a thermosiphon flow:

$$G_0^3 = -(\frac{dp^5}{2lDC_p})\{W_{a\chi} + C_\delta)\frac{dt_n}{d\theta} + U_T(t_n - t_a)\}\{2At_n + B\}f(s) \qquad (2.7)$$

equation (2.6) for G_0 is cubic. Finding magnitude t_n and dt_n / d_θ equation (2.4); by appropriate substitutions, one can determine G_0. Knowing G_0 and t_n приемная уравнения (2.4) и (2.7) можно также определить температуры t_3 and t_5 at the entrance and exit of the tank. Based on this, it is possible to determine all system parameters, as well as efficiency. solar receiver and the entire system.

Figure 2.4: Full-scale model of a flat solar collector.

Simulation Model of a Double-Circuit Solar Heating System with Thermosiphon Circulation

On the basis of theoretical studies, a simulation model of the power plant was created (**Figure 2.5**), which can be used to calculate the current and total values of the power generated, taking into account the technical characteristics.

In the displays, the current values of the generated power are shown taking into account the influence of solar radiation and the air temperature of the area, as well as the current value of the efficiency of the GEM. In addition, in the simulation model there are blocks for exporting data into tables for further processing.

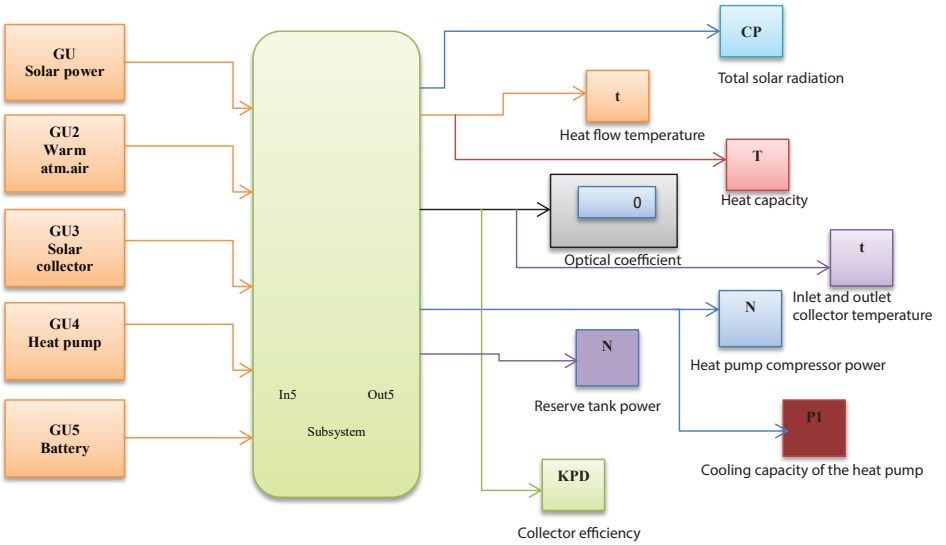

Figure 2.5: A simulation model for determining the value of the generated power depending on the parameters of the power plant.

GU Solar power	The block that records the arrival of solar energy
GU2 Warm atm.air	The block in which temperature of atmospheric air heat is recorded
GU3 Solar collector	The block in which the choice of solar collector is recorded
GU4 Heat pump	The block in which the set value of the heat pump is recorded
GU5 Battery	The block in which the set value of the power tank battery is recorded
N	A block showing the total value of the reserve tank power generated
The display showing the current and total values of the variable power plant are determined by blocks	
CP	Block, shows the current value of total solar radiation
N	The unit shows the power of the heat pump compressor
T	Block, shows heat capacity
t	Block, shows the current value of the heat flux temperature
0	Block, shows the total value of the optical coefficient of heat capacity
t	Block showing the temperature of the solar collector
P1	Block showing the cooling capacity of the heat pump
KPD	Block showing the efficiency of the solar collector

Table 2.1: Technical characteristics of the power plant are processed by the following blocks.

The simulation model has the opportunity to observe online the graphs of changes in daily, monthly and annual solar radiation, reserve tank power values, heat output of the heat pump and the current efficiency of the solar collector. The given simulation model meets two basic requirements of the proposed simulation models:

- Reflects the logic of the functioning of the system under study in time.
- Provides the possibility of conducting experiments.

The results of the study. Find $\frac{dt_n}{d\theta}$ temperature change in thermosyphon. Express $\frac{dt_n}{d\theta}$ from equation (2.8).

$$\frac{dt_n}{d\theta} = (\eta_n F_k E(\tau\alpha) - U(t_n - t_a))/W \tag{2.8}$$

The equation was simulated in MatLab Simulink software. The following data is initialized in (**Table 2.2**).

Variable	Value	Description
U	16	Heat sink coefficient
E	0.85	Average monthly radiation of 90
ta	10	Initialized System Temperature
n	0.85	System efficiency
Fk	1780	Aperture area
W	1000	

Table 2.2: Initialized Data.

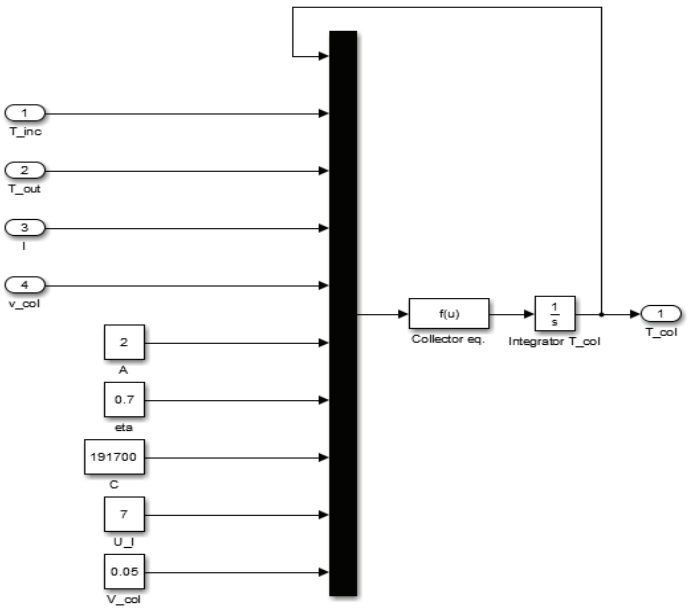

Figure 2.6: The block diagram of the model in Simulink.

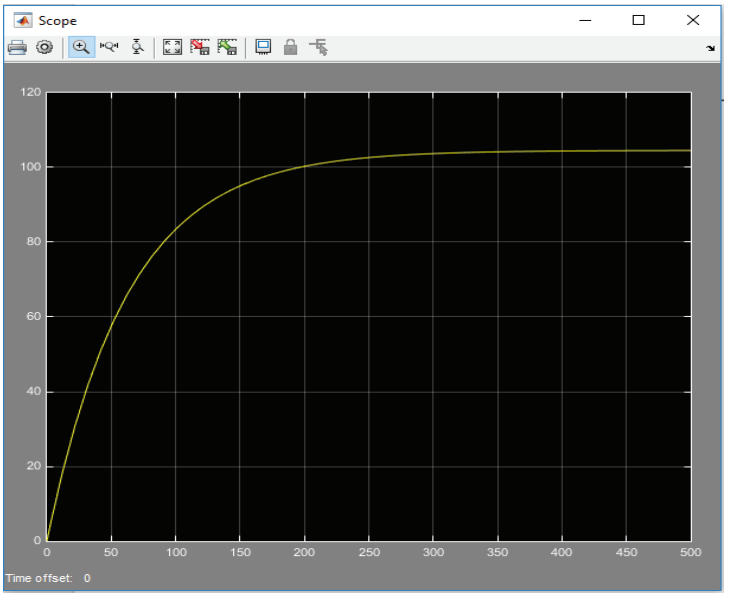

Figure 2.7: Dependence of ambient temperature and outlet.

This graph shows the same results with the solution of the differential equation, using numerical methods - the function ode45, which is based on the Runge-Kutta formula. The solution of the differential equation (6,7,8) $\frac{dt_n}{d\theta}$ - values were taken from the solution of diff. equations (2.8). A plot of thermosyphon flow versus temperature (**Figure 2.8**).

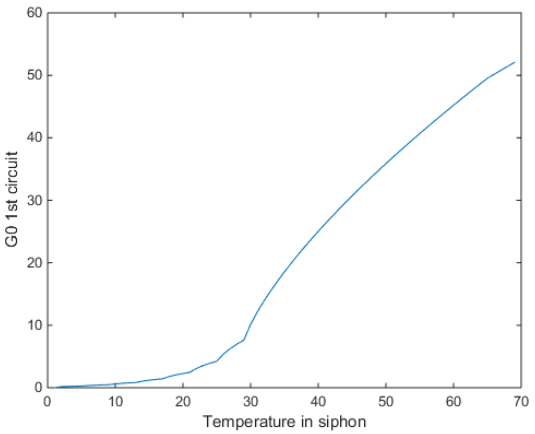

Figure 2.8: Dependence of thermosiphon flow on temperature.

We find the efficiency η_n with temperature change in thermosyphon. Express from the equation $\frac{d\eta_n}{d\theta} = (\frac{dt_n}{d\theta}W + U(t_n - t_a))/F_k E(\tau\alpha)$ The solution will be performed using numerical methods - the function ode45, which is based on the Runge-Kutta formula [28].

The result of the solution graph below, the dependence of the ambient temperature and the output. Graph the dependence of the ambient temperature and output (**Figure 2.9**).

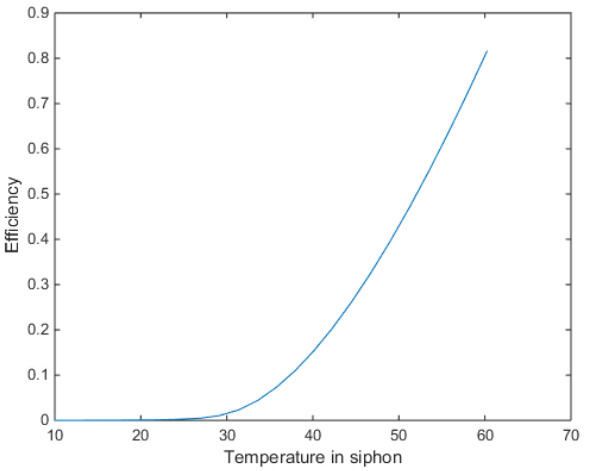

Figure 2.9: Dependence of ambient temperature and outlet.

In this section, a simulation model of a two-circuit solar heating system with a thermosiphon circulation was presented. The simulation model has the opportunity to observe online the graphs of changes in daily, monthly and annual solar radiation, reserve tank power values, heat output of the heat pump and the current efficiency of the solar collector.

Chapter 3

Modeling of the Basic Parameters of a New Type of a Solar Collector Design

Authors
Amirgaliyev Y.N, Kunelbayev M, Kalizhanova A.U, Kozbakova A. Kh, Daulbayev S.M, Auelbekov O. A, Kataev N.S, Yedilkhan D, Merembayev T, Ormanov T. A, Sundetov T.

*__Corresponding author:__ Ministry of Education and Science of the Republic of Kazakhstan Committee of Science Republican State Enterprise Institute of Information and Computational Technologies, E-mail: murat7508@yandex.kz

Analysis of the Main Parameters for New Types of Solar Collectors

For rational heat picking up from heat transmitting solar collectors and simplifying the solar system's operation, it is worth that the system operates with a thermo siphon circulation. Therefore, to define the solar installation's thermal regimes it is necessary to set the dependence of the performance on the solar radiation density's mode characteristics, heat removing factor, ambient temperature, temperature difference, etc.). Let us consider a single circuit system (**Figure1**) in the solar circuit, in which there is carried out the following: cold water (T1) out of the pressure tank (2) or the conduit is fed to the solar panels (1), heated and inlet into the accumulator tank, from where it is supplied to the consumers (3). On the motion path it is mixed with source cold water until reaching the appropriate temperature.

Let us assume, that the solar collector has a width of (b) and the slope angle to the horizon φ. Then at the solar collector's square F its length l = F/b; height $h = F\sin\varphi/b$.

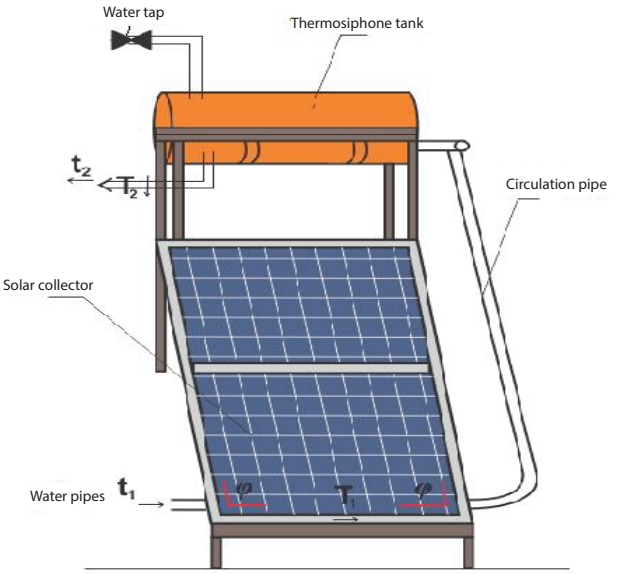

Figure 3.1: Solar system with thermo siphon circulation.

Circulation Motion's Magnitude

$$\mathrm{H} = g\frac{h}{2}(T_2 - T_1) = \frac{Fgn(T_2 - T_1)}{2h} \tag{3.1}$$

where n is the specific augmentation of the solar circuit heat conductor's volumetric mass under cooling for 1 degree (for temperature interval 40+80^{O}C n≈0,45 kg/m^2*grad(гра$\mathcal{Д}$)); F - total square of the solar collector (m2); T_2, T_1- final and initial temperature of the heat conductor in the solar circuit.
Circulation motion equals to the head loss in the solar circuit:

$$SG^2 = \frac{Fng(T_2 - T_1)sin\varphi}{2b} \tag{3.2}$$

Where S - solar circuit hydraulic characteristics Pa /$(\mathrm{kg} * \mathrm{h})^2$.
The heat quantity, absorbed by the thermosiphon is defined according to the formula:

$$G_1C_1(T_2 - T_1) = 3600E\gamma FF'\left[\left(\tau_0 - \frac{U_1}{E}\right)\left(\frac{T_2 + T_1}{2} - T_0\right)\right] \tag{3.3}$$

Hereunder γ– is the thermal detector's filling factor, which is equal to the ratio of square, radiated by the sun to the total square; C_1 - solar circuit thermal conductor' heat capacity; G_1- heat conductor's flow rate in the solar circuit; E-density of total solar radiation falling on the solar collector's surface;

τ_α- the solar collector's reduced absorption capacity; U_1 - losses factor in the solar collector; T_0- ambient temperature; F'- solar collector's efficient factor.

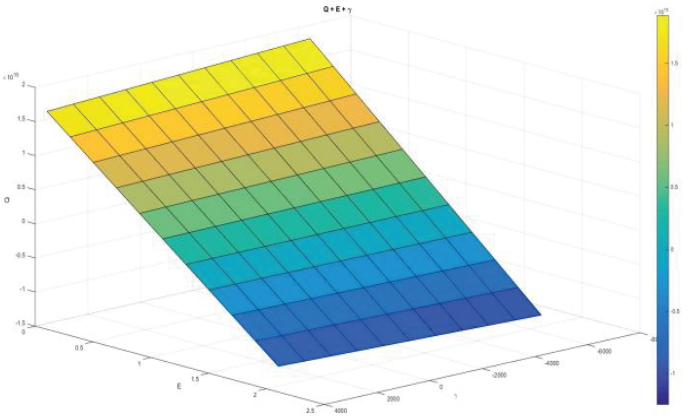

Figure 3.2: Heat quantity dependence on the solar radiation density.

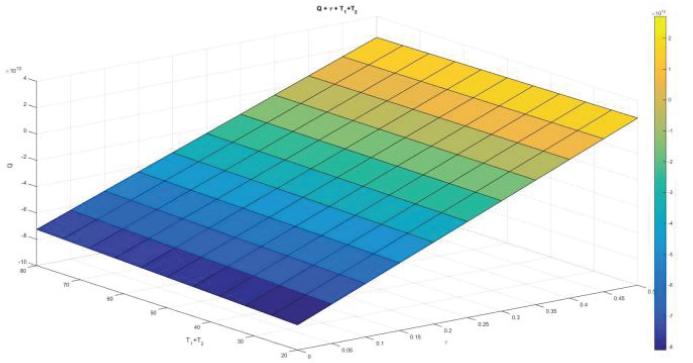

Figure 3.3: Heat quantity dependence on temperature difference.

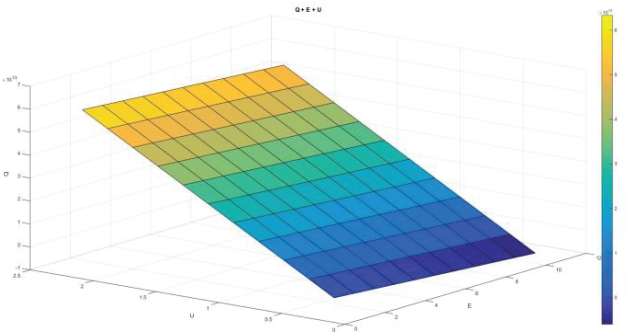

Figure 3.4: Heat quantity dependence on the coefficient of heat loss.

Finding the capture coefficient of a flat solar collector

Flow of the solar radiation falling onto the flat heat receiver, consists of two components [29]: $E_{\text{solar radiation}}=E_{\text{solar radiation}}+ E_{\text{scattered radiation}}$, where $E_{\text{solar radiation}}$ - is the flow of direct solar radiation $E_{\text{scattered radiation}}$ - is the flow of scattered radiation.

The equation of power balance, heat receiver's element separate layer will be of the following form [30] :

$$q_v + \frac{t_{v+1} - t_v}{\frac{1}{k_{v+1}} - \frac{1}{k_0}} = \frac{t_v - t_{v-1}}{\frac{1}{k_v} - \frac{1}{k_{v-1}}} + c_v \cdot p_v \cdot \frac{dt_v}{d\tau}$$

Capture factor - the principal optical-thermal characteristics of the solar in its magnitude is less than the overall coefficient.

The equation solution in respect of the capture factor can be finally presented as follows:

$$\gamma = \frac{q_p + k(t_p - t_v) - e^{-\frac{\tau\kappa}{c}}}{E} \tag{3.4}$$

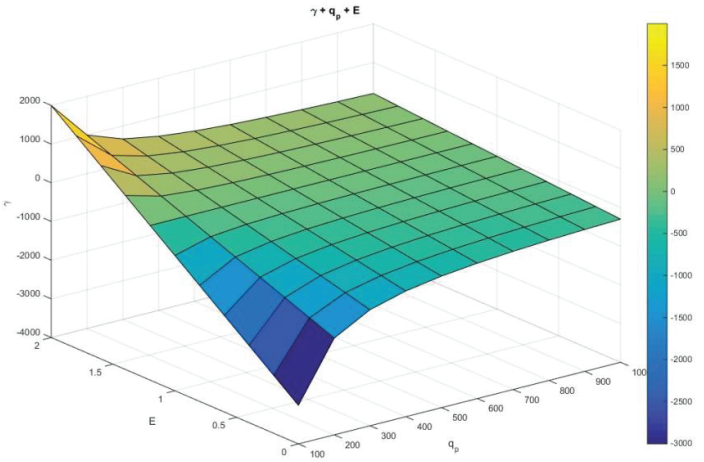

Figure 3.5: Dependence of the flat-plate solar collector's capture factor on the density of the total solar radiation and heat quantity.

As it is seen in the Figure 6 the collector's radiation capture factor complies with exponential regularity, which is dependent on the time. Having used the equation (6) there has been executed the computation, which allows defining the functional dependence of the capture factor on the time, solar radiation and thermal-physical parameters of the collector.

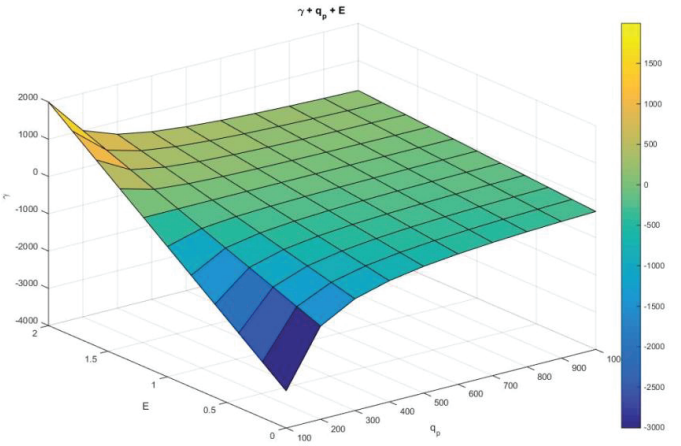

Figure 3.6: Capture factor dependence of the solar radiation on the time.

(**Figure 3.6**) contains the chart of the solar radiation factor dependence on the time, which shows the total solar radiation falling within the total time interval.

Defining the solar installations performance

By technical-economic calculations it is possible to define the capability utilization index of the solar system, if we know the breakdown of radiation frequency at different magnitudes, which plays a significant role upon the solar systems manufacturing.

As the capability utilization index is considered as the ratio of the installation output for the definite time period to the performance for the same time interval upon the installation operation at the gross installed capacity, it is necessary to define the solar installation's capacity for the considered time period. Since the performance G of any solar system in the first place depends on the radiation income and is its function i.e., G =ƒ (S), and radiation income regimes, in turn, are specified by the function of distributing the radiation real values F_1(S), the installation performance within the time T in general case might be represented as follows:

$$G = T\phi(E)f(S)\ F_1(S),dS$$

where ϕ(E) – is the installation performance dependence on the solar radiation microstructure, i.e. the so called working feature;
ƒ(S) - is the probability density of continuous stochastic process of the solar radiation micro structure for the same period of time.

Upon installation's output calculation the dependence integration process is usually replaced by approximate summing:

$$G = \frac{T}{100}[t_1 f_1(S_1) + t_2 f_2(S_2) + \ \dots \ + t_{max} f_{max}(S_{max})]$$

where $S_1, S_2, \dots, S_{max}$ - value of class mark on the chart of daily or hourly radiation sums, $t_1, t_2, \dots, t_{max}$ - radiation occurrences relative times of corresponding intervals (referred to the intervals mid-points).

$T = n m_1$

n - number of days per month,

m_1- installation's actual work average duration per day in hours.

The only argument defining the performance will be the radiation average value E for the given estimated period (for instance, month), which is specified for practical computations in the form of integral curves. Depending on the provision norm there has been calculated the average, the performance computation outcome will correspond to the same norm.

E, cal/sm^2 min	0.55	0.65	0.75	0.85	0.95	1.05	1.61	1.25	1.35	1.45
G_{m^3}	0.50	0.55	0.6	0.65	0.70	0.75	0.80	0.85	0.90	1.0

Table 3.1: Performance dependence on the solar radiation.

90% - monthly average radiation equals to $\overline{E}$ = 0,88 cal/sm^2min.

For the obtained calculated average $\overline{E}$, in compliance with frequency of repeatability the installation performance in our case can be defined as follows:

$$G = \frac{31*13,5}{1000}[0,5*55+0,55*76+0,60*97+0,65*117+0,70*132+0,75*138+0,80*140+0,85*136+0,9*93] = \frac{31*13,5*6,27}{1000} = 262m^2$$

Calculation of monthly performance according to the actual observation data and standard calculation in the Table 1 showed that discrepancies do not exceed 5% with reliability 0,9.

Necessary and sufficient conditions for defining any design solar installations performance by the equation will be:

- Setting the working specifications of the solar installationsG = ϕ(E).
- Setting the calculation standard tables of relative repeatability (frequencies) of the solar radiation different intensity (**Table**). It is convenient to represent those frequencies dependent on a single argument - average $\overline{E}$ for the same period for which the performance is calculated.

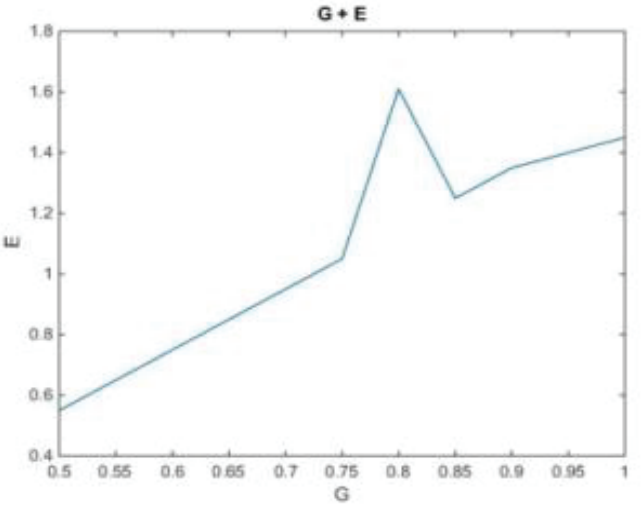

Figure 3.7: Chart of performance dependence on the solar radiation.

- Setting the distribution of the radiation average values $\overline{E}$ in the form of provision curves, $\overline{E}$= ƒ (P).

E	P												
	0,2-0,1	0,2-0,1	0,2-0,3	0,3-0,4	0,4-0,5	0,5-0,6	0,6-0,7	0,7-0,8	0,8-0,3	0,9-1,0	1,0-1,1	1,1-1,2	1,2-1,3
0,80	16,9	23,5	32,0	42,8	56,0	69,2	85,0	100,6	114,0	123,0	122,1	107,3	76,3
0,82	13,8	20,1	28,3	38,9	50,8	67,0	83,6	99,5	115,6	124,8	126,0	113,0	80,5
0,84	11,8	17,6	25,5	35,9	48,8	64,4	80,8	99,1	115,9	128,1	131,1	119,0	85,8
0,86	9,9	15,2	22,6	32,6	44,6	60,4	78,6	98,6	116,9	131,2	136,2	125,3	91,5
0,88	8,2	12,9	19,7	29,3	42,5	55,0	76,0	97,0	117,8	132,2	140,1	130,1	93,6

Table 3.2: Solar radiation frequency relating to Almaty city conditions in July.

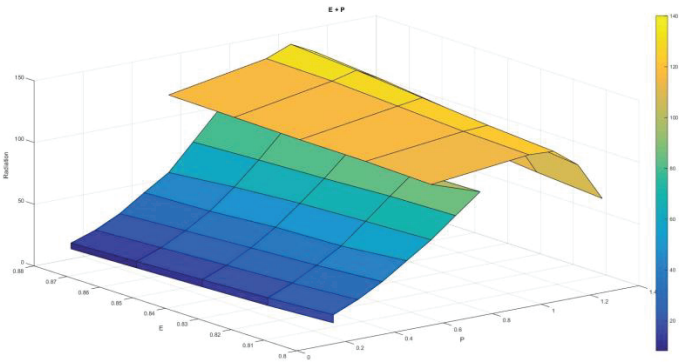

Figure 3.8: Chart of solar radiation dependence on the installation capacity.

The solar installation operation efficiency is assessed according to the capability utilization index, which is defined as the ratio of the installation performance at the radiation mode setting for the time T to the performance for the same time period upon the installation at capacity point.

Hereunder there has been calculated the heat quantity in the single circuit solar system with a thermo siphon circulation. As well, there has been computed the solar radiation capture index and the installation efficiency. Capture factor of radiation by the collector complies with exponential regularity. Solar system operation performance is assessed according to the capability utilization index, which is defined as the ratio of the installation capacity at the designed radiation regime for the time period T to the performance for the same time period at the installation operation with capacity point.

Give reasoning for incident angle of solar error collector

The performance of solar energy conversion systems is determined the amount of solar radiation collector that has reached an inclined surface, which is called the azimuthal angle or angle of inclination reservoir [**31**]. The sloped surface at any time is a global factor of radiation on a horizontal surface and the reflectivity of the earth that determine the amount of solar radiation.

Forty percent of the solar radiation incident on the solar collector is achieved by a tracking system [**32**]. However, the tracking systems are expensive, need energy for their operation, and are not always applicable, especially for small systems. Optimization of the angle of inclination is widely considered [**33-35**]. For the heating season a method for calculating the optimum angle for the collectors in the South was developed.

The design of system for hot water supply it is necessary to know the angle of solar collectors, which are determined by geographical latitude of terrain and operating conditions. Average values on a horizontal surface of solar radiation intensity given in handbooks, whereas the inclined surface there is no such data.

A common recommendation for determining the optimum angle to the horizontal plane commutator oriented in the south direction and used in the summer, is

$$S = \Psi - 15°$$

where Ψ - latitude areas for Almaty 43°.

The angles of inclination of solar collectors is recommended, based on the duration of the solar unit - for the summer $S_{recom.} = \Psi - 15°$, winter $S_{recom.} = \Psi + 15°$, $Syear_{recom.} = \Psi$.

With the use of work [**36**] we calculated the optimum angle for the TC conditions in Almaty [**37**].

Useful absorbed energy of the solar radiation incident on a horizontal surface, is defined as a normal vector component (H) from direct radiation flux vector (H_n).

$$H = H_n \cdot \cos\theta_z$$

where H - Vertical component of total solar radiation.

Normal flow vector of direct solar radiation incident on the inclined surface according to (**Figure 21**) is calculated by the formula:

$$H_T = H_n \cdot \cos\theta_t \quad (3.5)$$

In the reference material [**38**] there are the total value of the intensities, direct diffuse solar energy on a horizontal surface. In fact, the solar collector installed with an inclination angle θ_t, which is selected from the condition of maximum use of the absorbing area.

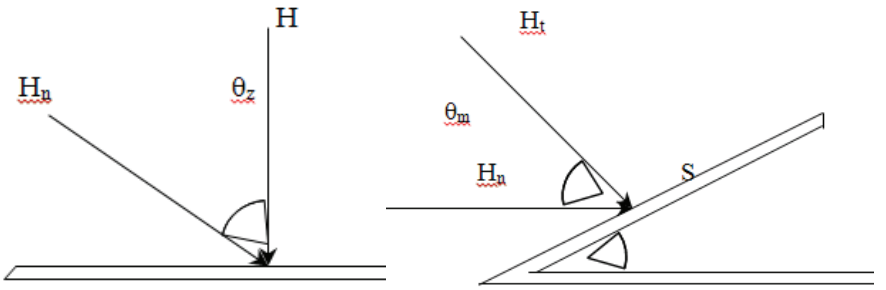

Figure 3.9: Parish radiation onhorizontal theand inclined surfaces.

The angle of the sun changes during the day. In the morning and in the evening it is maximum and minimum at lunchtime.

The ratio of H radiation flux$_t$ incident along the normal to the inclined surface of the corresponding flow on a horizontal surface is expressed through angles $\theta z\ \theta r$: .

$$R_B = \frac{H_t \cdot H_n \cdot \cos\theta_t \cdot \cos\theta_t}{H \cdot H_n \cdot \cos\theta_t \cdot \cos\theta_t}$$

Direct solar radiation incidence angle is defined by the formula:

$$\cos\theta = \sin\delta \cdot \sin\Psi \cdot \cos S - \sin\delta \cdot \cos\Psi \cdot \sin\Psi \cdot \cos\gamma + \cos\delta \cdot \cos\Psi \cdot \cos S \cdot \cos W + \cos\delta \cdot \sin\Psi \cdot \sin S \cdot \cos\gamma \cdot \cos W + \cos\delta \cdot \sin S \cdot \sin\gamma \cdot \sin W \quad (3.6)$$

where $\delta = 23{,}45 \cdot sin360 \cdot \left(284 + \frac{n}{365}\right)$– declination of the sun;

- Ψ - latitude areas.
- S - the angle between the horizontal plane considered and surface the of.

- γ - azimuth angle plane.
- W - hour angle.
- n - ordinal number of the day.

From (5) the formula for calculating the angle of incidence of radiation on the horizontal surface of the collector, i.e. if γ-S = 0. Then:

$$\cos\theta_Z = \sin S \cdot \sin\Psi + \cos\delta \cdot \cos\Psi \cdot \cos W \quad (3.7)$$

for A collector disposed at an angle to the horizon S:

$$\cos\theta_t = \cos\cdot(\Psi - S)\cdot\cos\delta\cdot\cos W + \sin(\Psi - S)\sin\delta \quad (3.8)$$

Substitutin (3.6), (3.7) into (3.8), gives the formula for calculating the correction factor for solar collectors predetermined angles of inclination.

$$R_B = \frac{\cos(\Psi - S)\cdot\cos\delta\cdot\cos W + \sin(\Psi - S)\cdot\sin\delta}{\cos\Psi\cdot\cos\delta\cdot\cos W + \sin\Psi\cdot\sin\delta} \quad (3.9)$$

The results of the calculation of the solar radiation using R_B according to Almaty GMO shows in accordance with Figures 7, 8, 9. The breadth of the area Ψ = 43˚, and the angles of inclination of solar collectors are 55˚, 45˚, 30˚ in the annual cycle.

The optimum angle at which the arrival of daily solar radiation, averaged for all non-heating season is the maximum in April, June, July, August (summer period) - 30˚, i.e. 2˚ above than conventional recommended value. For a transitional period – for March and September 45˚, also 2˚ higher if we take recommended value, as a year-round S = Ψ = 43˚. For winter - February, October, November optimum tilt angle is equal to the solar collector 55˚, i.e. on 3˚ less than conventional recommended (winter S = 58˚ for Almaty).

It is established that during operation of the tubular solar collector of solar energy when heating occurs an elongation of the plastic tube, which determines deviation of the surface pipe from the normal to the panel of the solar radiation on 5˚ lower than the calculated angle collector.

Based on this it is recommended during the operation to take into account this effect and respectively optimum angles in the annual cycle to take from the formula:

$$S = S_p + 5^\circ \quad (3.10)$$

where S_p - calculated angle.

Accordingly the optimum tilt angle to create a plastic solar collector year period at 35 ° i.e. higher than 7 ° $S_{recom.,}$ for March, September 50˚-is also higher than 7 ° $S_{recom,}$ for February, October, November 60 ° at 2 ° greater than S_{recom}.

Flat solar collectors absorb both direct and diffuse component of solar radiation. For use in practical calculations of the data incoming on a horizontal surface a total radiation, it is necessary to calculate a correction coefficient for the scattered.

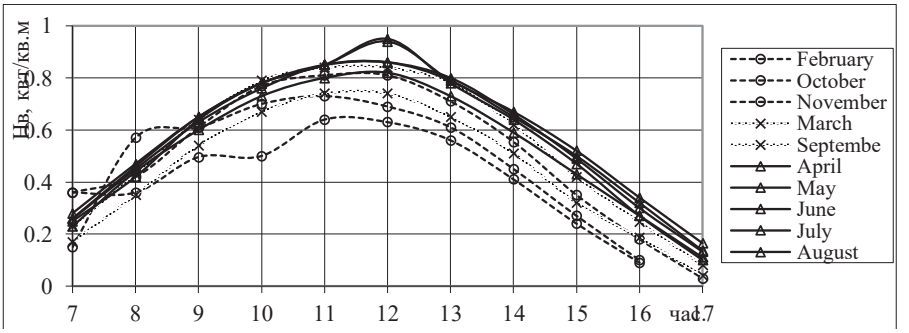

Month	II	III	IV	V	VI	VII	VIII	IX	X	XI
Amount per day, ∑	4,15	4,90	5,75	6,20	6,45	6,08	6,05	5,90	5,60	4,88
Avg. per day, E	0,43	0,44	0,52	0,56	0,49	0,55	0,55	0,53	0,50	0,48

Figure 3.10: Hourly and daily amount of direct solar Radiation on the inclined surface kw / m2.

The calculation of the total radiation on the inclined surface produced by the same method.

$$H_T = H_B \cdot R_B + H_d \cdot R_d$$

where H_B and H_d – direct and diffuse components of solar radiation horizontal surface; R_B - correction factor to direct radiation; R_d - the same for the diffuse component. The scattering of solar radiation can be directed, while $R_d = R_B$, i.e. the angular correction factor coincides with the coefficient for the line.

Hourly and daily amount of direct radiation onto the inclined surface 55 to tilt angles˚, 45˚, 30˚ given in accordance with figure 26. As can be seen, the maximum direct radiation coming have an orientation angle 30˚.

Hourly, daily and monthly amounts of total radiation scattered and are shown in accordance with **Figures 3.11** and **3.12**.

Month	II	III	IV	V	VI	VII	VIII	IX	X	XI
Amount per day, ∑	2,25	2,36	1,84	1,50	1,20	1,30	1,50	1,74	2,30	1,22
Avg. per day, E	0,23	0,21	0,16	0,13	0,10	0,12	0,13	0,16	0,20	0,20

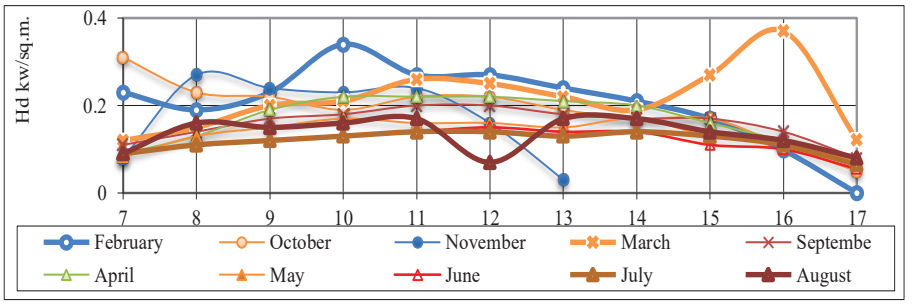

Figure 3.11: Hourly and daily amount scattered of solar radiation on the inclined surface, kW / m 2.

The values of reflectivity of the land surface in Almaty region under the calculation is 9.0... 10.0%, which should be considered in the design of solar installations.

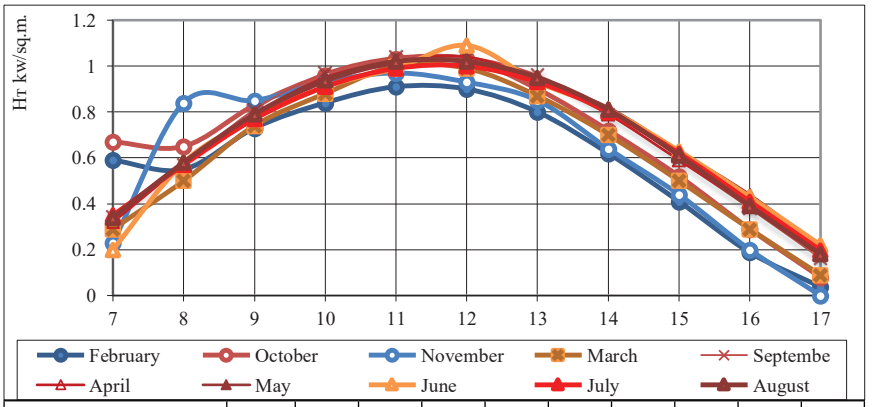

Month	II	III	IV	V	VI	VII	VIII	IX	X	XI
Amount per day, ∑	6,54	6,85	7,59	7,70	7,56	7,54	7,63	7,65	7,68	6,88
Avg. per day, E	0,59	0,62	0,69	0,70	0,68	0,68	0,69	0,69	0,69	0,68

Figure 3.12: Hourly and daily amount of total solar radiation on the inclined surface kW / m2.

The optimum angle at which the arrival of daily solar radiation, averaged for all non-heating season, the maximum is in April, June, July, August (summer) - 30˚, i.e. 2˚ above of conventional recommended value. For a transitional period - March to September 45˚, also 2˚ higher if we take the recommended, as a year-round S = Ψ = 43˚. For winter - February, October, November optimum tilt angle is equal to the solar collector 55˚, i.e. on 3˚ less than conventional recommended (winter S = 58˚ for Almaty).

Determination of heat loss coefficient and coolant temperature in a flat solar collector

The flat plate of the solar collector is the main component of solar heating and heating systems. The energy equation is not taken into account for analyzing the efficiency of solar collectors, so this is not a sufficient criterion for the efficiency of a solar collector [**39**]. It is necessary to optimize the design of the solar system and work. In papers [**40-42**], the efficiency and entropy of solar collectors were considered. Bejan et al. Found that solar collector systems depend on the irreversibility of heat transfer [**43**].

The heat recovery coefficient from the collector Fr is determined by the useful energy obtained from the useful energy at which the temperature of the entire is equal to the temperature of the transferring agent.

$$F_R = \frac{GC(T_{inlet} - T_{outlet})}{SU_L(T_{outlet} - T)}$$

where: G - heat flow in a single collector area:

or:

$$F_R = \frac{GC}{U_L}\left[1 - \frac{SU_L - (T_{inlet} - T_{outlet})}{SU_L - S(T_{inle}t - T)}\right] = \frac{GC}{U_L}(1 - e^{-U_L F^1 GC_P})$$

To bring this equation to the graph (**Figure 3.13**), we introduce the coefficient of solar-collector flux (**Table 3.3**):

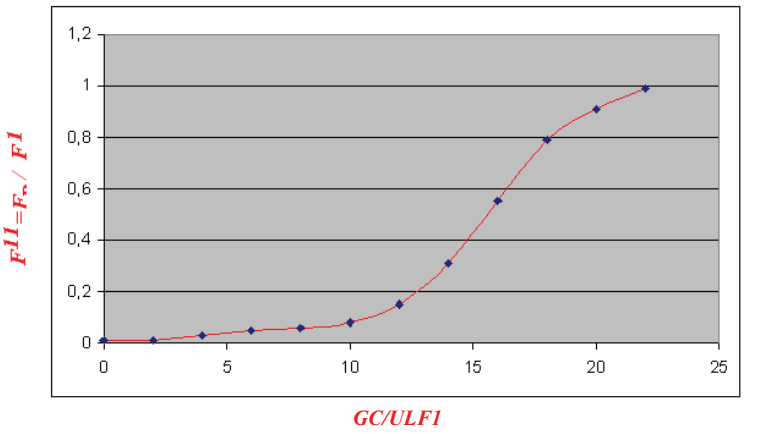

Figure 3.13: Graph of flow coefficient versus flow and spacing of the solar collector.

$\frac{GC}{U_L F^1}$	$F^{11} = \frac{F_R}{F^1}$	$\frac{GC}{U_L F^1}$	$F^{11} = \frac{F_R}{F^1}$
2	0,97	12	0,66
4	0,96	14	0,54
6	0,87	16	0,51
8	0,8	18	0,38
10	0,74	20	0,33

Table 3.3: Heat loss coefficient of a flat solar collector.

It is also possible to find the optimal pipe length of a flat solar collector (**Figure 3.14**), by combining the solar collector flow coefficient and the dependence of the interconnecting pipelines and the efficiency of the connection of the connector and the pipe with one graph.

It is also possible to find the optimal pipe length of a flat solar collector (**Figure 3.14**), by combining the solar collector flow coefficient and the dependence of the interconnecting pipelines and the efficiency of the connection of the connector and the pipe with one graph.

Determination of the temperature of the coolant. The heat generated by the solar collector is transferred to the coolant in the heat transfer pipeline. In the technical calculation of the efficiency and effectiveness of existing drives, it is currently not possible to ignore the temperature gradient along the perimeter of the pipe transported by the coolant.

Consider the movement of the coolant inside the pipe t1 and t2 (t1 ≠ t2) of the walls of the panels (absorber) of the solar collector walls absorbed in (**Figure 3.15**).

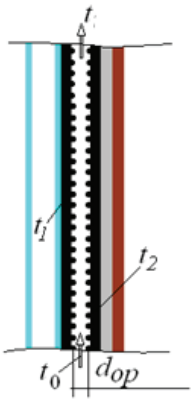

Figure 3.15: Section of the drain pipe.

Consider the width of the wall under consideration (average pipe diameter) δ, height h. Temperature inlet pipe temperature t_0. If we consider the radial direction of a moving transport agent moving away from the pipeline, as close to zero, then the energy distribution equation for the tube in question will be as follows.

$$u\frac{\mathrm{dt}}{\mathrm{dx}} = a\frac{d^2t}{\mathrm{dy}^2} \tag{3.11}$$

(3.11) boundary conditions for solving the problem:

x>0	y>0	t= t_1
x<0	y<0	t= t_2
	x=0	t=t_0

(3.12)

(3.11) equation (3.12) in general form when setting the limits:

$$T(x,y) = t_1 + \frac{y}{\delta}(t_2 - t_1) + \frac{4}{\pi}\left[t_0 - \frac{y}{\delta}(t_2 - t_1)\right] \cdot \sum_{n=1}^{\infty} \frac{(-1)^{n+1}\exp\left[-\left(\frac{2n-1}{2}\right)^2 \frac{4ax\pi^2}{U_{op}\delta^2}\right]}{2n-1} \cdot \sin(2n-1)\pi\frac{y}{\delta}$$

Where:

a is the temperature coefficient.

- Average speed of the heat carrier on the heat transfer pipeline.

The temperature of the heat transfer pipe is determined by the temperature of the transport agent (t) and the average temperature of the coolant in the pipe:

$$t_{losses} = \frac{1}{\delta}\int_0^{\delta} t(h,y)\mathrm{dy} \approx \frac{t_1+t_2}{2} + \frac{8}{\pi}\cdot\left(t_0 - \frac{t_1+t_2}{2}\right)\cdot\exp\cdot\left(-\frac{\pi^2 ah}{U_{cp}\delta^2}\right),$$

$$\bar{t}_f \approx \frac{t1+t2}{2} + \frac{8}{\pi^4}\frac{U_{cp}\delta^2}{ah}\cdot\left(t_o - \frac{t_1+t_2}{2}\right)\cdot\left[0.99 - \exp\cdot\left(-\frac{\pi^2 ah}{U_{aver}\delta^2}\right)\right]$$

When determining the temperature of the coolant in the heat transfer pipe, you can get half the temperature of the wall at different temperatures.

$$t_{losses} = t - \frac{8}{\pi^2}\cdot(t - t_0)\cdot\exp\cdot\left(-\frac{\pi^2 ah}{U_{cp}\delta^2}\right) \tag{3.13}$$

$$\bar{t}_f = t - \frac{8}{\pi^4}\frac{U_{cp}\delta^2}{ah}\cdot(t - t_0)\cdot\left[0.99 - \exp\cdot\left(-\frac{\pi^2 ah}{U_{cp}\delta^2}\right)\right] \tag{3.14}$$

here: $t = \frac{(t_1+t_2)}{2}$

The cost of the coolant is 55 kg / hour. The average speed of the coolant in the heat transfer pipeline:

$$U_{pipeline}=3600\cdot\frac{4G}{\rho\pi d^2} = 0{,}0017943;\ м/sec$$

Determining the temperature of the coolant in the flat collector of the coolant (absorber) on the basis of the equations of energy distribution (3.13) and (3.14). The heat conductor is made of thin-walled stainless steel with a width of 1 m and a height of 2 m, an average diameter of 0.015 m. The surface of the heat transfer pipeline is heated by the action of bitumen, which is exposed to sunlight. Lower lateral temperature 3-5° C below the surface.

Investigation of the thermosiphon circulation and finding the thermosiphon flow

Hot water production is one of the most interesting applications in solar energy and the demand for hot water is increasing significantly, especially in the residential sector. Components of solar hot water systems are solar collectors and a heat storage tank. The storage tank plays an important role in the solar energy system by storing when it is available and delivering heat when needed. The operation of solar heating systems is highly dependent on thermal stratification.

Since the 1970s, stratification in the reservoir has been intensively studied [**44-46**], and low consumption was thermally stratified and showed that storage tanks deliver 17% more solar energy [**47-51**]. The authors noted that thermal stratification has the advantage that the solar system heats the water. Cristofari et al. [**52**] found that with a high degree of stratification, energy conservation is higher (5.25% per year of use) than a fully mixed reservoir. However, a hotter tank, the degree of thermal stratification of which is determined by temperature, as the temperature difference between the upper and lower parts of the tank, is designed to meet energy demand and is very important for the efficient operation of solar panels of energy systems. The performance of thermal storage is influenced by many parameters as reservoir geometry [**53-56**], reservoir volume and reservoir area [**57-60**], therefore, many solutions have been proposed and a number of models developed. Among the most popular models are one-dimensional models [**51,61**], which provide good estimates of the temperature distribution in the tank. When working with thermal stratification, the primary and essential element that affects system performance is mass flow from a hot source (solar collectors) or / and load. For direct coupled systems (SDHW -Solar Domestic Hot Water), it is known that the mass flow entering the storage tank is the same flow outlet from the collector.

The efficiency of the siphon solar collector is influenced by a number of factors, such as the intensity of solar radiation, ambient temperature, the geometric parameters of the solar siphon collector, the thermophysical parameters of the absorber and the coolant, the material of the elements, as well as other factors affecting the final temperature and system operation . Also the flow time $\tau = f(d, H, G_0)$, pipeline geometry $\hat{a} = f(d, d, R)$, fluid temperature in the solar collector $t = f(F, I, V, \rho, m)$ and the temperature of the liquid in the tank - battery $t_{áà} = f(d, h, V)$.

In order for the solar collector with siphon to work with maximum efficiency, it is necessary to ensure a certain ratio of the geometric parameters of the siphon, the metering tank with the geometric parameters of the collector, and also to establish a rational outflow of the coolant from the SC.

Let us determine the influence of the geometric parameters of the siphon on the time of filling and outflow of fluid through the siphon.

To solve the problem, we consider the computational model shown in **(Figure. 3.16)**.

Baseline estimates of the adopted model:

H - liquid head, m; h is the length of the pipeline before the start of the knee (siphon height), m; d - diameter of siphon, m; Fosn - the area of the base of the metering tank, m2; v - fluid velocity, m / s; V - dispenser tank capacity, m^3; G - fluid flow in the dosing tank, m^3/s.

1 - siphon tank dispenser; 2 - tank dispenser; 3 - pipeline with valve for cold water.

The volume of fluid in the dosing tank can be calculated as:

$$V = F \cdot H$$

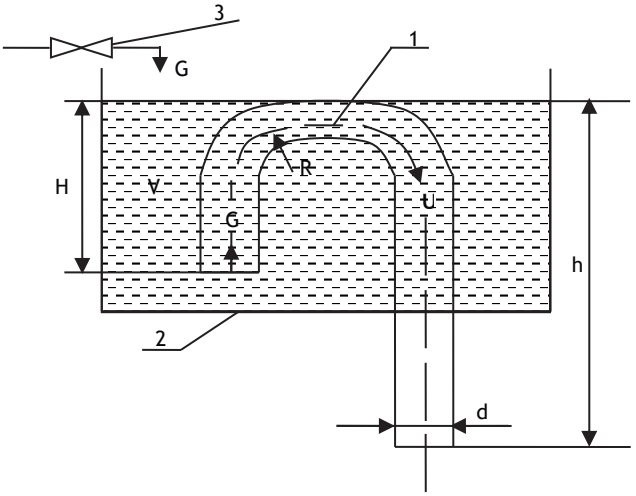

Figure 3.16: Calculated physical model of the dispenser tank with siphon.

where F – base area of the metering tank, m^2, H – liquid head, m. At the same time filling the tank τ_1 is defined as follows: $\tau_1 = \frac{V}{G}$, where V – volume of fluid in the dosing tank, m^3; G – fluid flow, m^3/s.

Determine the flow time of the coolant through the siphon, which in general is a function of the head H, the diameter of the pipeline d, and the flow through the siphon G_0

$$\tau_2 = f(d, H, G_0)$$

In general, the time the fluid flows through a siphon can be defined as:

$$\tau = \frac{V}{G_0},$$

where G_0 is the flow rate through the siphon, $ì^3/ñ$.

In turn, the flow rate can be represented as (as follows):

$$G_0 = \vartheta \cdot f,$$

where ϑ - fluid velocity, $ì/c$; f - cross sectional area, M^2.

Calculate the cross-sectional area of the siphon f as:

$$f = \frac{\pi \cdot d^2}{4},$$

where d - pipe diameter, m. And the magnitude of the velocity of the fluid ϑ we determine from the condition of free flow of water from the vessel. Then:

$$\vartheta = \sqrt{2g \cdot H},$$

where g - acceleration of gravity, $ì/ñ^2$; H – head, m. Taking into account (6), (5) and (4) expression (3) takes the form:

$$\tau_2 = \frac{F \cdot H}{\sqrt{2g \cdot H}\, \pi d^2 / 4}.$$

As is known, when a fluid flows through a siphon, a pressure loss occurs, which is a sum of friction losses. h_{mp} in the pipeline and losses due to local resistance h_k (knee loss):

$$H_{ïîò} = h_{ò} + h_k,$$

where h_{mp} - pipe length loss; h_k - knee loss. Head losses due to friction of round pipes are determined by the well-known Darcy-Weisbach formula / 1 /:

$$h_{òð} = \lambda \frac{\ell}{d} \frac{\vartheta^2}{2g},$$

where ℓ - the length of the pipeline, in our case, it is respectively equal to $\ell = H + h$; λ - coefficient of hydraulic friction in turbulent fluid flow;

$$\lambda = 0{,}11 \cdot \left(\frac{K_y}{d} + \frac{68}{R_i} \right) \cdot 0{,}25 ;$$

$R_0 = \frac{\vartheta \cdot d}{\nu}$ - Reynolds number for round tubes; $\nu = 1 \cdot 10^{-6}\ M^3 / c$ - kinematic viscosity of water.

Loss of pressure in the knee are due to changes in the direction of fluid flow and are determined by the formula:

$$h_k = \xi \cdot \frac{\vartheta^2}{2g},$$

where ξ - dimensionless coefficient of local resistance. When turning the pipe 900, it is determined by the Altshul formula / 2 /:

$$\xi_{90^0} = \left[0{,}2 + 0{,}001(100 \mathrm{x} \lambda)^8 \right] \times \sqrt{\mathrm{d}/\mathrm{R}} ,$$

$R = \frac{d}{4}$ - hydraulic radius for round pipes. When turning at any angle takes the form:

$$\xi = \xi_{90^0} \times a ,$$

where $\grave{a}$ - coefficient depending on the angle of rotation, a=1,33/104,105/

When a fluid flows through a siphon, the movement of the fluid is unsteady. In this case, the head H changes over time, therefore, the flow rate also changes G.

Consider the expiration process: at some point in time the liquid level is at a height h. For an infinitely small period of time $d\tau$, the level will change to a small amount *dh*. During $d\tau$ fluid movement can be considered steady. Then during the time $d\tau$ a volume of liquid flows out of the siphon:

$$dV = Gd\tau \quad \text{or} \quad dV = d\sqrt{2ghd\tau} ,$$

on the other hand

$$dV = Fdh .$$

Equating the right sides of the obtained equations, we get:

$$Fdh = d\sqrt{2ghd\tau} ,$$

or

$$d\tau = \frac{Fdh}{d\sqrt{2gh}} .$$

The outflow time of a fluid from the level H_1 to the level H_2 is the integral from $h = H_1$ before $h = H_2$

$$\tau = \int_{I_1}^{I_2} \frac{Fdh}{d\sqrt{2gh}} \text{ or}$$

$$\tau = \frac{2F}{d\sqrt{2g(I_1 - I_2)}} \cdot (I_1 - I_2).$$

At the time when the liquid level reaches the lower edge of the suction side of the siphon $\acute{I}_2 = 0$, full expiration time is determined by the formula:

$$\tau = \frac{2FI}{d\sqrt{2gI_1}} \cdot$$

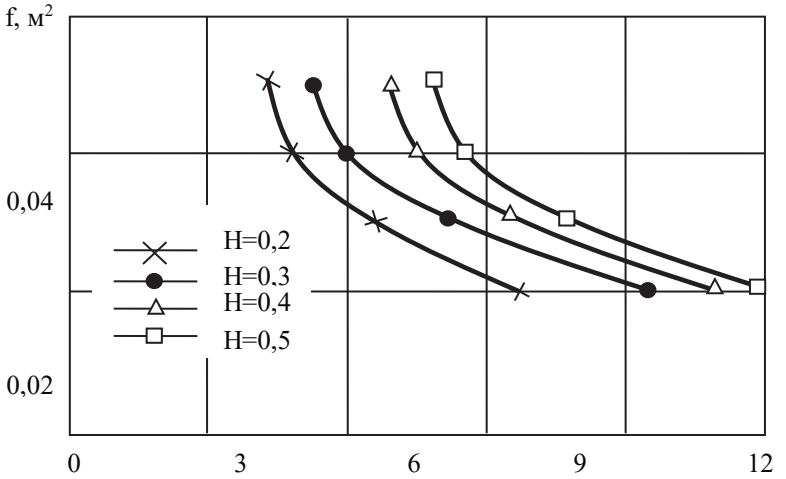

Figure 3.17: Dependence of the cross-section of the pipe on the time of fluid flow at various values of pressure.

The dependences obtained allow us to trace the relationship between the flow time through a siphon, depending on the size of the siphon head H and its geometrical parameter (cross-sectional area of the siphon). (**Figure 3.17**) presents diagrams of these dependences, where it is shown that the intensive drop in the time of expiration is the greater, the larger the cross section of the siphon pipe. You can also see that with increasing siphon pressure, the flow

time increases. This can be explained by the fact that as the pressure increases, the hydraulic resistance (friction and local resistance) of the siphon increases, which leads to a decrease in the velocity of the fluid.

Chapter 4

Scientific Research And Experimental Design Works on the Selection of A Constructive Model and Development of Calculation Methodology

Authors
Amirgaliyev Y.N, Kunelbayev M, Kalizhanova A.U, Kozbakova A. Kh, Daulbayev S.M, Auelbekov O. A, Kataev N.S, Yedilkhan D, Merembayev T, Ormanov T. A, Sundetov T.

*__Corresponding author:__ Ministry of Education and Science of the Republic of Kazakhstan Committee of Science Republican State Enterprise Institute of Information and Computational Technologies, E-mail: murat7508@yandex.kz

Experimental Testing of a Solar Heating System Based on Flat Solar Collectors

Every day the resources of traditional sources of energy are depleted. To balance global energy resources, we need the development of renewable energy technologies that are important for the future. For the generation of hot air for many years, the tube has been used to heat water. Evacuated pipes made of glass composition have widespread use and popularity in the world because they have better performance.

Studies show that significant efforts have been made in the field of tubular solar collectors. In [**62**], an empirical relation was calculated to find the total heat loss coefficient of a tubular collector. On the basis of the vacuum tube of a solar collector, thermal characteristics have been investigated [**63**].

In the glass tubes, water was found in the glass concept using the method of heat extraction and developed evacuated tube collectors [**64**]. Experiments on vertical tubular collectors were carried out and described in [**65**]. The collector had a tubular absorber and can use solar radiation from all directions. It was found that the results of the calculations have a high degree of similarity between the measured and calculated results of the model. The thermal performance of the evacuated solar collector was compared with the thermal performance of the flat plate of the solar collector with optimal inclination and orientation. Characteristics of solar water heaters in glass and an estimate of the rate of circulation in asymmetric pipes are given in [**66**].

Experimental Tests of Solar Systems and Technical Characteristics of the Solar Collector

The purpose of the current experiment is to determine the temperature of the coolant in the heat sink channel of the tubular heat sink. The experimental setup is set at latitude of the terrain Ψ =43˚, and the angles of inclination of the solar collectors are 55˚, 45˚, 30˚ in the annual cycle of Kazakhstan, Almaty.

The solar-electric installation consists of a storage tank, a solar collector, an electric heater, and a support frame. The storage tank has a thermally insulated cylindrical case with a branch pipe for intake of hot water and heat-insulated branch pipes and for connecting solar collectors. On the cover of the tank there is a nozzle for air release when filling the system.

Between the body of the tank and the casing laid insulation. At the bottom of the tank mounted rack for attachment to the support. An electric heater (heater) is installed at the bottom of the tank. The solar collector consists of a register of black polyethylene pipes with cellular insulation, tied up at the bottom with hydraulic collectors, and the length of the pipes is at least 2.5 meters. A specific feature of the collector is that the end pipes are made of metal, which make it possible to adjust the tension of the register of thin-walled pipes, thereby giving rigidity to the tubular solar collector in the plane of absorption of solar radiation and exclude the “body assembly”.

To carry out tests on the helio site, the GU-500 was installed with tubular solar collectors. The tests were carried out in the following mode: the storage tank (BA) was filled with water at 9 hours, through the float system, i.e. filling is done automatically. There is no water from the storage tank during the day. At the end of the working day - 17h. all the water from the BA is drained.

To determine the technical and operational characteristics of the installation, the readings of the temperature sensors were recorded. Chromel-Copel thermocouples were used as temperature sensors, with which the temperature was measured at 6 installation points. The registration of thermocouple readings was performed by a KSP-4 recorder. In parallel with thermocouples, mercury thermometers were installed at a number of points for control measurements.

In the course of the experiments, the following quantities were continuously recorded:

- Flux density of total solar radiation on the surface of the collector E.
- Outdoor air temperature t_3.
- Wind speed in undisturbed flow v.
- Temperature of cold tap water t_3.
- Water temperature at the inlet and outlet from the system of solar collectors t_1, t_2.
- Water temperature in BA in three sections along the height of the tank at a distance of 0.1, 0.3 and 0.4 m from the bottom t_5, t_6, t_7.
- Water temperature given to the consumer t_8.
- Water flow in the circulation circuit G.

All the above-mentioned parameters were measured every hour during daylight, starting at 9 am The measurement results were used to determine the mean values of the total solar radiation flux at the collector surface $\bar{E}$, outside air temperature $\bar{t_3}$, wind speed $\bar{v}$, and inlet water temperatures $\bar{t_1}$ and output $\bar{t_2}$ from the collector system. These values were found by planning the areas bounded by the x (τ) curves, where x is any of the above values in the time range of the experiment. Next, the heat output of the solar installation was calculated:

$$Q = G * c1 * (t2 - t1) * \tau + \Delta Q1$$

where τ- experience time; ΔQ1- the heat accumulated in the circuit by the end of the experiment, which, as a rule, did not exceed 0,05 and η - daily efficiency of her work.

$$\eta = \frac{Q}{\sum E \cdot \sum S}$$

where ΣE=$\bar{E}$τ- the total amount of total solar radiation falling during τ per 1m^2 of the area of the solar collector and ΣS - is the total area of the heat-receiving surface of the solar collectors. The test results for the GU-500 with a tubular solar collector are shown in Table 4.1. The average values of meteorological parameters were in experiments $\bar{E}$=375-888 W / m^2; $\bar{t_3}$=14-20°C; $\bar{v}$=1,0-4,5 m/s, and the flow rate of the water in the circulation circuit varied within 73,1-157,5 kg/h. The result is a wide range of efficiency values from 0.2 to 0.64. The results of experiments with consumption G=2-3 kg/s approximated by linear dependence.

$$\eta=0,782–11,3(\Delta\ \bar{t}/\ \bar{E})$$

These experimental data of the tubular solar collector and the numerical deviations cannot be explained by the experimental error. It can be shown that when calculating a parameter $\Delta \bar{t} / \bar{E}$ directly on the water temperature at the outlet of the collector all experimental points, including the corresponding flow rates G = 2-3 kg / s, practically lie on one straight line.

date	Heating time		Expenditure	Solar Radiation Intensity	Air temperature	Inlet temperature to collector	Temperature output	The temperature in the booming	The temperature in the tank is final	Heat output	Installation efficiency	Specific heat output	Heat output
	initial	final											
	$\tau_{н}$	$_{к}$	G	$\bar{E}$	$\bar{t}_0$	$\bar{t}_1$	$\bar{t}_2$	t_3	t_4	Q	η	$Q_{ul.}$	
	h, min		kg/h.	W/m^2	°C	°C	°C	°C	°C	W/h.	%	W h./ m^2	
22.07.18	11:30	16:30	121,5	827	27,3	23,6	34,1	16	36	7400	0,59	493	525150
23.07.18	11:50	17:50	157,5	888	27,5	25	31,7	18	38	7400	0,46	411	300
24.07.18	10:05	16:05	120,9	822	26,4	25	33,3	18	37	7030	0,47	390	
27.07.18	11:05	17:45	135	833	25,8	25,4	34,1	17	41	8880	0,54	455	150
28.07.18	11:30	16:30	130,7	883	25,6	27,4	37,1	19	39	7400	0,55	493	150
30.07.18	9:55	16:55	109	880	26,6	31,9	41,5	18	50	8537	0,46	406	
22.08.18	9:25	16:25	47,9	868	24,3	26,7	39	17	47	5324	0,29	253	
23.07.18	9:10	17:10	91,3	809	24,4	33,9	41,8	16,5	54	7090	0,36	295	170
26.08.18	9:30	14:30	110,7	665	25,6	21,4	28,1	16	29	4343	0,43	289	
27.08.18	10:15	17:15	110,3	920	25,9	35,4	42,2	27	48	6090	0,325	290	
14.09.18	9:30	16:30	73,1	916	26,4	30,7	40,5	20	49	5820	0,49	277	
16.09.18	14:45	17:10	97,9	824	27,4	48,1	53	44,5	53	6221	0,314	254	
7.09.18.	9:45	16:45	76,4	517	26	30,1	43,8	22	45	8510	0,48	405	145

Table 4.1: Solar test results with a tubular collector.

Results of a change in water temperature in a flat heliocollector with different volumes of water

(**Figures 4.1-4.3**) show the results of a change in water temperature with different volumes of water. The most optimal is the volume of the tank 70-100 liters per square meter. With increasing volume, the temperature of the water in the tank decreases, so for 250l-55-57°C, 300l-50-53°C, 400l-46-48°C, 500l-45-47°C.

According to known data, at a latitude of less than 54°, 90% of simple single-circuit solar power plants without a doubler with a natural circulation circuit for hot water supply of seasonal heat consumers are used.

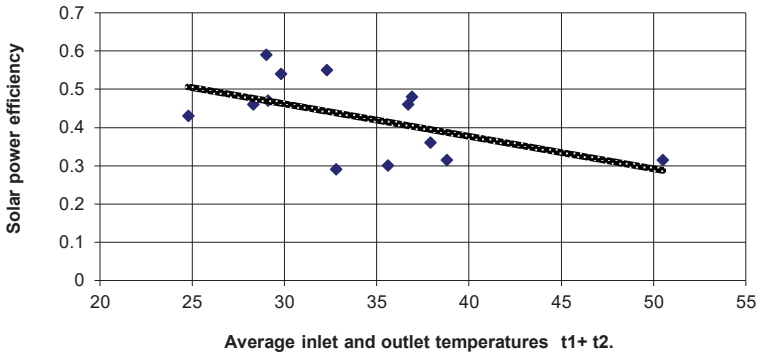

Figure 4.1: The dependence of the efficiency of the solar system from the average temperature at the entrance and exit of the flat collector.

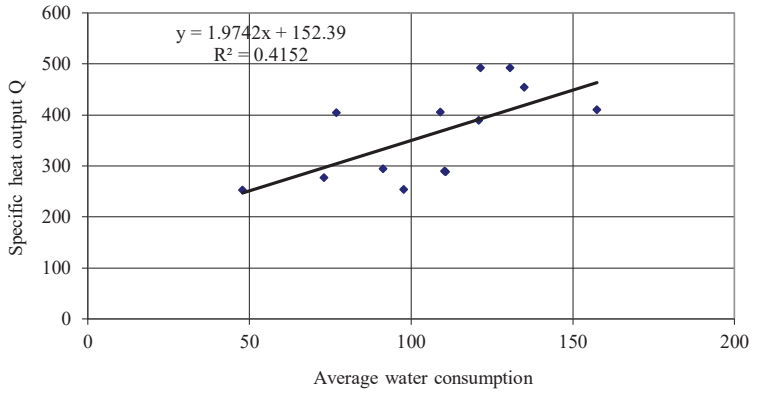

Figure 4.2: Dependences of specific heat output from water consumption in GU-500.

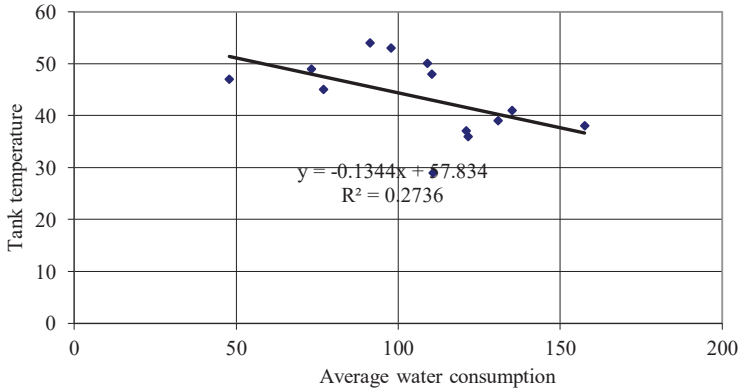

Figure 4.3: Dependence of the temperature of heating water in the tank from the flow of water in the solar circuit.

As an example, (**Figure 4.1** and **4.2**) show the results of the test setup. During the experiment (from 9.00 to 17.00) 0.5 m^3 of water with a temperature of about 50° C was released to the consumer. The distribution of water temperature along the height of the storage tank was revealed. These data well illustrate the degree of stratification of water in the tank. The temperature difference in the upper and lower layers was at noon 10-15° C. The high level of heat losses is due to the fact that the total length of the connecting pipelines of the solar collector system is about 5m and poor insulation, i.e. instead of polyurethane insulation used foam insulation.

Processes of manufacturing different types of solar collectors

The solar collector frame is made of an alloy of profile aluminum with polymer painting. The glass is glued to the frame with a special silicone on the inside, thereby ensuring complete tightness of the collector. Tempered glass is selected to ensure rigidity and safety (**Figure 4.8**).

Figure 4.8 Solar collector frame.

The solar collector absorber is made of 1 mm thick copper sheet. Copper tube with a wavelength of 50 mm and sealed on a copper sheet. The sheet itself is painted with a matt black polymer paint with a thickness of 200 microns (**Figure 4.9**).

a) Absorber solar collector b) General view of the solar collector

Figure 4.9: Solar Collector.

The heat insulating layer is realized from two components (**Figure 4.10**). a) Polyethylene foam with reflective mirror foil 5mm thick. b) Penoplex with a thickness of 30 mm.

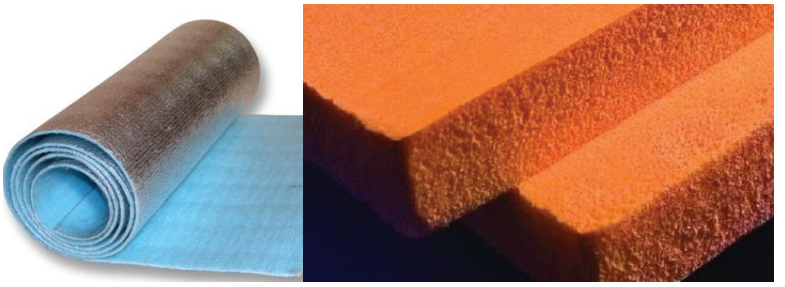

a) Penofol b) Penoplex

Figure 4.10: Thermal Insulation Components0.

(**Figure 4.11**) shows the design of the solar collector using the full area of the absorbent surface. The design differs in that it lacks a serpentine-shaped tube, which must be welded onto an absorbent copper sheet. The back wall is made of sheet steel 1 mm thick and painted with polymer coating. The wall is glued to the case of the solar collector using silicone and self-tapping screws, which ensure complete tightness.

a) Rear view b) Front view

Figure 4.11: The design of the solar collector, using the full area of the absorbent surface.

The storage tank is made of 1 mm thick copper sheet with a diameter of 210 mm and a height of 320 mm (**Figure 4.12**). Inside the cylinder there is a spiral heat exchanger made of copper pipe with a diameter of 9.5 mm and a total length of 9 meters. The diameter of the spiral is 100 mm and the height is 270 mm, which in turn, the heat exchanger from the spiral is connected to the solar collector. The storage tank is thermally insulated with polyethylene foam and

has two pipes designed to connect water. The battery case is sheathed with a 400 micron galvanized steel sheet.

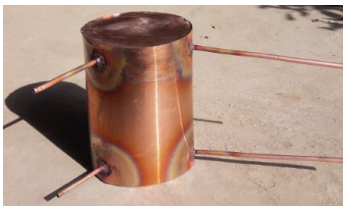

a) View of the completed battery tank

b) Inside view of the tank

c) Type of sheathed insulation

Figure 4.12: Tank battery.

(**Figure 4.13**) shows a general view of a solar collector with an area of 2 meters square, having four strips of heat pipes made of copper. The water distribution of this solar collector is 3.8 liters. The advantage of this design is the separation of the working fluid into four lanes. This design provides rapid warm-up and increase the efficiency of the solar collector.

Figure 4.13: General view of the solar collector.

(**Figure 4.14**) shows the current laboratory sample. A copper sheet with a size of 600x420 mm and a thickness of 1 mm is used as an absorber. The surface of the absorber is covered with a copper oxide layer obtained by chemical processing. The thickness of this layer is 80 microns. The absorption coefficient of solar radiation of this layer is 90-95%. The reflection coefficient is 5-7%, respectively.

Figure 4.14: Valid laboratory sample.

Thus, the conducted studies confirm the viability of the proposed solar hot water installation using a siphon collector.

For the first time, a relationship has been established that determines the expiration time depending on the geometric parameters of the solar collector. In general, as we observe from the calculations proposed by us, the developed method allowed to establish that local hydraulic resistance and friction exert a significant value on the coolant flow.

Chapter 5

Models and Methods for Calculating the Efficiency of a Solar Collector with a Thermosiphonic Circulation

Authors
Amirgaliyev Y.N, Kunelbayev M, Kalizhanova A.U, Kozbakova A. Kh, Daulbayev S.M, Auelbekov O. A, Kataev N.S, Yedilkhan D, Merembayev T, Ormanov T. A, Sundetov T.

*__Corresponding author:__ Ministry of Education and Science of the Republic of Kazakhstan Committee of Science Republican State Enterprise Institute of Information and Computational Technologies, E-mail: murat7508@yandex.kz

This section discusses the graphoanalytic method for determining the energy and optical characteristics of a flat solar collector. The total solar radiation on the inclined surface of flat solar collectors was calculated. In the research methodology, the city of Astana was taken as an example of calculating the total total solar radiation. According to experimental data, it can be seen that the duration of solar radiation falls in the summer. Thus, the distribution of the direct solar radiation flux density, the optical efficiency of the direct solar radiation flux density, and the total flux to the receiver were calculated by the graphic-analytical method. Optical efficiency was 66%. This suggests that the parameters of the solar collector are correctly selected.

Studies were carried out on the development and application of the F-diagram method for a dual-circuit solar system with thermosiphon circulation. The f-chart method is based on the correlations of a large number of simulations calculated on dimensionless variables. The simulation conditions varied in the corresponding ranges of the parameters of the practical designs of the dual-circuit solar system with thermosiphon circulation. Using the F-chart method, monthly values of the ambient temperature with a correction coefficient were calculated, which show that the degree of heating of the monthly average daily temperature and direct solar radiation, which varies depending on weather conditions [**65**].

An exergy analysis of a double-circuit flat solar collector with thermosiphon circulation has been done. The project presents a mathematical model of the exergy analysis of flat solar collectors, as well as the effects of ambient temperature, solar radiation, inlet fluid temperature and fluid flow rate, exergy rates and energy loss rates. The estimated optimum fluid inlet temperature is 70° C and the maximum usable exergy rate is 250W. The exergy efficiency is 4%, and the largest exergy loss is the difference between the surface of the absorber plate and the sun, which is 52.86% of the total exergy rate. [**66**].

A technique is presented for calculating the generation of entropy and studying the thermal characteristics for a thermosiphon flat collector. Heat losses in flat solar collectors are calculated using the upper heat loss coefficient. The paper discusses a methodology based on the 2nd law of thermodynamics, which provides an accurate way of estimating heat losses in flat solar collectors. The generation of entropy in the collector is associated mainly with heat conduction and convection modes. Heat collector losses occur mainly due to these heat transfer modes. The amount of heat transferred by radiation to the inner surface of the solar collector glass was also calculated [**67**].

Graph-Analytical Method for Determining the Energy and Optical Characteristics of a Flat Solar Collector

The scale of the man-made impact on the environment and the steady demand for energy underlines the urgent transition to renewable energy sources. The market for solar thermal collectors is 8 times larger than two decades ago, since the solar collector is more efficient than the photovoltaic system for generating heat [**68**]. In addition, cheaper storage, comparable to batteries, has made solar thermal collectors a better choice for heat production than Photovoltaic. Solar thermal collectors are usually divided into three categories based on coolant temperature (HTF). a low-temperature solar collector (less than 100° C) includes a flat plate and evacuated tubular collectors (ETC), which are capable of providing hot water and air for residential premises, a high-temperature collector (more than 300° C) [**67,68**]. Such as linear Fresnel collectors and parabolic troughs are mainly designed to provide steam for steam

generators [**69**]. Finally, the less studied category is a medium temperature reservoir (100-300° C) with a wide range of applications, for example, desalination [**70**], mining, vaporization [**71**] and zero liquid [**72**].

Various approaches to optical analysis have been carried out by various researchers. Jose analyzed the distribution of the flow in the focal spot of the solar furnace taking into account the effect of darkening along the edge of the Sun [**73**]. Evans used the integral dependence to determine the intensity distribution for both flat absorbers and cylindrical parabolic concentrators under ideal conditions with the assumption of a solar disk [**74**]. Dali used the back-ray tracking procedure to find the flux distribution over the solar concentrator [**75**]. Nicolas performed a two-dimensional analysis of the flow distribution on parabolic collectors and included the influence of the angle of incidence on the flow distribution for flat surfaces [**76**]. Jeter analyzed the intensity distribution around circular receivers using a semi-infinite formula, treating the sun as a point source. The effect of declination on flow distribution has also been investigated. Jeter developed a semi-infinite model for calculating the flow distribution by considering the effects of a glass tube by incorporating the transmission and absorption functions [**77**]. Kaushika developed the basic analytical models of optics for paraboloid concentrators and analyzed the operation of experimental concentrators [**78**]. Kalogiro used artificial neural networks to determine the flow distribution in a cylindrical absorber for different angles of incidence of solar energy [**79**]. Gombert et al. worked on surface surfaces with a long-wavelength anti-reflective coating and reported an increase in transmittance compared to the existing anti-reflective coating [**80**]. Eck and Steinmann developed an analytical model for direct steam production. A correlation is presented for the minimum mass flow to avoid stratified flow. The minimum temperature at the inlet to the collector was also discussed to avoid pressure instability [**81**].

Grena optically simulated a parabolic trough collector using the Monte Carlo simulation method taking into account tracking error, angle of incidence and refraction in a glass tube [**82**]. Yang et al. analyzed the flow distribution in the parabolic trough collector using the Monte Carlo method [**83**]. Kumar and Reddy used an analytical method to determine the intensity distribution in flat receivers. The influence of surface errors is included in the scattering angle. The variance error is calculated over the image width using the analytical approach [**84**]. Y.L. He et al. Integrated Monte Carlo simulations with the finite volume method to obtain a temperature gradient along the walls of the receiver. To calculate the flow intensity, uniform values of the transmittance of the glass tube and the absorption capacity of the receiver are taken [**85**].

In this section, we consider the graphoanalytical method for determining the energy and optical characteristics of a flat solar collector. To study the graphoanalytical method, the developers studied a new flat solar collector, as well as conducted experimental studies of energy and optical characteristics.

The graphoanalytical method for determining the energy characteristics of concentrating systems is based on geometric constructions that allow one to determine the display at the receiver of a beam of rays reflected by an elementary mirror platform [**86**]. In this case, the law of specular reflection is used and either a parallel beam of rays or diverging with an angular size ϕ0 ≥ ϕC is considered. The radiation distribution in the beam along the directions is assumed to be uniform, and if it is necessary to take into account the uneven distribution, the reflected beam is divided into a number of elementary beams

Figure 5.1: Map of solar radiation in Kazakhstan. (National Atlas of the Republic of Kazakhstan).

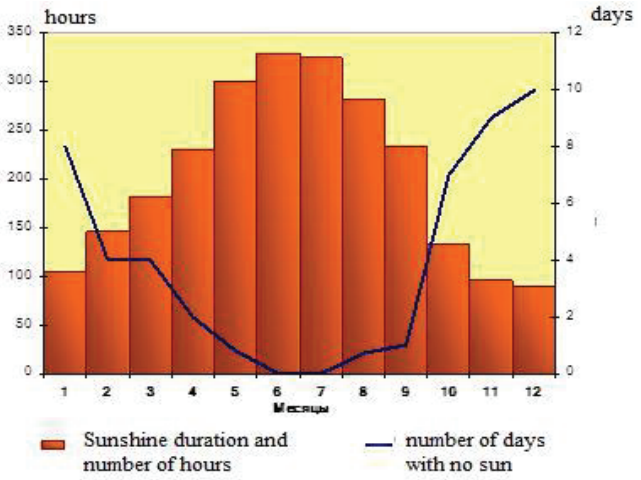

Figure 5.2: The duration of sunshine and the number of days without sun in Astana.

The study of solar collectors with reflectors and transparent insulation from the accumulated double-glazed windows provides a calculation of the energy and optical characteristics of solar collectors with reflectors (concentrators) and VSP, including a graph-analytical method for calculating the optical efficiency of a solar collector with reflectors. Reflectors are designed so that the reflected rays hit the back of the heat receiver. For the equilibrium state, the calculation of the heat balance of the solar collector with reflectors is performed according to the equation [**87**].

$$H\tau\eta_{opt}\ \Theta = q \text{ heat flux density} + q \text{ heat from the density} \qquad (5.1)$$

where H is the density of the total solar radiation, W / m2, τ is the transmittance of transparent insulation; ŋ_opt - optical system efficiency; Θ-coefficient of capture of solar radiation; q_ (sp.iz) - heat flux density through transparent insulation, W / m2; q_ (heat from) the density of the heat flux through the insulation, W / m2.

It is proposed to calculate the optical efficiency ŋ_opt of the system using the graphoanalytic method, which consists in dividing the solar flux incident on the solar collector (normal incidence is considered) into zones by the amount of reflection from the solar collector.

The total stream incident on the receiver will consist of the direct stream coming to the front side of the receiver and the stream reflected from the concentrator to the back side of the receiver (provided rpr ≤ r ≤ Rap and rpr = r0) [**88**].

$$Q = \alpha\ q\pi[(r_n{}^2 - r_{n-1}{}^2)\rho^n + (r_{n-1}{}^2 - r_{n-2}{}^2)\rho^{n-1} + (r_{n-2}{}^2 - r_{n-3}{}^2)\rho^{n-2} + \cdots + (r_1{}^2 - r_0{}^2)\rho^1 + \delta_0 r_{\text{ref}}{}^2\rho^0] \qquad (5.2)$$

where q is the direct solar radiation flux density, W / m2; rn = Rap is the radius of the large circle of the concentrator (aperture); rn-1 is the inner radius of the peripheral ring and the outer radius of the ring following it; ρn is the reflection coefficient of the concentrator to the degree n; αpr - absorption coefficient of solar radiation by the receiver; r0 is the radius to the axis of the semicircle; rpr is the radius of the receiver; δ0 ≥ 1 - coefficient taking into account the scattered radiation incident on the front side of the receiver.

In collectors, the sun's rays fall on the surface of the absorber, which is heated and then transfers thermal energy through the liquid absorber.

$$Q = 2\alpha_{\text{ref}}\ qL_k[(r_n - r_{n-1})\rho^n + (r_{n-1} - r_{n-2})\rho^{n-1} + (r_{n-2} - r_{n-3})\rho^{n-2} + \cdots + (r_1 - r_0)\rho^1 + \delta r\ \rho^0] \qquad (5.3)$$

where Lk is the length of the concentrator, m; rpr, rn in this case is the width of the receiver and the width of the zone, respectively, m.

The optical efficiency ŋ opt of the "hub - receiver" system is determined as follows.

$$\eta_{\text{optical efficiency}} \frac{Q}{\delta_0 q * A_{ap}} \quad (5.4)$$

where A_{ap} is the area of the reflector aperture.

For the solar collector, reflectors ηopt = 66% at ρ = 0.9.

(**Figure 5.3**) shows a model of a flat solar collector. The essence and novelty

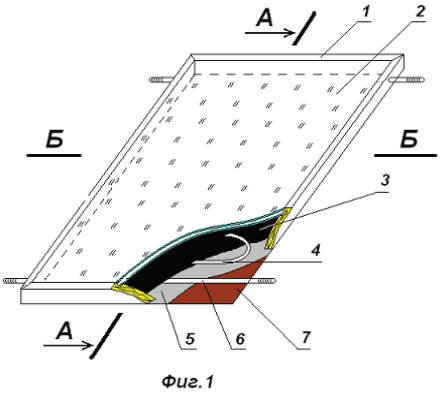

Figure 5.3: Flat solar collector.

is that, unlike the well-known design principle, the collector contains a transparent double-glazed window 2 with double glass and with reduced pressure, as well as a perimeter frame 1. The bottom of the wooden frame 7 is made of plywood 8 mm thick. and heat-insulating film 5 with foil is glued to them. In the gap formed between the double-glazed window and the bottom of the frame, a flexible thin-walled stainless corrugated tube 4-16 mm is laid in the form of a coil. The ends of the tube are attached to the inlet and outlet protruding pipes 6.

Figure 5.4: Full-scale model of a flat solar collector.

(Figure 5.4) shows a full-scale model of a flat solar collector. The solar collector is the main heat generating unit of the solar installation. To achieve this goal, we have developed a fundamentally new flat solar collector, on the basis of which a type size range of solar plants for heating water and heating the building and the room will be created.

Options	Value
Adsorbent plate material	Copper
Adsorber plate dimensions	1000 × 2000 mm2
Adsorber plate thickness	0.4 mm
Glazing material	Knee glass
Glazing dimensions	1000 × 2000 mm2
Glazing thickness	4 mm
Insulation	Penopleks (polyurethane foam)
Collector angle	450
Thermal conductivity of the absorber	401 W / (m K)
Thermal conductivity of insulation	0.04 W / (m K)
Transmittance-absorption coefficient	0.855
Visible Sun Temperature	4350 K
Ambient temperature	303 K
Radiation intensity	1000 W / m2

Table 5.1: Technical indicators of a flat solar collector.

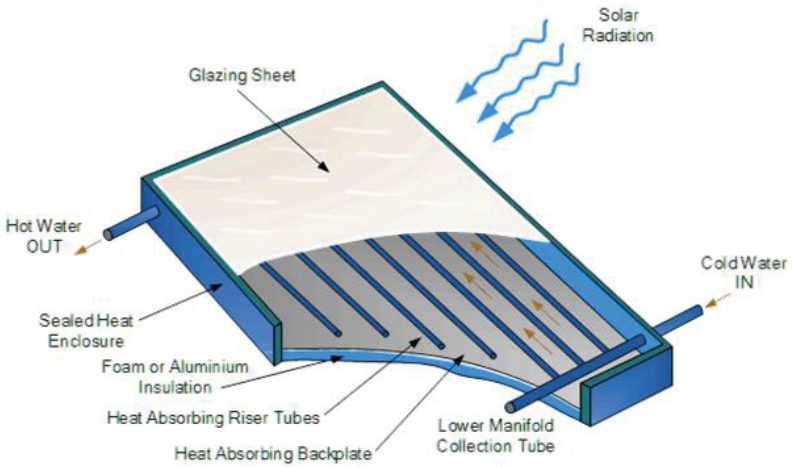

Figure 5.5: The penetration of solar radiation on a flat solar collector.

As shown in (**Figure 5.5**), absorbed solar radiation reaches the inside of the collector, either by passing through a wall to the inner surface of the wall from which it is supplied and emitted, or by hot air passing through the air gap. The wall loses energy to the environment due to conduction, convection and radiation through the glazing.

When solar radiation penetrates a flat solar collector due to additional accumulation of solar heat on the surface of the absorber, a change in the flow rate of the working fluid is inevitable. Therefore, the correct selection of the material of the absorber and the working fluid plays an important role in the collection of heat flux.

From (**Table 5.2**) it is seen that at the same flow rates of the heat carrier (water), the maximum temperature is reached in the solar collector with reflectors and transparent insulation and is 94° C. This temperature is quite high with a concentration coefficient of 2. The efficiency of a solar collector with reflectors is 40.1%, which is 10.8% higher than the efficiency of a solar collector with reflectors and single glazing.

Type of glazing	o W/m²	H, Wt*h/m²	Нприх, Wt*h/m²	t_{inlet} o_C	t_{outlet}, o_C	t_{outlet} °C	G kg/h*m²	Q, W/h*m²	η, %
One glass	20,5	715	732,7	22	78	56	3,3	214,4	29,3
Double glazing, clearance 3 mm	17	722	739,9	19	82	63	3,4	248,5	33,6

Table 5.2: The parameters of the environment and the solar collector by various types of glazing with maximum heating of the coolant.

Designations in the Table: tc - ambient temperature, N - solar radiation; Nprih - the amount of solar radiation per hour; tin - the temperature of the coolant (water) at the inlet of the SC, tout - the temperature of the coolant at the outlet of the SC; G is the coolant flow rate, Q is the heat energy received in the collector in 1 hour; η is the efficiency.

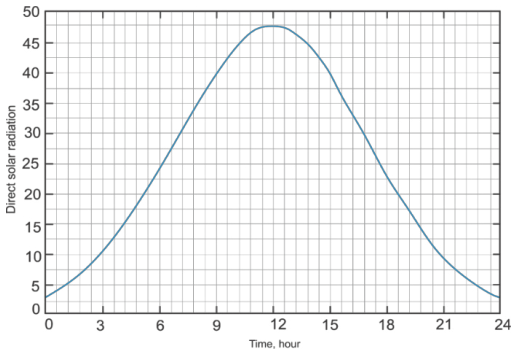

Figure 5.6: Distribution graph of direct solar radiation flux density, W / m2 in 24 hours.

(Figure 5.6) shows that in one day, that is, in 24 hours, the direct solar radiation flux density is effective in the middle of the day, that is, when the sun is at its zenith. The dependence also shows that the higher the direct solar radiation flux density, the higher the air temperature

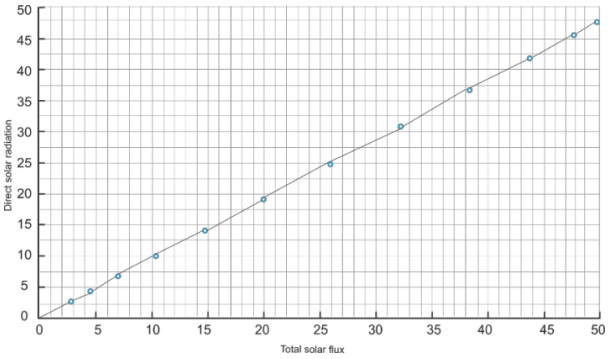

Figure 5.7: Graph of the dependence of optical efficiency on the flux density of direct solar radiation and the total flux to the receiver.

(Figure 5.7) shows that the higher the optical efficiency of the solar collector, the higher the flux density and the total flux to the receiver. Also, the higher the total flux to the receiver, the higher the optical efficiency of the solar collector.

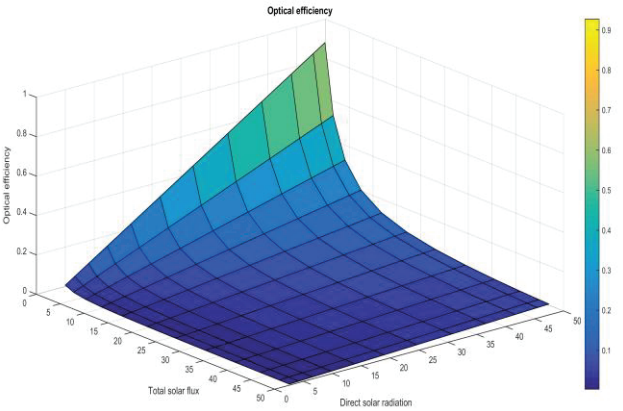

Figure 5.8: Dependence of direct solar radiation flux density on the total flux to the receiver.

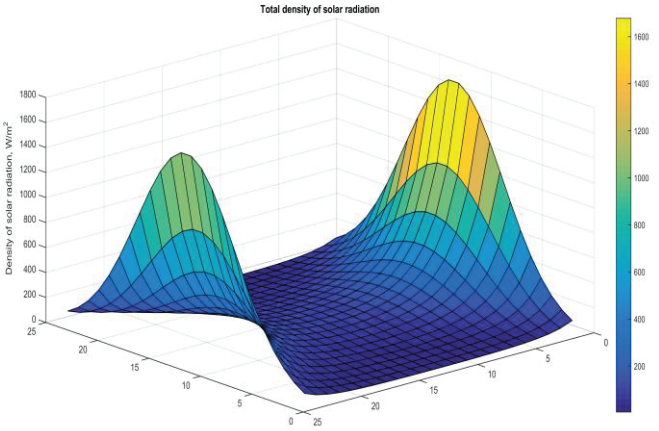

Figure 5.9: The values of the density of total solar radiation obtained by calculation from the equation for the equilibrium state of the calculation of the heat balance of the solar collector with reflectors.

The arrival of solar radiation on a horizontal surface with a clear sky at noon on the flat part of the territory is 0.33-0.81 kW / m2, in the mountains - 0.46-1.02 kW / m2. the presence of cloudiness reduces incoming solar radiation and radiation balance.

The total radiation is determined by the total arrival of direct and diffuse radiation on a horizontal surface. The total radiation in the entire territory of the republic reaches its maximum intensity in May-July. The intensity of the total radiation varies for foothill areas from 280 to 925 mJ / m2. In high mountain areas, it ranges from 360 to 1120m J / m2.

F-Chart Method for a Double-Circuit Heating System with Thermosiphon Circulation

$$Q = Q_{hotwater} + E = \Delta U \tag{5.5}$$

Where Q is the Monthly Heat, The Productivity of the Solar Installation:

Q_ (g.v) is the monthly load of hot water supply, E is the total amount of energy received during the month, ΔU is the change in the amount of energy in the storage unit.

With the sizes of the batteries commonly used in solar heating systems, the difference ΔU is small compared to Q, Q_ (g.v) and E and can be taken equal to zero. Then equation (5.5) can be represented as [89].

$$f = \frac{Q_{\text{hot water}} - E}{Q_{\text{hot water}}} = \frac{Q}{Q_{\text{hot water}}} \tag{5.6}$$

where f is the fraction of the monthly heat load provided by solar energy.

Equation 5.6 cannot be used directly to calculate f, since Q is a function of incident radiation, ambient temperature, and thermal loads. However, consideration of the parameters on which Q depends, suggests that the substitution coefficient f can be empirically associated with two dimensionless complexes [**29**].

$$X=F_K K_K (T_a - T_b) \frac{Ät}{Q_{\text{hot water}}} \quad (5.7)$$

$$Y = \frac{F_k \eta_0 E_k n_Д}{Q_{\text{hot water}}}, \quad (5.8)$$

where T_a is the base temperature, taken equal to 1000° C, T_b is the average monthly outdoor temperature, °C, Δt is the time change, E_k is the average monthly daily arrival of the total solar radiation on the inclined surface of the flat collector, J / (m2 * day).

The f-chart method is based on the correlations of a large number of simulations in terms of easily calculated dimensionless variables. Modeling conditions varied in the corresponding ranges of parameters of the practical system designs. The resulting correlations give f, the fraction of the monthly heating load (in this case, space heating and hot water) provided by solar energy, as a function of two dimensionless parameters. One of them is related to the ratio of collector losses to thermal loads (X), and the other to the ratio of absorbed solar radiation to thermal loads Y. As a result of modeling the systems for which the f-diagram was applied, we used to develop a correlation between dimensionless variables and f - the monthly share of the loads carried by solar energy. The dimensionless parameters X and Y are determined as follows [**90, 91**]:

$$X=\frac{\text{Collector energy loss during a month}}{\text{Total heating load during a month}} \quad (5.9)$$

$$Y=\frac{\text{Absorber solar radiation}}{\text{Total heating load during a month}} \quad (5.10)$$

Parameters X and Y can be written as in equations 5.11 and 5.12, respectively.

$$X=\frac{A_C F/ U_{L(T_{ref}} - T_a)\Delta\tau}{L} \quad (5.11)$$

$$Y=\frac{A_C F/ R(\overline{\tau\alpha})\bar{\bar{H}}N}{L} \quad (5.12)$$

For ease of calculation, the values of the dimensionless parameters X and Y in equations 5.9 and 5.12 are usually located as in equations 5.13 and 5.14, respectively. The reason for this device is that the values of the coefficients LR UF and n RF are obtained from the test results of a standard collector. The F'R / FR ratio corrects various temperature differences between the collector and the storage tank and is calculated by methods generalized in [**90**] and [**91**]. The ratio (τα) / (τα) n is also estimated by the methods described in [**90**].

$$X=FRUL\frac{F/_R}{F_R}(T_{ref}-T_a)\Delta\tau\frac{A_C}{L} \quad (5.13)$$

$$Y=FR(\tau\alpha)n*\frac{F/_R}{F_R}*\frac{\overline{\overline{(\tau\alpha)}}}{(\tau\alpha)_n}*\overline{\overline{Ht}}*N*\frac{A_C}{L} \quad (5.14)$$

Efficiency of a Liquid-Based Solar Heating System Using the F-Chart Method

In this section, the thermal characteristics of the solar heating system shown in (**Figure 5.20**) will be analyzed using the f-chart method. The monthly share of solar energy (the contribution of solar energy for each month), the heat load and the contribution of solar energy on an annual basis. The fraction f of the monthly total load coming from the solar heating and water heating system (liquid system) is presented as a function of X and Y in (**Figure 1.21**). The ratio of X, Y, and f in the form of an equation is [**91**].

$$f = 1{,}029Y – 0{,}065X – 0{,}245Y2 + 0{,}0018X2 + 0{,}0215Y \quad (5.15)$$

where $0 < Y < 3$ и $0 < X < 18$.

Due to the nature of equation (5.15), it should not be used outside the ranges shown by the curves in Figure 5.21. If the calculated point is outside this range, the graph can be used for extrapolation with satisfactory results [**90**]. For simplicity, the simple "degree-day" method is used to calculate the average monthly load on space heating required for the system in this study. The method for assessing the degree of heating in degrees-days is based on the principle that the energy requirement for heating a room primarily depends on the temperature difference in the room and on the street. It is assumed that the monthly load on the heating of rooms in which the temperature is maintained at 24° C is proportional to the number of degree days in the month DD [**90**].

$$LS=(UA)h*DD \quad (5.16)$$

where Ls is the load on the heating of the room, and (UA) h is the product of losses by the area of the building. For this study, a building with (UA) h 467W/m2oC was taken from the building design. The number of days in degrees (DD) per day is the difference between 18.3° C and the average daily ambient temperature

(the average of the maximum and minimum daily ambient temperatures). If the average daily temperature exceeds 18° C, the number of days in degrees is taken equal to zero [**91**]. For the city of Almaty, the number of days with a degree of heating, monthly average daily solar radiation and ambient temperature are given in (**Table 5.3**).

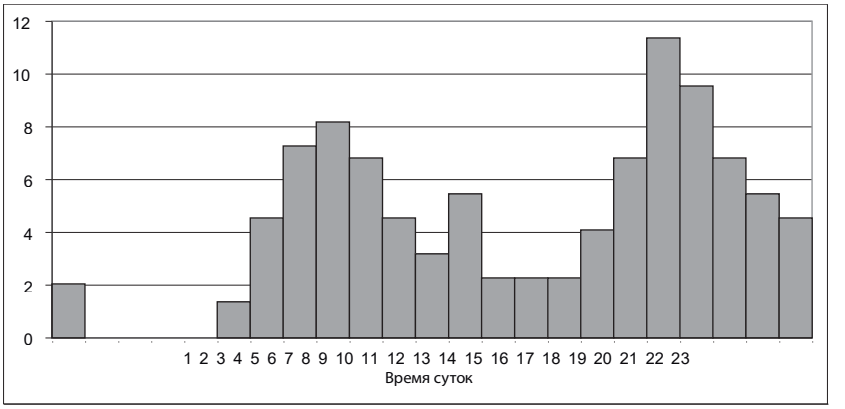

Figure 5.21: The average monthly daily solar radiation for the city of Almaty.

Another load included in this study using the f-chart method is the load on heating water for domestic consumption (the amount of energy needed to heat water for domestic purposes). It greatly depends on the lifestyle of the residents of the building. On average, in Almaty, the estimated water demand and consumption is 300 liters per person per day [**93**]. The monthly load of water heating, Lw, is set by pmwpw.

$$Lw=N*Np*V*(Tw-Tm)*\rho * Cp \quad (5.16)$$

where N is the number of days in a month; Np = number of people in the family; Tw = minimum permissible temperature of hot water: it is ~ 60° C [**91**]. V - daily water consumption per person in m3. Tm is the temperature of the main supply water (0C): ρ is the density of water in kg / m3: Cp is the specific heat of water (4190 J / kg * 0C). The monthly total load (L) is the sum of the load for heating the room (LS) and the load for heating domestic water (Lw), as in [**91**].

$$L = LS + Lw \quad (5.17)$$

The contribution of solar energy per month is the product of f and the total heating load L for this month. The fraction of the annual heat load supplied by solar energy is the sum of the monthly contributions of solar energy divided by the annual load, as in the following equation:

$$F = \frac{\sum f_i L_i}{\sum L_i} \quad (5.18)$$

Months	$\overline{\overline{T_a}}$(0C)	$\overline{\overline{H}}$ (MJ/ m2*day)	Months	$\overline{\overline{T_a}}$(0C)	$\overline{\overline{H}}$ (MJ/ m2*day)
January	-17	-16,0	July	30	20,0
February	-20	-18,63	August	28	19,12
March	7	6,2	September	22	17,00
April	12	10,5	October	15	13,0
May	18	18,4	November	7	6,2
June	25	19,0	December	-10	-9,2

Table 5.3: The degree of heating and the monthly average daily temperature and global radiation for Alm.

Consider a method for calculating the characteristics of a solar heat supply system for conditions when the load of hot water supply is predominant or unique.

The following is the result of the required heat load, the proportion of the load supplied by the solar energy system for various collector zones, and parametric studies.

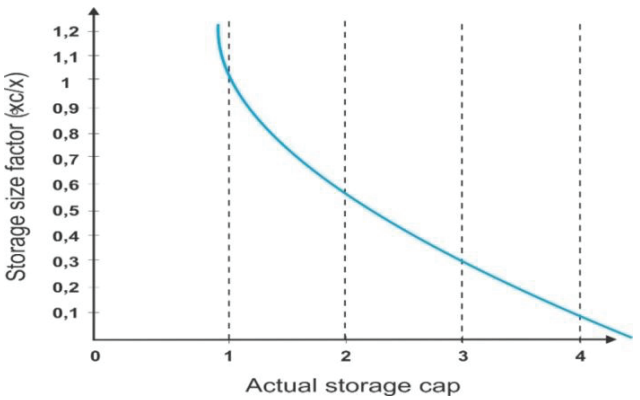

Figure 5.22: The dependence of the monthly value on the correction factor for hot water systems.

(**Figure 5.22**) shows that the graph of the monthly value of the correction coefficient using the f-chart method shows that the degree of heating, the monthly average daily temperature and direct solar radiation are lowered depending on weather conditions.

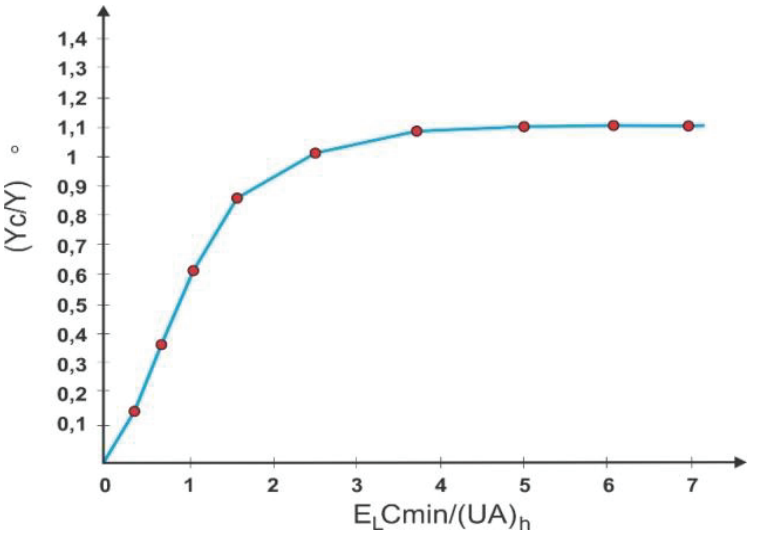

Figure 5.23: The dependence of the monthly value on the modified correction factor Yc / Y for hot water systems.

(**Figure 5.23**) shows that the modified correction factor Yc / Y from the ambient temperature has an exponential function, which, as the correction coefficient increases, increases the annual share of the load provided by solar energy.

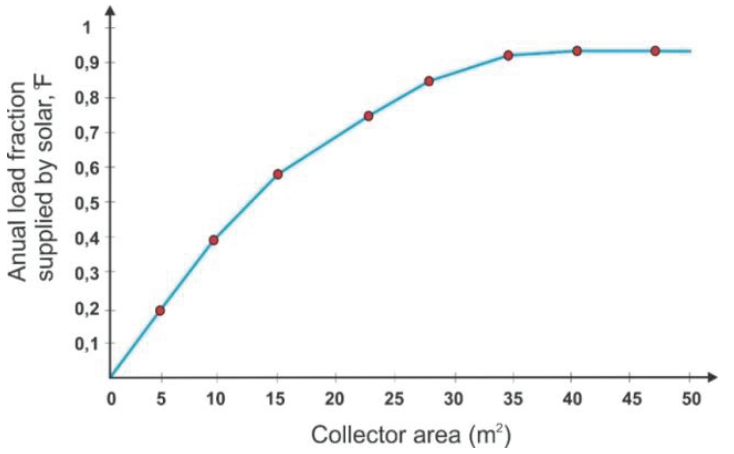

Figure 5.24: Dependence of the change in the monthly share of the load for different collector areas during the year for hot water systems.

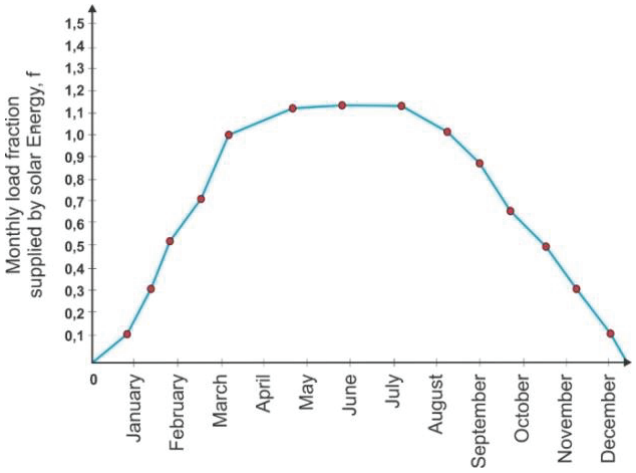

Figure 5.25: Change in the heating load of the room and heating water for domestic consumption depending on the months of the year.

From (**Figure 5.24**), you can see that the monthly load fraction increases with increasing collector area. It also shows that the monthly share is higher in the summer months in Almaty (Kazakhstan) (July is the highest value) and lower in the winter months (January, February is the lowest value). In (**Figure 5.25**) it is observed that the lowest heating load is observed in the summer months of the year. The figure also indicates that the load on the room heating is available only for three months, namely: December, January and February. The rest of the time, the heating load is almost zero. This is a very interesting result due to the fact that the load corresponds to peak winter demand, during which a heating load is required, and this result also provides an important advantage from an economic point of view by reducing the total cost of fuel / electricity, which could otherwise the case is spent on the energy needed for the heat supply needed in the winter.

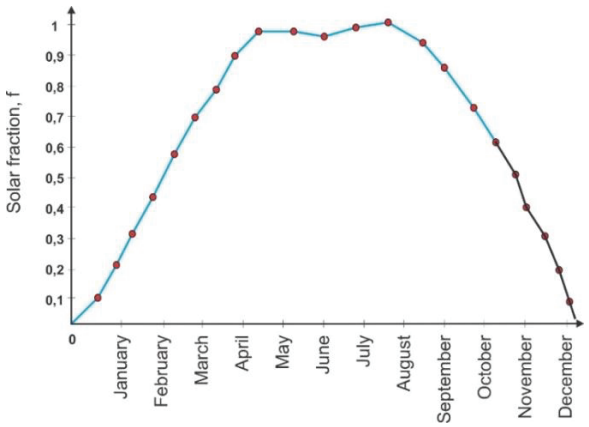

Figure 5.26: The effect of the actual storage capacity in liters per m2 of collector area on the annual share of the load provided by solar energy.

(**Figure 5.26**) shows that the annual load share increases by a small amount, and a large share is observed in a larger collector area. In particular, if the storage capacity exceeds approximately 50 liters of water per m2 of collector area, only a slight increase (improvement) is observed in the annual proportion of the load provided by solar energy.

Exergy Analysis of a Double-Circuit Flat Solar Collector with Thermosiphon Circulation

To heat water when it is necessary to significantly reduce the cost of energy, you can use solar energy. Thermosiphon solar collector is a type of passive heater that can be easily built and can be easily used without any complexity.

[**94**] presented a theoretical model of energy and exergy analysis of flat plate solar collectors, through which it is possible to study the effect of all the calculated parameters on the performance.

After the experimental data of the model, the influence of such parameters as the fluid flow rate and temperature, the type of working fluid and the thickness of the back insulation on the energy and efficiency of the collector exterior was analyzed, and based on the analysis and comparison of the results, the optimal operating state of the system was determined. According to the results, designing a system with an inlet water temperature of 40° higher than the ambient temperature, as well as a lower flow rate, will increase overall productivity.

To a greater extent, when tracking the generation of entropy, exergy analysis using the second law of thermodynamics can lead to optimization of the system [**95,96**].

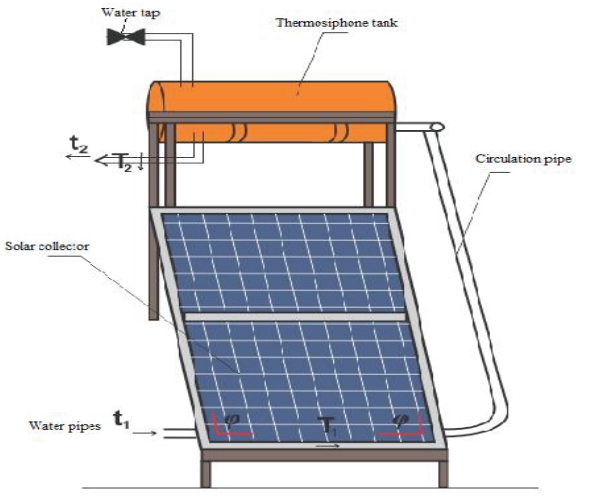

Figure 5.27: General view of the solar water heater.

The rationale for the structural-technological scheme. Taking into account the requirements of increasing the device's performance, a circuit diagram of a double-circuit solar installation with a heat pump was developed (**Figure 5.27**), where the investigated diesel generator sets are made up of four main units: thermosiphon 1, solar collector 2, heat pump 3, and storage tank (BA) 4.

Justification of the structural-technological scheme. Given the need to improve the operational characteristics of the installation, a circuit diagram of a dual-circuit solar installation with a heat pump has been developed (**Figure 5.28**).

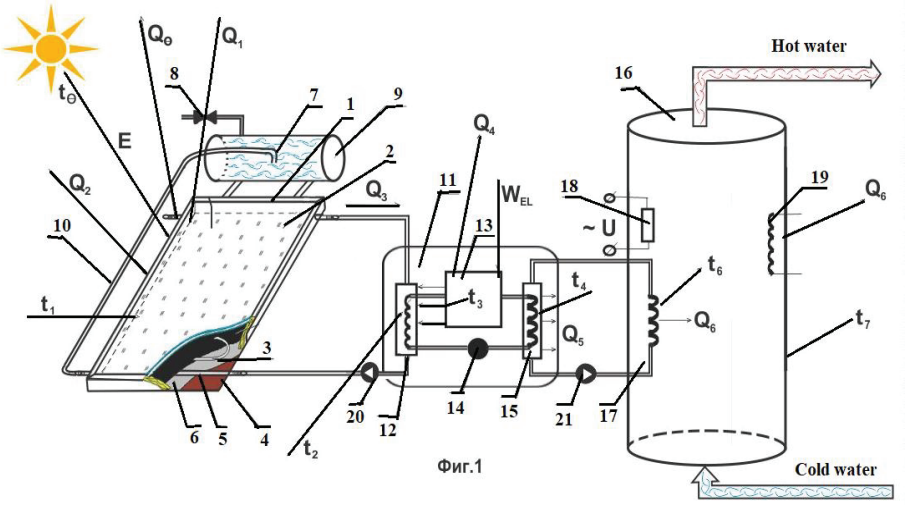

Figure 5.28: Schematic diagram of a dual-circuit solar system with thermosyphon circulation.

The work of the proposed installation is as follows. Solar energy E with a temperature t0 is absorbed by a solar collector 1, with a temperature t1, heating a stream of solar energy passes through a translucent insulating glass 2. Heat received from a solar stream heats the liquid in the coils 3, which is removed from the collector, and cold water comes in its place from the pipeline with a valve for cold water 8, and from the siphon of the dispenser tank 7, a constant thermosiphon circulation occurs using the circulation pipe 10. Next, the liquid enters the heat pump 11, which consists of and a condenser evaporator 12 with a temperature t2, in which the heat exchanger is made in the form of a spiral, absorbing heat from the heat carrier, lowers its temperature below the temperature of atmospheric air (Q2) using a throttling valve 14, thereby contributing to the additional absorption of heat from atmospheric air. The diagram also shows solar radiation reflected from a translucent coating (Q0) and the surface of the absorbing panel (Q1). In the heat pump, energy of the coolant with a relatively low temperature is transferred to the coolant of the heat exchanger of the condenser 15 in the form of a spiral with a higher temperature t2, which increases the area, as well as the heat exchange rate. To

carry out such a cycle, a compressor 13 with a temperature of t3 is used, with an electric drive 17. Further, by means of a heat exchanger of a condenser 15 with a temperature of t4, heat from the heat pump (Q5) is transferred to the tank from the heat exchanger Q6 with a temperature t6 of heating system 18. Since the installation has two circuit, it is equipped with automatic circulation pumps 19 and 20 for circulating liquid between the solar collector and the evaporator, condenser and storage tank. The water temperature is brought to the required technological level and is supplied to the consumer for the purpose of hot water supply and heating.

Energy and exergy model. The instant useful energy collected by the solar collector is calculated according to the following equations [**97-99**].

$$Q_u = A_c F_R [I_T(\tau\alpha) - U_l(T_{in} - T_a)] = mC_{p,wa}^{\cdot} (T_0 - T_i) \quad (5.19)$$

Alternatively, the instantaneous net energy collected by the solar collector can be calculated as [**97**].

$$\dot{Q}_u = \dot{m}\, C_{p,wa}(T_{out} - T_{in}) \quad (5.20)$$

The instantaneous collector efficiency is calculated [37].

$$\eta_{en} = \frac{Q_u}{I_T A_C} \quad (5.21)$$

The solar radiation equations given by Duffy and Beckman [**97.98**] can be used to estimate the total instantaneous solar radiation. The temperature distribution between the tubes and collector efficiency is discussed in detail [**97**].

The heat extracted from the heat pump heat exchanger, Qu, is calculated according to the following equation [**98**]:

$$Q_u = \dot{m}\, C_p(T_{out} - T_{in}) \quad (5.22)$$

The heat transfer coefficient in the condenser is calculated as [**34**].

$$\dot{Q} = \dot{m}(h_2 - h_1) \quad (5.23)$$

The heat transfer rate in the evaporator is [**34**].

$$\dot{Q} = \dot{m}(h_1 - h_4) \quad (5.24)$$

Compressor input speed [**100**].

$$W_{com} = \frac{\dot{m}_{ref}(h_2 - h_1)}{\eta} \tag{5.25}$$

where η is energy efficiency.

The efficiency of the entire COPsys system, which is the ratio of the capacitor load to the total cost of the compressor and circulation pumps, is calculated according to the following equation [**101**].

$$COP_{sys} = \frac{\dot{Q}_u}{(\dot{W}_{com} + \dot{W}_{pumps})} \tag{5.26}$$

The working inlet to the circulation pump [36].

$$\dot{W}_{pump} = \frac{\Delta PV}{\eta} \tag{5.27}$$

where ΔP is the pressure loss, V is the volumetric flow rate of the water-glycol mixture, and ηmec is the mechanical efficiency of the pump.

ΔP is the pressure loss, which is written as follows [**101**]:

$$\Delta P = 0.5 f \frac{L}{D} \rho U^2 + \sum \zeta \tag{5.28}$$

where U is the velocity, f is the loss of fraction, ζ is the specific loss of resistance, and L is the length of the pipe.

The exergy rate is calculated by the following equation [**101**]:

$$\dot{E}_x = \dot{m}_{ref}[(h - h_0) - T_0(s - s_0)] \tag{5.29}$$

Exergy damage in the heat exchanger (condenser and evaporator), in the expansion valve and the solar collector are calculated as follows:

Heat exchanger:

$$\dot{E}_{\chi dest,HE} = \sum \dot{E}_{\chi in} - \sum \dot{E}_{\chi out} - \sum \dot{E}_{\chi dest} \tag{5.30}$$

$$\dot{E}_{\chi dest,HE} = \dot{m_{wa}}(\psi_{in} - \psi_{out}) + \dot{Q}_r \left(1 - \frac{T_0}{T_{ground}}\right) \tag{5.31}$$

Heat pump.

$$\dot{E}_{\chi dest,pump} = \dot{W}_{pump} - \left(\dot{E}_{\chi out} - \dot{E}_{\chi in}\right) \tag{5.32}$$

Expansion valve:

$$\dot{E}_{\chi dest,valve} = \dot{m_{ref}}(\psi_{in} - \psi_{out}) \tag{5.33}$$

A driving method that is used as a solar collector:

$$\dot{E}_{\chi dest,col} = \dot{m_{wa}}(\psi_{in} - \psi_{out}) + \dot{Q}_u\left(1 - \frac{T_0}{T_s}\right) \quad (5.34)$$

$$\dot{E}_{\chi dest,col} = \dot{m_{wa}}(\psi_{in} - \psi_{out}) + A_C I_T\left(1 - \frac{T_0}{T_s}\right) \quad (5.35)$$

The exergy efficiency of the heat exchangers (condenser and evaporator) is determined by the increase in cold flow exergy divided by the decrease in hot flow exergy based on speed, as follows:

$$\varepsilon_{HE} = \frac{\dot{m}_{cold}(\dot{\psi}_{cold,out} - \dot{\psi}_{cold,in})}{\dot{m}_{hot}(\psi_{hot,in} - \phi_{hot,out})} \quad (5.36)$$

The exergy efficiency of the circulation pumps is determined

$$\varepsilon_{pump} = \frac{\dot{E}_{\chi out} - \dot{E}_{\chi in}}{\dot{W}_{pump}} \quad (5.37)$$

GSHPS Exergy Efficiency Calculated

$$\varepsilon_{sys} = \frac{\dot{E}_{\chi out}}{\dot{E}_{\chi in}} = 1 - \frac{\sum \dot{E}_{\chi dest}}{\sum \dot{E}_{\chi in}} \quad (5.38)$$

In this study, an energetic and exergy study was conducted to analyze a double-circuit flat solar collector with thermosiphon circulation. Figure 5.29 shows the hourly change in solar radiation intensity and ambient temperature relative to the city of Almaty, Kazakhstan (longitude / latitude: 77 degrees east longitude and 43 degrees north latitude).

To assess the potential of solar energy falling on the territory in a particular area, it is necessary to have data on the potential of solar energy. Based on a generalization of actual observations and theoretical calculations, there is data: the annual and latitudinal variations of the possible monthly and annual amounts of direct solar radiation entering the perpendicular surface under clear sky conditions, information about the duration of sunshine, the daily course of solar radiation for typical days of the year, distribution maps over the territory of average monthly radiation sums for June and December, as well as the distribution map of “technically applicable and economically viable solar power”, developed nnye their criterion for defining this concept. The basis of all the calculated indicators of solar systems in assessing the solar energy resources of the territory of Kazakhstan is the quantitative characteristics of direct solar radiation on a horizontal surface, from which it is possible to recalculate from horizontal to inclined plane of any orientation. According to the results of statistical processing of the mean values of direct total radiation and the duration of sunshine, five zones were identified and a histogram

was drawn up characterizing the possibility of introducing solar installations throughout Kazakhstan [**102**].

To calculate the exergy analysis, a computer simulation program (MATLAB ode45 subroutine) was used, using the fourth-order Runge-Kutta method.To ensure the accuracy of the developed numerical model, the numerical results of water productivity were confirmed by the corresponding experimental temperatures.

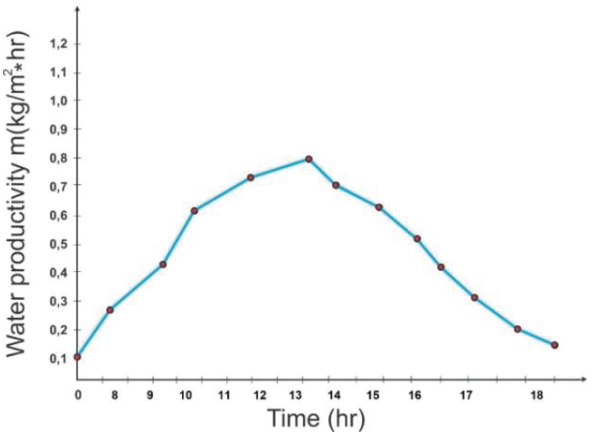

Figure 5.29: Dependence of hourly water productivity on time.

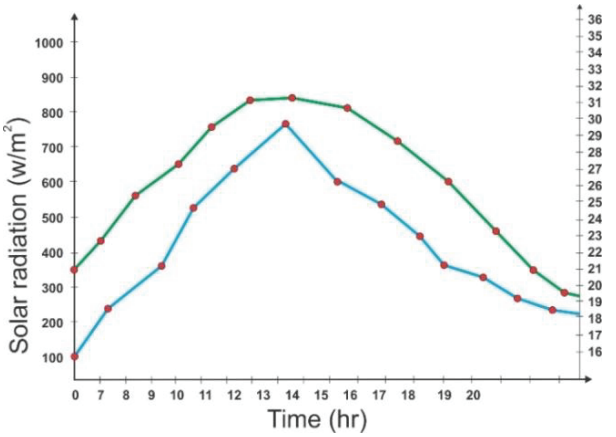

Figure 5.30: Dependence of solar radiation on hourly variation of meteorological conditions in Almaty (Kazakhstan).

(**Figure 5.29-5.30**) shows the hourly variations in the changes in the energy and exergy efficiency of the proposed system and the exergy rate of destruction of all components. According to this dependence, it can be said that the intensity of solar radiation for the city of Almaty in the summer time is of greatest importance at lunchtime, since the total solar radiation reaches its peak value.

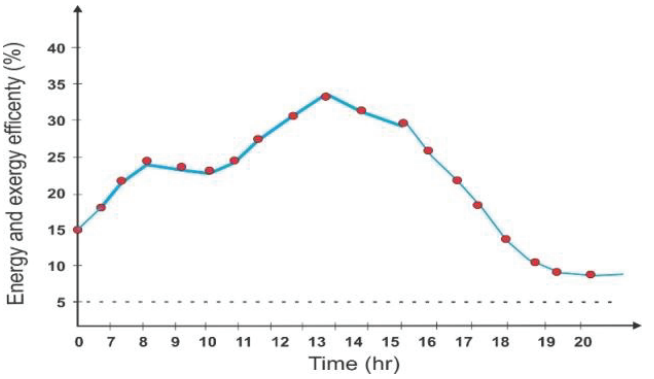

Figure 5.31: Dependence of energy and exergy efficiency on hourly variation of meteorological conditions in Almaty (Kazakhstan).

In (**Figure 5.31**), the maximum values of energy efficiency and exergy at noon are 32.5% and 2.23%, respectively. Despite the fact that the two graphs show approximately the same trend, energy efficiency is much higher than exergy efficiency. The reason for this behavior is a significant deterioration in energy quality based on the concept of exergy. To clarify this point, the high temperature of the Sun (6000 K) is reduced to a relatively low temperature of water.

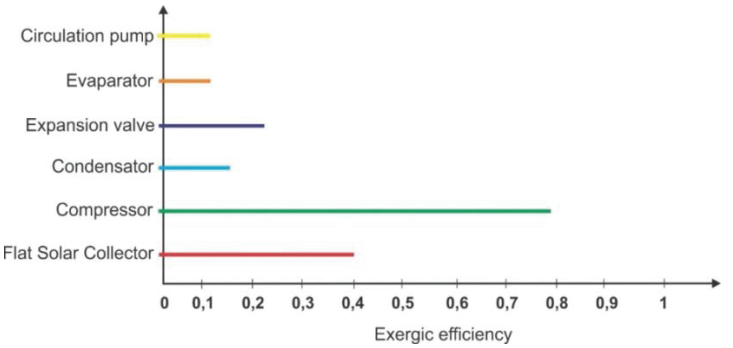

Figure 5.32: Exergy efficiency indices of a double-circuit flat solar collector with thermosiphon circulation.

(**Figure 5.32**) shows the exergy efficiency of a double-circuit flat solar collector with thermosiphon circulation. As we see from the figure, the greatest irreversibility of the process in terms of thermodynamic parameters is due to the heat pump compressor. This is due to the large degree of overheating achieved at the end of the compression and evaporation processes, which leads to large temperature differences associated with the initial phase of heat transfer based on the heat pump cycle. The value of exergy efficiency for the entire system is 70. The reasons for the destruction of exergy in the system include a compressor, a heat exchanger (condenser and evaporator),

and circulation pumps. Thermodynamic properties of water and refrigerant (working fluid, R218 were obtained from the NIST database.

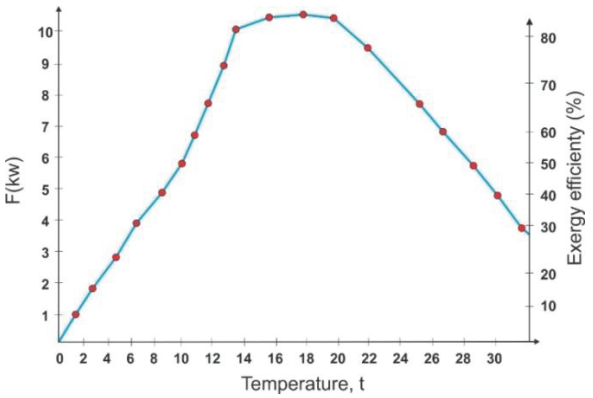

Figure 5.33: Temperature dependence of the exergy efficiency of a double-circuit flat solar collector with thermosiphon circulation.

(**Figure 5.33**) shows that in the summer period, exergy efficiency increases with increasing ambient temperature at lunchtime, when the total total solar activity is at its peak value.

An exergy analysis of a flat solar solar collector with thermosiphon circulation is based on the calculation of the heat loss coefficient, collector heat transfer coefficient and plate exposure coefficient. However, the accuracy of the calculation will lead to better accuracy. In this work, it was proved that the maximum level of exergy can be achieved in the temperature range, but the efficiency of the heat pump decreases, while the ambient temperature has a positive effect on thermal efficiency, while it negatively affects the exergy efficiency. It was also proved that with a circulating solar water system, exergy efficiency of about 4% can be expected.

Methodology for Calculating the Generation of Entropy and Study of Thermal Characteristics for a Thermosiphon Flat Solar Collector

For solar heating systems, studies on the generation of entropy are not widespread. The analytical method proposed by Bezhan [**103**] for determining the generation of entropy in solar collectors was adapted for Kalogirow concentrating collectors [**104**]. In this method, entropy generation is a function of the incident solar radiation, the usable heat delivered to the user, and the heat loss at the receiver. The study [**105**] showed that the generation of entropy due to heat transfer and friction of the liquid inside the absorber tube gives almost the same optimal flow rates as the analytical method [**106**]. The method used in our study [**107**] directly calculates the generation of entropy using computational fluid dynamics in accordance with the equations obtained by Kok and Herwig [**105**].

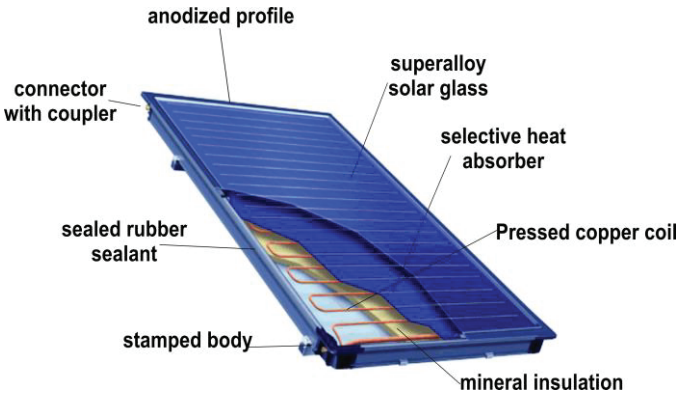

Figure 5.34: Schematic diagram of a flat solar collector.

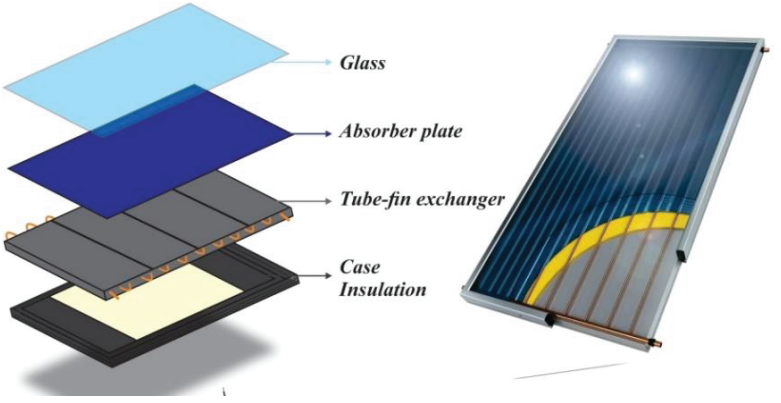

Figure 5.35: Schematic diagram of a flat solar thermal collector disassembled.

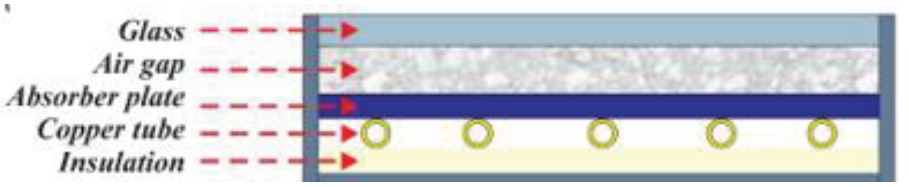

Figure 5.36: Cross section of a flat solar collector.

As shown in (**Figure 5.36**), solar energy passes through the glass and hits the absorber plate, which heats up, converting solar energy into thermal energy. Heat is transferred to the working fluid, which passes through tubes attached to the absorber plate. The basic equations for stationary and three-dimensional turbulent flow are the continuity, momentum, and energy equations given in [105]. Continuity equation.

$$\frac{\partial(\rho u_i)}{\partial x_i} = 0 \tag{5.39}$$

Momentum equation

$$\frac{\partial}{\partial x_j}(\rho u_i u_j) = -\frac{\partial \rho}{\partial x_i} + \frac{\partial}{\partial x_j}\left[\mu_{eff}\left(\frac{\partial u_i}{\partial x_j} + \frac{\partial u_j}{\partial x_i}\right) - \frac{2}{3}\mu_{eff}\frac{\partial u_i}{\partial x_i}\delta_{ij} - \rho u_i' u_j'\right] \tag{5.40}$$

Energy equation

$$\frac{\partial}{\partial x_j}(\rho u_i c_p T) = \left[\frac{\partial}{\partial x_j}\left(\lambda\frac{\partial T}{\partial x_j} + \frac{\mu_t}{\sigma_{h,t}}\frac{\partial (c_p T)}{\partial x_i}\right) + u_j\frac{\partial p}{\partial x_j}\frac{\partial u_i}{\partial x_i}\right] \tag{5.41}$$

The additional terms in these equations represent the effects of turbulence and the Reynolds criteria, which are emphasized by $\rho u_i u\_j$. u_i, u_j are the time-averaged velocity components in the directions i and j, respectively, and T is the time-averaged temperature. The effective viscosity is defined as $\mu\_eff = \mu\_t + \mu$, and λ is the thermal conductivity of the liquid. The most common approach is the Reynolds criterion, which is associated with average velocity gradients through [**105**]

$$\rho u_i u_j = 2\mu_t S_{ij} - \frac{2}{3}(\rho k + \mu_t\frac{\partial u_i}{\partial x_i})\delta_{ij} \tag{5.42}$$

$$\rho u_i u_j = \mu_t\left(\frac{\partial u_i}{\partial x_j} + \frac{\partial u_j}{\partial x_i}\right) - \frac{2}{3}(\rho k + \mu_t\frac{\partial u_i}{\partial x_i})\delta_{ij} \tag{5.43}$$

where k is the turbulent kinetic energy per unit mass, defined as

$$k = 1/2(u'^2 + v'^2 + w'^2) \tag{5.44}$$

In this study, a feasible k-ε model was used to close turbulence. Additional equations necessary for the transfer of turbulent kinetic energy and the velocity of turbulent dissipation in the implemented k-ε model are given in [**105**]. For k

$$\frac{\partial}{\partial x_j}(\rho k u_j) = \frac{\partial}{\partial x_j}\left[(\mu + \frac{\mu_t}{\sigma_k})\frac{\partial k}{\partial x_j}\right] + G_k - \rho\varepsilon \tag{5.45}$$

$$\frac{\partial}{\partial x_j}(\rho\varepsilon u_j) = \frac{\partial}{\partial x_j}\left[(\mu + \frac{\mu_t}{\sigma_\varepsilon})\frac{\partial \varepsilon}{\partial x_j}\right] + \rho C_i S\varepsilon - \rho C_i\frac{\varepsilon^2}{k+\sqrt{\nu\varepsilon}} \tag{5.46}$$

where G_k represents the production of turbulent kinetic energy and is modeled in the same way for all k- models as the k-ε model as

$$G_k = \rho u_i u_j \frac{\partial u_i}{\partial x_i} \quad (5.47)$$

In accordance with the Boussinesq hypothesis.

$$\mu_t = \rho C_\mu \frac{k^2}{\varepsilon} \quad (5.48)$$

A detailed definition of C_μ is given in [40]. Constant in the model for realizable k-ε models.

$$C_1 = \max\left(0.43, \frac{\eta}{\eta+5}\right), \eta = S\frac{k}{\varepsilon}, S = \sqrt{2S_{ij}S_{ij}}, C_2 = 1{,}9, \sigma_k = 1, \sigma_\varepsilon = 1.2, S_{ij} \quad (5.49)$$

represents the rate of linear deformation of a fluid element. In total, there are three components in three dimensions, three of which are linear components of elongation strain and six components of shear and deformation [**106**].

$$S_{ij} = 1/2\left(\frac{\partial u_i}{\partial x_j} + \frac{\partial u_j}{\partial x_i}\right) \quad (5.50)$$

Solar radiation absorbed by the collector is distributed to heat loss and useful energy gain. For flat solar collectors, losses occur mainly from above and are usually estimated using the upper heat loss coefficient. An improved formulation of this coefficient was given by Agarwal and Larson [**107**]:

$$U_t = \left[\frac{N}{(C/T_p)((T_p - T_0)/(N+f))^{0.33}} + \frac{1}{h_w}\right]^{-1} + \left\{\frac{\sigma(T_p^2+T_0^2)(T_p+T_0)}{(\varepsilon_p+0.05N(1-\varepsilon_p))^{-1}+\frac{2N+f-1}{\varepsilon_g}-N}\right\} \quad (5.51)$$

where C = 250 (1−0.0044 (ϕ − 90)) with ϕ slope, f = (1−0.04hw + 0.005hw2) (1+ 0.091N), T0 and Tp are the ambient and absorber temperatures, respectively, hw - wind heat transfer coefficient, N is the coating number, σ is the Stefan-Boltzmann constant, and εp and εg are the emissivity of the absorber and coating, respectively.

Equation (5.51) can be used to study the role of many parameters that affect the performance of solar collectors. However, forecasts based on formula (5.39) are also less reliable when there is data with phase transition materials or emitting gases that are used to capture solar energy.

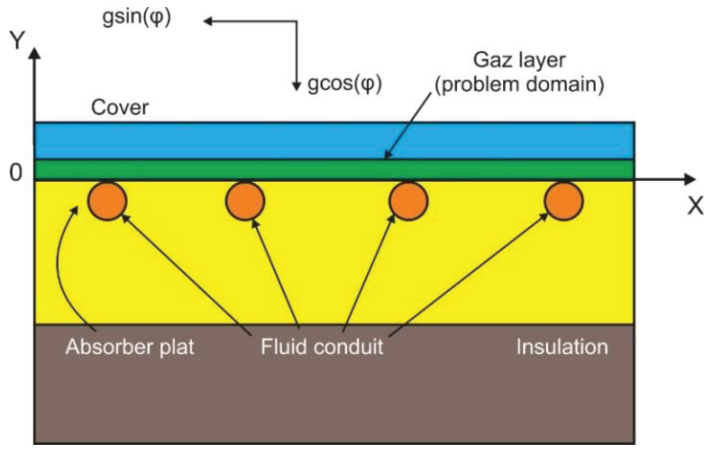

Figure 5.37: Solar collector circuit and problem area.

The influence of the inclination of the collector. The entropy generation in the collector is mainly associated with the modes of heat conduction and convection. The heat loss of the collector, therefore, occurs mainly due to these heat transfer modes.

As a result, the temperature value for a flat solar collector depends on the level of solar insolation and the ambient temperature [**108**].

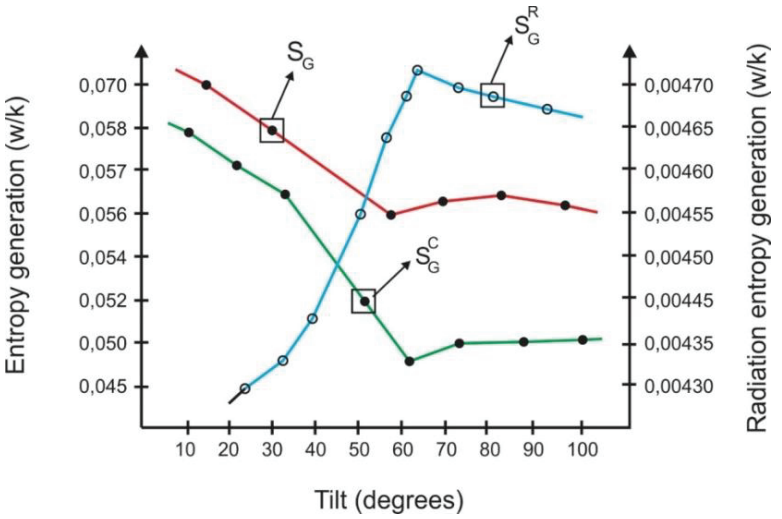

Figure 5.38: Dependence of the generation of entropy on the slope of the solar collector and the generation of radiation entropy.

(**Figure 5.38**) shows the generation of entropy from the inclination of the solar collector and the generation of radiation. As can be seen from Figure 5.38, entropy generation occurs in two cases: one due to heat transfer by irreversibility through a finite temperature difference and the other due to fluid friction. From an experimental study, it was shown that for small Reynolds numbers, the irreversibility of transmission through a finite temperature difference is an important component, and for large Reynolds numbers, friction of the liquid in the tube of a flat solar collector is important.

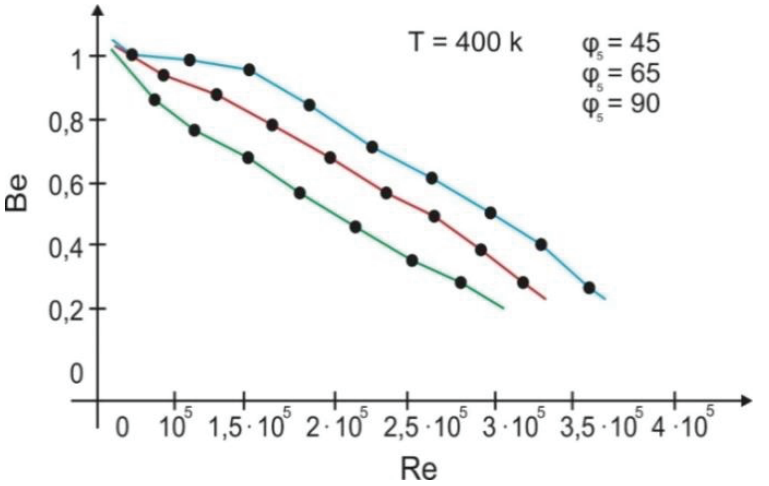

Figure 5.39: Dependence of the Bejan number on the Reynolds number of the generation of entropy.

As can be seen from Figure 5.39, at a temperature of 400K, the Bejan number is close to 1, the irreversibility of heat transfer dominates and for the Bejan number is close to 0, the irreversibility of fluid friction dominates.

The entropy calculation methodology is used to estimate the heat loss in solar collectors. This technique identified critical places in a dual-circuit heliosystem with thermosiphon circulation. Consider a method for calculating the characteristics of a solar heat supply system for conditions when the load of hot water supply is predominant or unique. If the monthly values of X are multiplied by the correction factor determined by the expression below, then the f-method for calculating liquid solar heating and hot water systems can be used to determine the monthly values of f achieved in solar hot water systems.

Chapter 6

Design and Computer Modeling of the Construction Features of the New Type of the Solar Collector

Authors
Amirgaliyev Y.N, Kunelbayev M, Kalizhanova A.U, Kozbakova A. Kh, Daulbayev S.M, Auelbekov O. A, Kataev N.S, Yedilkhan D, Merembayev T, Ormanov T. A, Sundetov T.

*__Corresponding author:__ Ministry of Education and Science of the Republic of Kazakhstan Committee of Science Republican State Enterprise Institute of Information and Computational Technologies, E-mail: murat7508@yandex.kz

Analysis of Heat Loss of a Solar Flat Collector Using Numerical Simulation

This section discusses a theoretical study of calculating the heat loss of a flat solar collector for subsequent modeling of a solar water heating system for climatic conditions in Kazakhstan. For various climatic zones with increasing energy costs or the lack of central heating systems, the search for ways to improve the energy efficiency of the solar system is promising. In the course of research, we believe that the system consists of a flat solar collector installed inside the heat exchanger tank and pumps for heating, as well as for supplying hot water. The solar system is modeled in

Double Circuit Solar Thermal Installation With Thermosiphon Circulation **by Amirgaliyev Y.N, Kunelbayev M, Kalizhanova A.U, Kozbakova A. Kh, Daulbayev S.M, Auelbekov O. A, Kataev N.S, Yedilkhan D, Merembayev T, Ormanov T. A, Sundetov T.**

Matlab + Simulink and is based on a mathematical model of energy analysis. The main modeling problem is the mismatch between the simulation result and the real values; in order to solve the problem, various physical parameters were studied in the study, such as the loss coefficient, thermal conductivity coefficient, Nu, Ra, Pr values that affect the efficiency of the solar flat collector and for the heat loss of the system . All these parameters are the main indicators for modeling. The developed mathematical models, the design and composition of the software and hardware complex, automated control and monitoring systems allow the solar hot water supply system to increase the energy efficiency of the life support and heating systems of buildings, reducing energy costs for heat supply.

Each year, renewable energy becomes an important role in our daily lives. Using renewable energy can reduce energy consumption and reduce our dependence on fossil energy. The most obvious way to use renewable energy is solar energy, which allows you to get clean energy without pollution. In the world, research is being conducted on models, designs and comparisons of solar heating systems for residential buildings.

One of the studies is devoted to the evaluation of data on solar heating of hot water and analysis in South Korea over 3 years [**109**]. Work was carried out to install a solar water heating system for multi-family housing for 1179 families in 14 units. The results of the study showed that, compared with a conventional boiler for heating water (COP = 85%), the solar water heating system showed a positive effect on the environment and is estimated as a reduction of 71.9 l / year of oil and a reduction of 186.3 tons of CO2. Identical studies were conducted in [**110**]. A numerical study of a centralized solar hot water system has been developed for a multi-story residential building in Hong Kong.

Another type of research related to the solar hot water system was described in [**111**]. The solar system was simulated with a flat collector, storage tank and circulation. Two designs of hot circulation were analyzed: water - water and water - air. The result of the study showed that the design of water - air is not effective. In a study [**112**], a review of articles in the field of solar energy absorption by a solar system with various types of liquids was presented. The focus of the study is on solar-powered absorption cooling systems, diffusion absorption systems, ejector-based absorption systems, compression absorption systems and cogeneration / trigeneration absorption systems. The thermodynamic properties of the most common working fluids were examined using a ternary mixture in solar absorption systems. The author Soteris A. Kalogiru [**113**] calculated the optical, thermal and thermodynamic analysis of the solar collector, described the methods that were used to evaluate the efficiency.

In [**114**], a study was conducted of the design and efficiency of the solar hot water supply system. The geometry and dimension of the solar system were determined based on the resulting thermal properties of the materials. Authors Carlos Eduardo Camargo Nogueira, Magno Luis Widotto, Fernando Tonyazzo, Gilson Debastiani [**115**] demonstrated software developed by Matlab and their own algorithms for calibrating a small solar hot water system.

Thermal characteristics can be calculated on the basis of the first law of thermodynamics (energy), but this does not allow estimating the losses of a solar flat collector [**116**]. The second law of thermodynamics (exergy) is used to estimate various losses in a flat solar collector and allows to evaluate the efficiency of the solar hot water supply system [**117, 118**].

Currently in Kazakhstan, much attention is paid to the development of a solar hot water heating system, the price of the system is expensive, therefore it is not available to all customers. To solve this problem, it is necessary to develop a new hybrid energy system with mathematical methods and computer modeling, software and hardware. One way to improve energy efficiency is to use a new energy source (renewable and environmentally friendly) in the fuel and energy system of Kazakhstan. Therefore, the development of an energy system based on a dual-circuit solar system with a heat pump is an urgent and urgent problem of autonomous energy supply.

Kazakhstan has the potential for the development of solar energy, as our article [**119**], based on actual observations and theoretical calculations, analyzes the most favorable period and region for the use of solar energy in the Almaty region. This article discusses a solar collector with a storage tank, a heat exchanger and pumping stations for hot water. Modeling was performed for various temperature conditions and solar radiation for the Almaty region. The simulation was performed in Matlab + Simulink, as a tool often used for modeling various processes and, in particular, for modeling a solar hot water heating system [**120, 121, 122**]. Modeling can allow assessing the technical feasibility of a solar water heating system and indicate the system nodes that should be changed and improved for the weather conditions of Kazakhstan.

The solar system consists of several parts, to simplify the process of description and modeling, we describe each part of the system separately. (**Figure 6.1**) shows a solar hot water heating system with a heat exchanger in a storage tank. The heat exchanger coil is installed inside the storage tank and allows heating water for consumption. The system is used for heating and hot water supply.

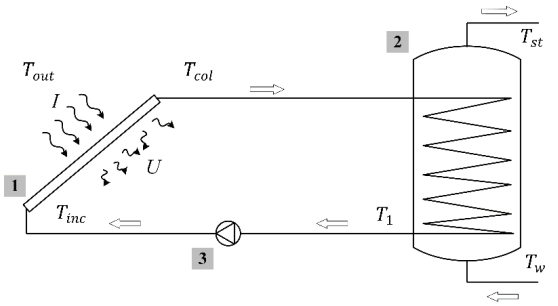

a) The scheme of the solar hot water supply system.

b) The solar hot water supply system was built.

Figure 6.1: Solar hot water system. a - a solar flat collector; b - storage tank with heat exchanger; 3 - pump.

In the central object of study (solar flat collector), we separately described the mathematical model of the solar flat collector (Figure 2.2) and conducted an analysis of energy and exergy. The mathematical model of the reservoir is defined as a function: T_col = f (T_inc, v_p, I, T_out, U), where T_col is the temperature of the fluid at the outlet of the collector, T_inc is the temperature of the fluid at the inlet of the collector, v_col is the volumetric flow rate in the collector cycle, I - solar radiation, T_out - collector ambient temperature, U - collector heat loss coefficient.

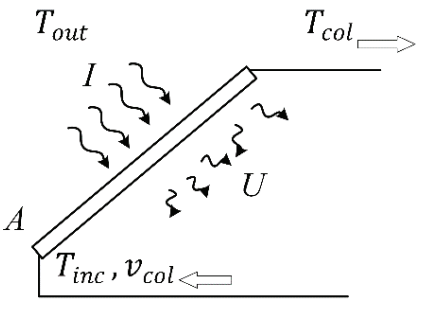

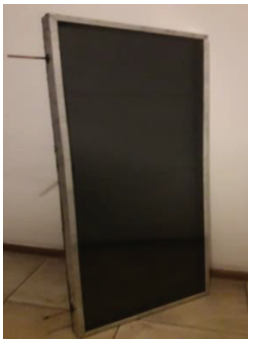

Scheme of a solar flat collector Natural view of a flat solar collector.

Figure 6.2: Solar flat collector.

Energy analysis. Based on the solar energy absorbed by the collector plate, the coefficient of heat loss of the collector and the heat absorbed by the liquid, the energy balance equation can be defined as [58]:

$$\frac{dT_{col}(t)}{dt} = \frac{A\eta}{C} I(t) - \frac{UA}{C}\left(T_{avg}(t) - T_{out}(t)\right) + \frac{v_{col}}{V_{col}}\left(T_1(t) - T_{col}(t)\right) \quad (6.1)$$

where C = ρ_col c_col V_col is the equation for calculating the total heat capacity of the fluid, T_avg (t) = (⟦T_1 (t) + T⟧ _col (t)) / 2 is the average temperature of the fluid in the reservoir.

The input values of the solar flat collector are described in table 6.1. We used these collector parameters to do a heat loss coefficient analysis.

Options	Values	Units measuring
Plate to cover distance	30	mm
Radiation plate	0.95	
Wind heat transfer coefficient	10	W/m^2 ◦C
Collector tilt	45	Degree
Glass emission	0.88	
Area	2	m^2

Table 6.1: Input values of a solar flat collector.

In order to simplify the calculation of differential equations for calculating heat losses, it was proposed to use general loss factors for the solar collector, similar calculations were performed in [**120**].

Consider a solar flat collector for a single glass coating system. The calculation of the loss coefficient for the upper surface is carried out according to the formula:

$$U_t = \left(\frac{1}{h_{c,p-c}+h_{r,p-c}} + \frac{1}{h_w+h_{r,c-a}}\right)^{-1} \quad (6.2)$$

The convection coefficient between the absorbed and the glass coating h_ (c, p-c) is calculated using the parameters of Nusselt, Rayleigh and Prandtl. The heat transfer rate between two plates, inclined at a certain angle to the horizontal, is of obvious importance when working flat collectors. Convective

heat transfer data are usually correlated in terms of two or three dimensionless parameters: the Nusselt number Nu, the Rayleigh number Ra, and the Prandtl number Pr.

$$Nu = \frac{hL}{k} \tag{6.3}$$

The dependence of the Nu and Ra parameters was calculated in [63].

$$Nu = 1 + 1.44\left[1 - \frac{1708(\sin 1.8\beta)^{1,6}}{Ra\cos\beta}\right]\left[1 - \frac{1708}{Ra\cos\beta}\right]^{+} + \left[\left(\frac{Ra\cos\beta}{5830}\right)^{1/3} - 1\right]^{+} \tag{6.4}$$

$$Ra = \frac{g\beta'\Delta TL^3}{v\alpha} \tag{6.5}$$

where h is the heat transfer coefficient:

L is the distance between the absorbent and the glass.

k is the conductivity.

g is the gravitational constant.

β ^ 'is the coefficient of volume expansion.

ΔT is the temperature difference between the boards.

v is the kinematic viscosity.

α is the thermal diffusivity.

To calculate the thermal conductivity coefficient h_ (c, p-c), we use the formula (6.3):

$$h = Nu\frac{k}{L} \tag{6.6}$$

The dependence of the temperature difference between the receiving surface and Ra, is calculated by the formula (6.5). From this formula, we can build the relationship between the Ra number and the temperature difference between the receiving surface and the absorbed one (**Figure 6.3**). From this graph, it can be noted that with a large difference between the surfaces, the number Ra is minimal, which affects the calculation of the number Nu.

The ratio between Ra and Nu is calculated by the formula (6.4). (**Figure 6.4**) is displayed in a logarithmic format. Ra values were generated in the range [**103-105**] and for 5 different collector tilt angles.

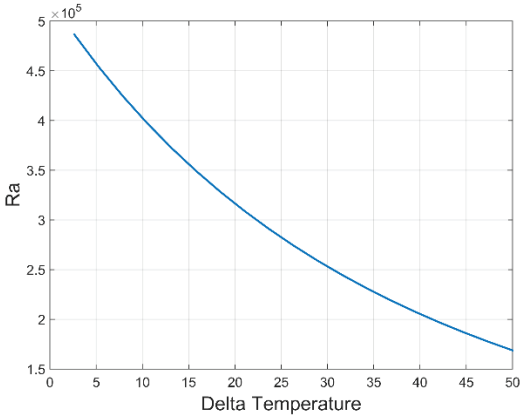

Figure 6.3: Dependence of temperature difference on Ra.

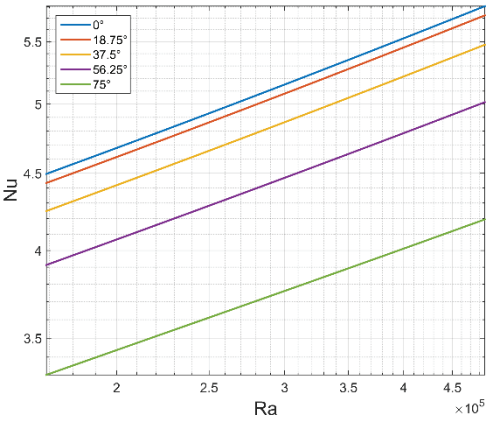

Figure 6.4: The ratio of Ra and Nu at different scales.

(**Figure 6.5**) shows the thermal conductivity, Nu, and heat transfer coefficient between absorbed and glass coating. The maximum values of Nu and thermal conductivity gave the maximum value of the heat transfer coefficient, this must be taken into account when designing a solar flat collector. Our main goal is to collect maximum solar radiation and heat water as quickly as possible.

After calculating the thermal conductivity coefficient, it is necessary to calculate the emissivity from the glass coating to the absorber.

$$h_{r,p-c} = \frac{\sigma(T_p^2+T_c^2)(T_p-T_c)}{\frac{1}{\varepsilon_p}+\frac{1}{\varepsilon_c}-1} \tag{6.7}$$

where ε_c - absorbing emission - 0.88, ε_p - glass emission - 0.95, T_p - absorbent temperature - 100, T_c - glass surface temperature - 50, σ - Stefan - Boltzmann constant - 5.670367x10-5 W m2 K-4.

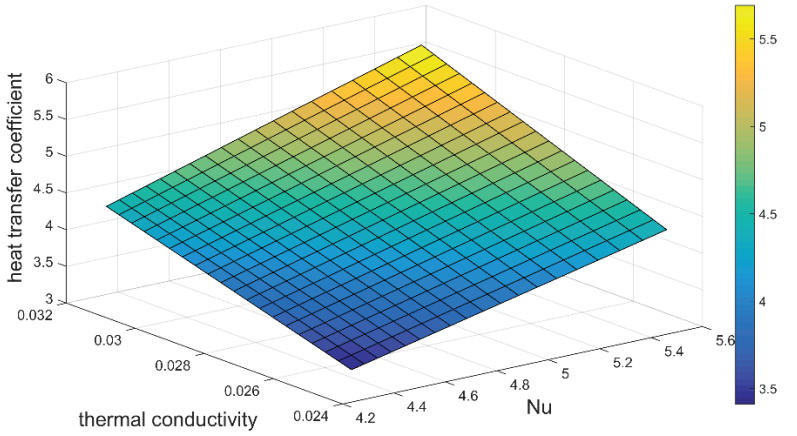

Figure 6.5: Dependence of thermal conductivity Nu on the heat transfer coefficient.

The calculation of the emissivity between the surface of the glass and the air is calculated by the formula:

$$h_{r,c-a} = \varepsilon_c \sigma (T_c^2 + T_a^2)(T_c + T_a) \tag{6.8}$$

The calculation of the surface temperature of the glass is calculated by the formula:

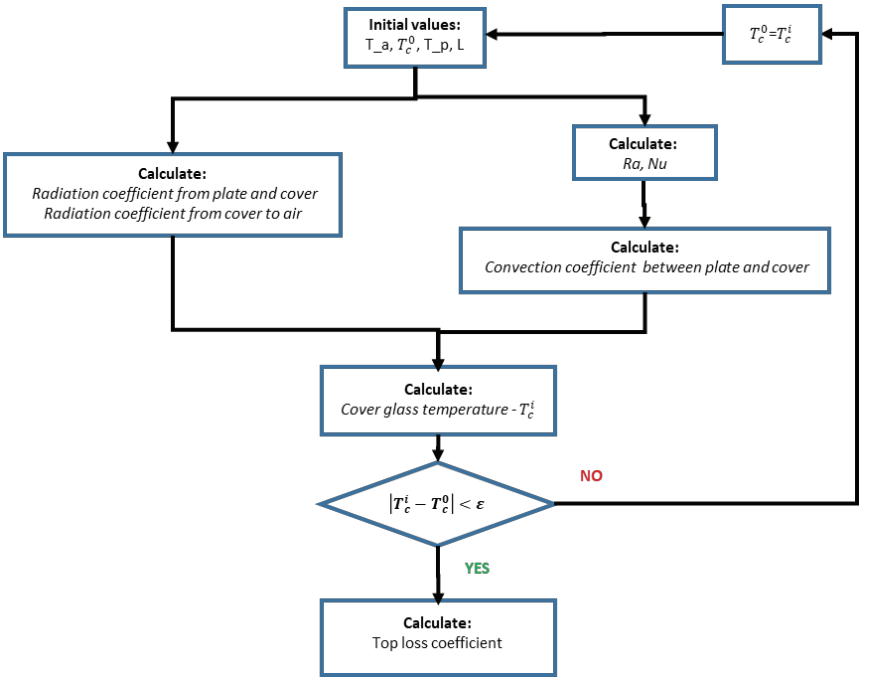

Figure 6.6: The block diagram of the calculation of the coefficient of upper losses.

$$T_c = T_p - \frac{U_t(T_p - T_a)}{h_{c,p-c} + h_{r,p-c}} \quad (6.9)$$

The process of calculating the loss coefficient for the upper surface is iterative and depends on the temperature of the glass surface, in (**Figure 6.6**) is a block diagram of this calculation.

In the calculation, we get the following result for the coefficient of maximum loss:

Input data		**Calculated data**		**Result**	
Ambient temperature ° C	40	Ra	5.28E+05	Maximum loss factor from the collector plate to the environment, W / m2 ° C	7.5286
Coating Temperature ° C	50	Nu	5.4279		
Absorbent temperature, ° C	100	Convection coefficient between cooker and lid, W / m2 ° C	4.8829		
The distance between the coating and the absorbent, m	0.03	Emissivity from plate to cover, W / m2 ° C	8.6584		
		Emissivity for air coating, W / m2 ° C	6.9555		
		Cover glass temperature, ° C	66.6		

Table 6.2: The result of the calculation of the upper loss coefficient.

Based on formula (6.2), a loss coefficient range for the upper surface (one glass surface) was calculated, calculated for different indicators of the ambient temperature [40; twenty; -10], the temperature of the plates has a range from 0 to 200° C with a wind heat transfer coefficient of 10 W / m2C.

In (**Figure 6.7**), we obtained the relationship between the average plate temperature and the loss factor from above. You can notice that the temperature and the loss coefficient increased almost linearly, except from 0 to 60° C. Our calculated coefficient is 7.5286, in the figure this value is equivalent to an average plate temperature of about 120° C. This fact may be possible in the summer.

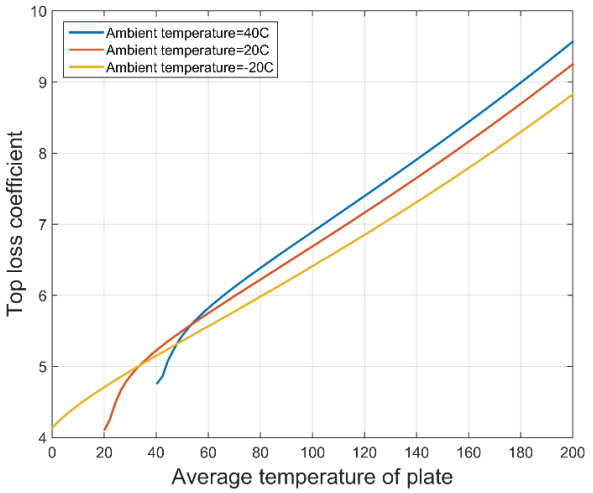

Figure 6.7: The relationship between the average temperature of the plate and the coefficient of losses from above.

The calculation of the loss coefficient for the lower surface of the collector is calculated by the formula:

$$U_b = \frac{k}{L} \tag{6.10}$$

where k is the thermal conductivity of the insulating material (material - 0.04 W / (mK)). L is the thickness of the insulating material.

The heat loss coefficient for lateral boundaries is usually small and often not calculated for the overall heat loss coefficient. If it is necessary to calculate the exact values of heat loss, the calculation will be performed according to the formula [64]:

$$U_e = \frac{(UA)_{edge}}{A} \tag{6.11}$$

where U is calculated by the formula (6.10), but for lateral isolation. Collector Thickness: 0.1 m; insulation thickness: 0.01 m.

The total loss coefficient will be calculated by summing all the coefficients.

$$U = U_t + U_b + U_e \tag{6.12}$$

Modeling and discussion results. MatLab / Simulink performed a simulation of the model, and the model used was taken from [**119**]. The created model was modeled entirely by a solar hot water supply system: flat collector, storage

tank and pumps. Based on the mathematical model of a solar flat collector, a Simulink block diagram was developed, a block diagram of the collector model is shown in (**Figure 6.8**). The result of the simulation is the temperature of the liquid at the outlet of the collector. We selected data for one year in the Almaty region. Input data: solar radiation and ambient temperature.

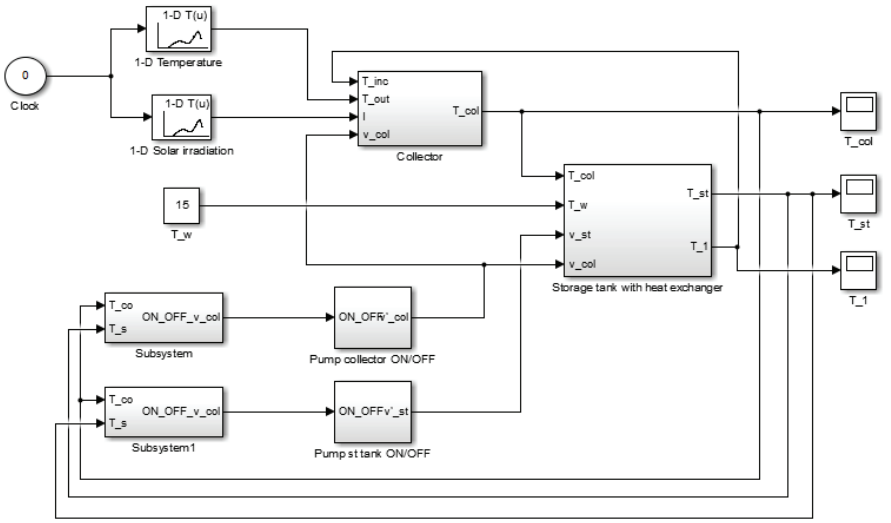

Figure 6.8: General block diagram of a solar hot water system.

The simulation result is shown in (**Figure 6.9**). Based on the figure, it can be noted that for the region, the solar hot water heating system will not provide an acceptable temperature in the flat collector and storage tank, from December to March. The best result (high temperature) of the system will be provided from June to mid-October.

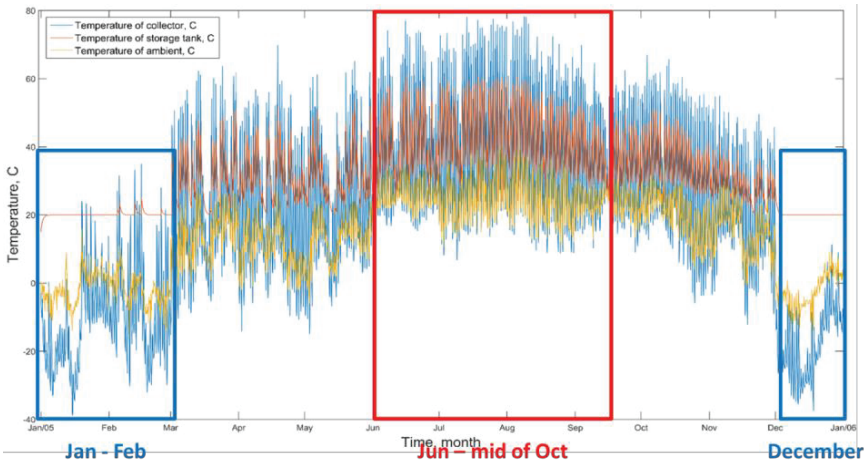

Figure 6.9: Simulation result for one year.

(**Figure 6.10**) shows a high correlation between solar radiation and temperature in the collector and reservoir. If the density of solar radiation is higher, then the temperature is more monotonous, and the standard temperature deviation in the storage is close to the average value, for example, from July to August.

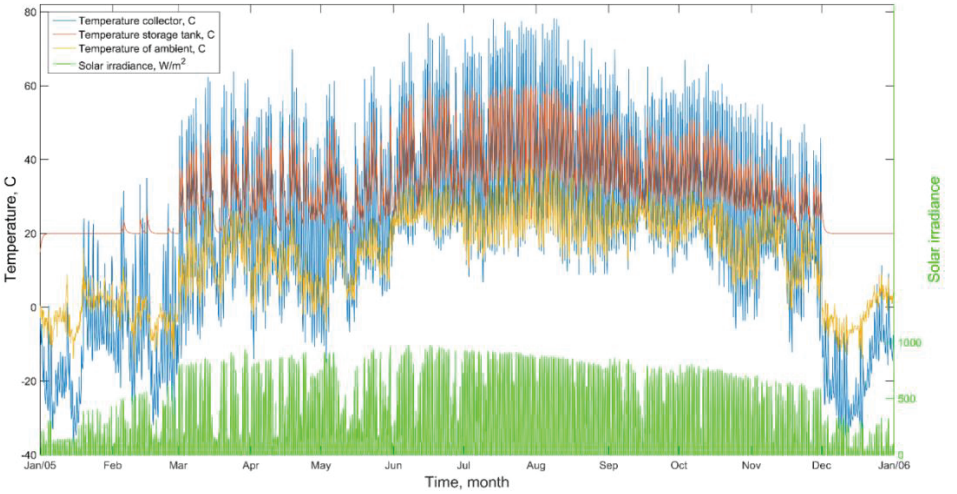

Figure 6.10: The result of the simulation with a comparison of ambient temperature and sunlight.

The pump workflow in the collector cycle depends on the achieved temperature in the collector cycle; we used the same limit values for pump activation as in the study [**119**]. (**Figure 6.11**) shows that in summer the pump switched to regular operation to transfer the achieved temperature from the collector to the storage tank. In winter, the pump is clearly not working.

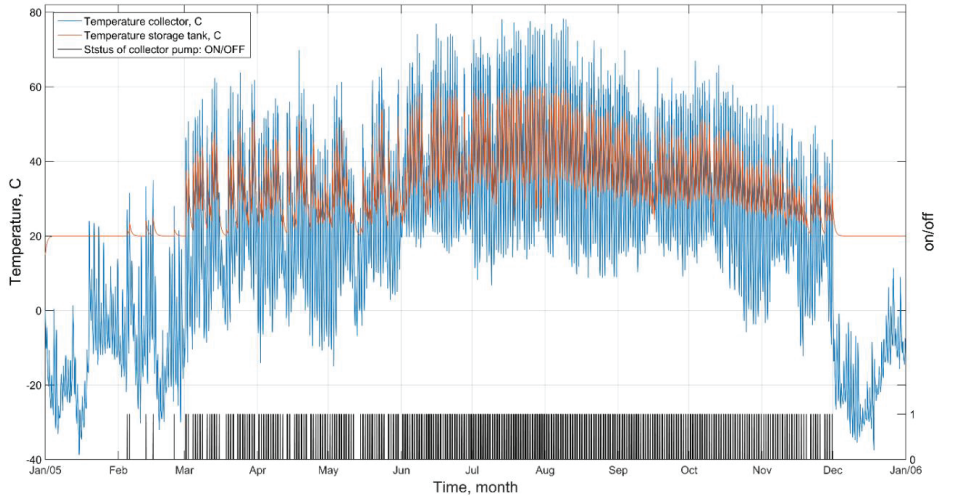

Figure 6.11: The result of the pump in the collector cycle.

For a detailed analysis of the simulation results, we modeled the data up to 3 days (July 1 - July 3). The simulation result showed the maximum water temperature in the storage tank 56.9° C in Almaty region and in the collector - 60.5° C (**Figure 6.12**).

The figure shows the temperature in the collector, tank and pump operating modes. We see a correlation between the ambient temperature and the temperature of the heated water. When the temperature in the collector reaches 40° C, the pump switches and starts transferring the heated liquid to the heat exchanger inside the storage tank and receives the cooled liquid in the collector cycle for heating. The second reason for cooling the liquid in the cycle is related to weather conditions (lower ambient temperature, sunset).

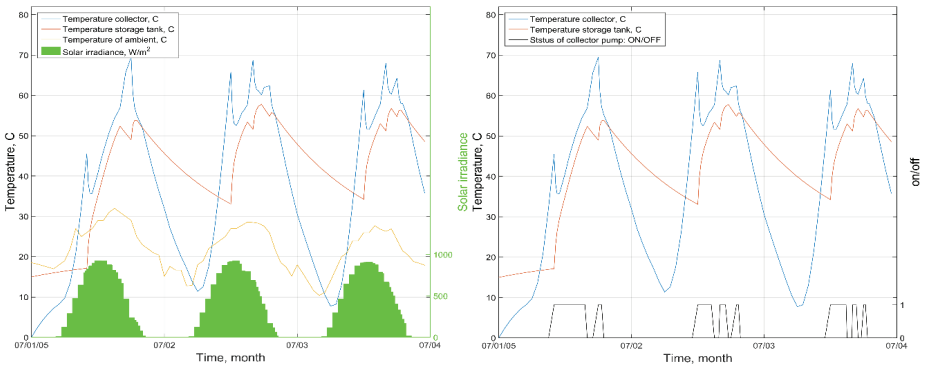

Figure 6.12: Ambient temperature and temperature in the collector and tank with the pump operating mode.

Before performing water heating simulations, it is necessary to analyze the technical characteristics of a flat solar collector, such as collector heat loss. This analysis takes longer, but allows you to simulate more accurate results. After calculating the values, you can begin to analyze the energy. The main goal of the simulation model is to determine the limit values of the installation and identify weak points of the installation for improvement. The developed simulation model allows you to simulate the operation of the solar hot water system in various climatic conditions (temperature and solar radiation) and various individual system parameters to increase the efficiency of the system in various climatic conditions of Kazakhstan.

The simulation result showed that in the daytime the temperature of the water in the collector is 70° C, and during this period it can be used at home. The main problem is the storage of heated water, since the heated water is cooled at night. Another task that we can determine from the analysis of modeling is to find a way to extend the period of operation of the system with high efficiency (April-October), perhaps it will be engineering, technical or programming controller solutions. This moment needs to be investigated and improved.

The next stage of research will be the numerical simulation of the reservoir design. It is necessary to define a design with high and low efficiency. We will determine the optimal system parameters for various climatic conditions, using machine learning algorithms to configure the parameters. We will conduct an experiment and a comparative analysis of the simulated and experimental data.

Building a Predictive Model Using the Lightgbm Machine Learning Program for Solar Controllers

Numerical solutions of statistical data and the construction of a predictive model using the LightGBM machine learning program for a solar heating system were carried out in the work. Gradient Boosting Decision Tree (GBDT) is a popular machine learning algorithm and has quite a few efficient implementations such as XGBoost and pGBRT. To solve a specific algorithm for solving the problem, thresholds are conditionally selected so that the target variable falls on the right, the input variables grow. We developed four algorithms that show how, with the help of the machine learning program LightGBM, the ability to build functional dependencies between input and output parameters was established. From the numerical experiments done, we can conclude. LightGBM is well trained enough, speeds up the learning process, which can be further said that the LightGBM package is well trained for solar heating systems.

One widely used machine learning algorithm is the Gradient Decision Tree (GBDT) [**127**], which is well-efficient, accurate, and interpretable. In many machine learning tasks, GBDT achieves the most advanced advances such as multi-class classification [**125**], click forecasting and rank training [**126**]. In recent years, GBDT has faced new challenges with the advent of big data (in terms of number of functions and number of cases), especially accuracy and efficiency. Conventional GBDT implementations should, for each function, scan all data instances to evaluate the gain in information of all possible split points. Therefore, their computational complexity will be proportional to both the number of functions and the number of instances. This makes these implementations very time consuming when processing big data.

LightGBM has target and input variables. To solve a specific algorithm for solving the problem, thresholds are conditionally selected so that the target variable falls on the right, the input variables grow. GBDT is an ensemble model of decision trees that are trained in sequence [**126**]. In each iteration, the GBDT examines decision trees by selecting n

Algorithm 1: Regression method

```
import pandas as pd
from sklearn.model_selection import train_test_split, RandomizedSearchCV
import lightgbm as lgb
from sklearn.metrics import mean_squared_error
import matplotlib.pyplot as plt
params = {
  'boosting_type': 'gbdt',
  'objective': 'regression',
  'metric': {'l2', 'l1'},
  'num_leaves': 31,
  'learning_rate': 0.05,
  'feature_fraction': 0.9,
  'bagging_fraction': 0.8,
  'bagging_freq': 5,
  'verbose': 0
}
%matplotlib inline
```

Using the LightGBM software package, a regression method was developed when the target variable is continuously discrete, as in the example of solar radiation, total solar radiation, and atmospheric air heat. Reads distances, that is, the metrics l1 and l2, where l1 is the sum of the absolute values of the difference, l2 is the sum of the squares of the differences. This algorithm has a collection of Boost class libraries, which shows the weight of the sample and serves as a good indicator of the importance of data instances. However, GBDT does not have its own sampling weights, and thus the sampling methods proposed for AdaBoost cannot be applied directly. For each data instance in LigtGBM provides us with useful information for data sampling. That is, if an instance is associated with a slight bias, the learning error for this instance is small, and it is already well trained.

Algorithm 2: Leaf count

```
data = pd.read_excel("D:\\temp\\mura.xlsx", skiprows=1)
data.columns = ["col%s"%ind for ind in range(11)]
```

In the second algorithm, the number of leaves is calculated, where the leaf is the end point, which allows you to set the accuracy of parameter prediction.

Algorithm 3: Learning speed

```
for ind in range(1,10,1):
data['col%s'%ind] = data['col%s'%ind].astype('float64')
INPUT = ['col1','col2','col3','col4']
OUTPUT = ['col5','col6','col7','col8','col9','col10']
ORIGIN = [u'T bak',u'T koll vyh',u'KPD',u'T sol rad',u'Hladoproizvod tep nas',u'Teploproizv Tep nas']
```

The 3 algorithm considers the learning speed, which allows you to adjust the selection step. In this algorithm, there can be not one threshold, but several thresholds. When solving this problem, for calculating the thermodynamic and thermotechnical parameters of the solar heat supply system, it is not necessary to normalize the input variables.

Algorithm 4: Test and training sets

```
def train_gbm(data,col,cnt):
    X_train, X_test, y_train, y_test = train_test_split(data[INPUT] , data[col], test_size = 0.20)
  # create dataset for lightgbm
  lgb_train = lgb.Dataset(X_train, y_train)
  lgb_eval = lgb.Dataset(X_test, y_test, reference=lgb_train)
  print('Starting training...',col)
  # train
  gbm = lgb.train(params,
            lgb_train,
            num_boost_round=20,
            valid_sets=lgb_eval,
            early_stopping_rounds=5)

  print('Saving model...')
  # save model to file
  gbm.save_model('model.txt')
```

```
    print('Starting predicting...')
    # predict
    y_pred = gbm.predict(X_test, num_iteration=gbm.best_iteration)
    # eval
     print('The rmse of prediction is:', mean_squared_error(y_test, y_pred) **
0.5)
    ax = plt.subplot(2,3,cnt+1)
    plt.plot(list(range(1,21,1)),y_test,'b')
    plt.plot(list(range(1,21,1)),y_pred,'r')
    ax.set_title(ORIGIN[cnt-1])
plt.figure(figsize=(15,15))
for cnt,col in enumerate(OUTPUT):
    train_gbm(data,col,cnt)
```

In order to test the prognostic model in 4 algorithms, they are divided into test and training sets with a ratio of 20 to 80. The resulting graphs when testing the thermal parameters along the abscissa from 0 to 20 are the numbers of test cases, and along the ordinate are the input and output parameters of the solar heating system

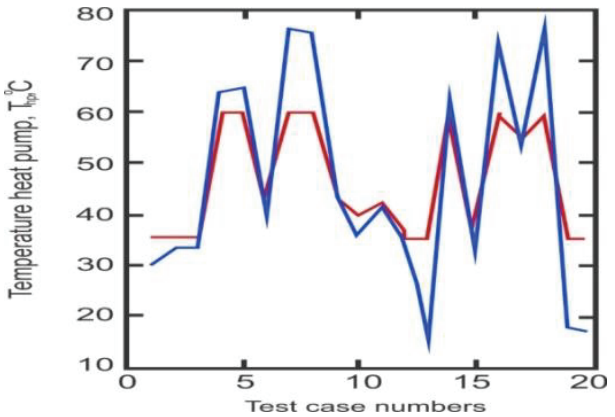

Figure 6.13: Dependence of the temperature of the storage tank on the number of test cases.

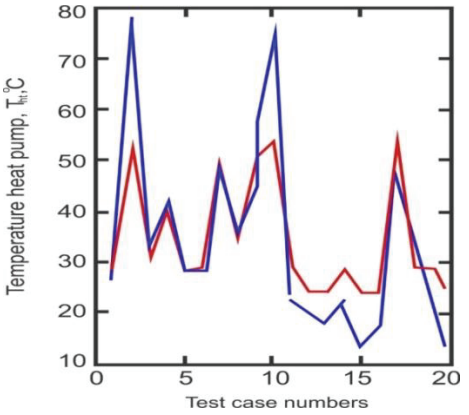

Figure 6.14: Dependence of the temperature of the heat output of the heat pump on the number of test cases.

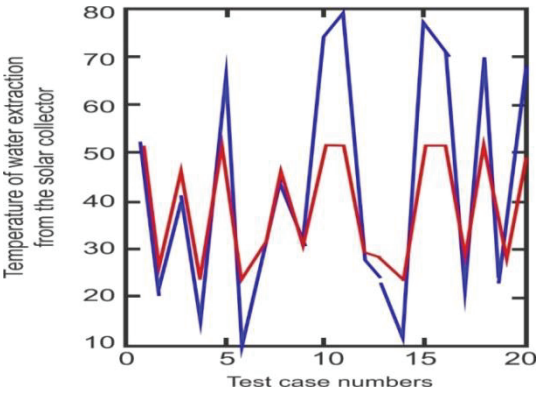

Figure 6.15: Dependence of the temperature of water outlet from the solar collector from the number of test cases.

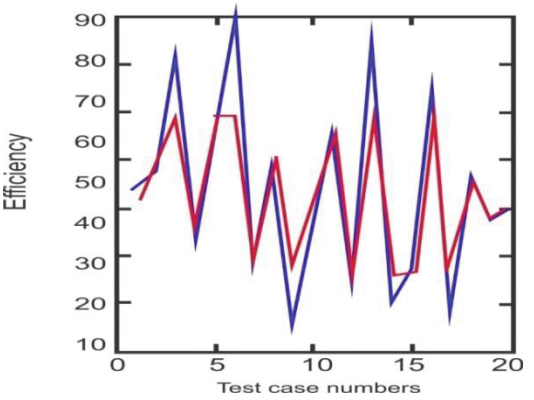

Figure 6.16: The dependence of the efficiency of the solar thermal installation on the number of test cases.

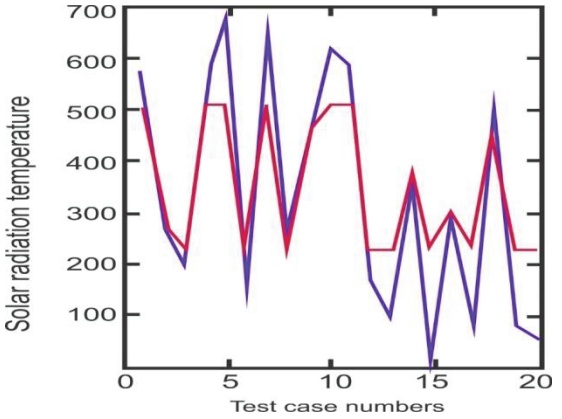

Figure 6.17: The dependence of the temperature of solar radiation in Almaty (Kazakhstan) on the number of test cases.

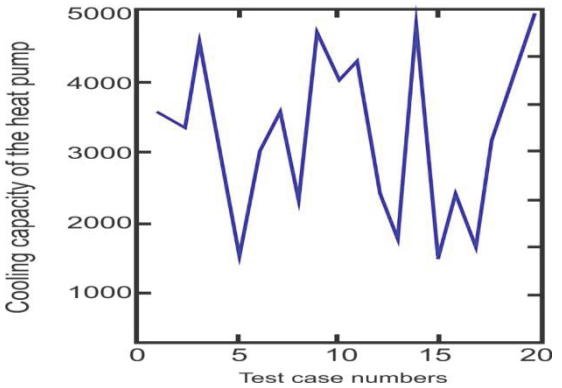

Figure 6.18: Dependence of the temperature of the cooling capacity of the heat pump of the number of test cases.

When modeling a predictive model using machine learning to develop a mathematical model of the solar collector + heat pump system, the forms are repeated according to the training model. As a result of numerical statistical experiments and the construction of a prognostic model, the possibility of constructing functional dependencies between input and output parameters was established. The error between the experimental (laboratory) numerical (statistical) methods is that the temperature of the battery tank is 7.775 degrees, the temperature of the hot water outlet from the solar collector is 4.49 degrees, the efficiency of the entire solar heating system is 7.74 degrees, the temperature of solar radiation is 4.66 degrees , the heat output of the heat pump is 87 degrees, and the refrigeration capacity is 15 degrees. From this we can conclude that in the future the LightGBM package is quite well trained. You can also expand the training set, which potentially improve the accuracy of parameter prediction.

Designing Architecture for Storing Data from Solar Collectors in the Network

This section discusses the problem of collecting and storing data from technical devices connected to a single control and monitoring network. As a technical device, a solar water heating system is considered. Basically, these systems do not contain sensors for collecting information about the system or sensors for controlling the system. Today, the data is very valuable for modeling, predicting and managing the system, therefore, digitalization of devices that will optimize the work process takes place in production. The study addresses the problem of collecting and storing data from systems that generate large amounts of data with a high frequency in time. Existing solutions to solve this problem are described. A solution based on the Orleans framework that is optimally suited for the task was chosen.

In industrial processes, the amount of data coming from one unit can reach 100 MB per day. At the same time, the number of sensors with which the unit is equipped, as well as the number of units in general, is not limited. In connection with such conditions, there are problems of constructing such an architecture of an information system that will be able to scale horizontally in order to increase throughput with an increase in data flow, and to reduce energy consumption while reducing load [**129-132**].

One solar collector can be equipped with an unlimited number of sensors that can operate in various modes of the frequency of information retrieval, as well as transmitting it to the control panel. At the same time, a well-established architectural solution today is to equip the unit with a central controller with predetermined technological characteristics for collecting data from sensors, aggregating them and transmitting them to a central control panel or in passive mode and providing an access interface to the accumulated data in queue mode. With the active mode - it is necessary to pre-configure the equipment and indicate the destination of data transfer. In passive mode, the controller collects data from the sensors into the operational data bank until the memory is exhausted, after which new data begins to be replaced by older ones according to the queue rule - FIFO.

Choosing a controller for the unit is an important decision. It is necessary to compare the operating modes with the acceptable operating modes of the controller. For example, technological equipment operating in high vibration mode (for example, turbines) require special types of controllers that can withstand physical impact for a long period of time. The same issues arise with temperature, humidity, pressure, and environmental aggressiveness.

The solar collector is a specialized unit for converting sunlight into heat. Today, the technological device has a number of implementations, starting with the simplest and ending with highly intelligent units that can adapt to a given

temperature regime, equipped with protection mechanisms from overheating and overcooling [**133**].

Within the framework of a given scientific research, the task was set of creating a centralized system for collecting information from geographically distributed solar collectors (**Figure 6.19**). Data collection will solve the following issues:

- Timely troubleshooting and notification of the user about the need for service.
- Building predictive models of efficiency through territorial interpolation.

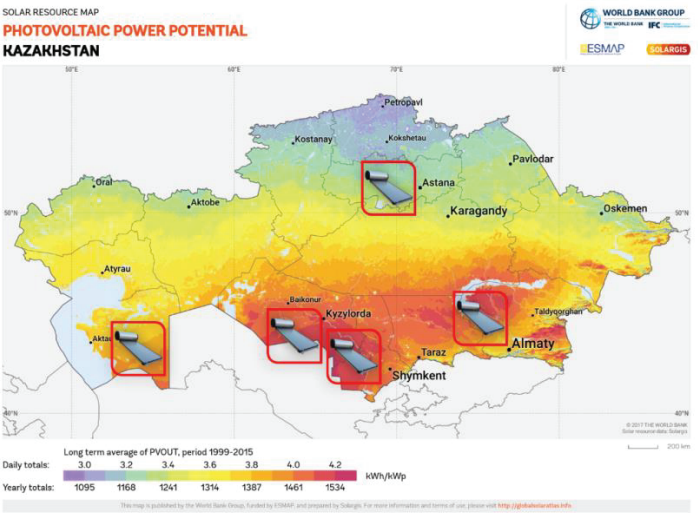

Figure 6.19: The potential location of the collector network in Kazakhstan.

The difficulty in implementing the system lies in the potential number of simultaneously active sessions between the unit controller and the data processing server. Any hardware has its own limits of possible loads and operating modes.

A typical, for example, parameter of simultaneously supported network connections for a standard operating system is 65 535 [**134**, **135**]. Accordingly, in order to connect the next unit, it is necessary that the session of the previous one be closed. In this mode, there are conditions for connection failure and flushing of the data buffer scheduled for writing. To solve these problems, a network of computing resources is organized, connected into a single information system, which is a cloud in modern language. At the same time, the task of dynamic proportional load distribution and fault tolerance with the possibility of connecting additional computing resources in case of an increase in the number of one-time sessions is set within the cloud [**136**].

The second example of organizational complexity of implementing such an information system is the choice of data warehouse architecture. Based on

the requirements for industrial technological processes - the storage should meet the criteria:

- High availability.
- Fault tolerance.

Data storage architecture.

Today, in the context of the tasks of the Internet of things, the inapplicability of classical relational information storage models has become apparent. Relational models do a good job of normalizing data, combating anomalies, and losing integrity. However, they poorly demonstrate their capabilities in terms of high availability and efficient storage. Therefore, such solutions appear as a column - oriented storages, graph - oriented storages, document - oriented storages, key-value, and time series storages [**137**]. Each of these types of storages in their own way uses the features of the hardware, the capabilities of the operating system and are designed to solve a specific narrow task that they solve better than other methods. It is clear that for the task of storing sensor data from various units, the primary goal is an effective mechanism for collecting and recording data in information stores. At the same time, the data arrives necessarily in chronological order, the volume of this data can be infinitely large, the intensity of data arrival also tends to infinity. Accordingly, a solution capable of infinite horizontal scalability is needed. Thus, if one magneto-mechanical hard drive is capable of maximum peak output / reception of data at 100MB per second, then the recording requirements of 1000MB per second make it necessary to use 10 hard drives at a time.

Currently, there are many different solutions for implementing a given information system. For example, the InfluxDB storage system, designed to use the storage mechanisms of historical data. A feature of this system is the physical model of data storage and the ability to scale and distribute data on disparate hardware resources. The second example that could be applied is the Akka framework (set of libraries and technological environment), built on the JVM infrastructure. The Akka framework implements the agent model proposed back in the 70s. The main point is the abstraction of the function performed from the physical location of the computing resource, which allows you to increase the number of outgoing agents from the given performance requirements. The agent model has been implemented in a variety of programming environments and languages.

Orleans framework. As part of the current study, it was decided to use a solution based on the Orleans framework [**138**, **139**, **140**]. One of the advantages of this framework being developed by Microsoft and now having the status of an open source project is the use of the widely used C # programming language. The C # language is an inheritor of the C language. Programs written on it are executed by the DotNet virtual machine. The language has laconicism and all

modern tools, and techniques for writing program codes, including the ability to use low-level programming techniques - working with pointers.

Orleans is a specialized system for distributed computing, designed for high loads, with the properties of fault tolerance. Implements an agent model, and calls it a virtual agent, since the location and state of the agent is not known. Each agent can be in two states - active / inactive (**Figure 6.20**).

The activation process of each agent is a simple request for it by identifier. If the object does not exist in the information environment, it will be created. If necessary, agents are deleted from the memory, then their status is treated as inactive (**Figure 6.20**).

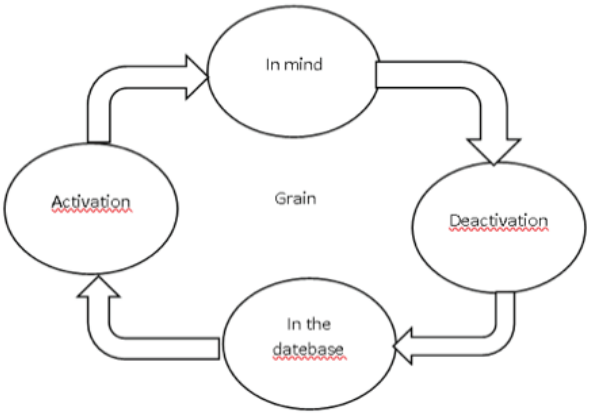

Figure 6.20: Object state graph.

Thus, even if one of the machines of the information infrastructure fails, and all agents located on this machine disappear, then when they are requested by their identification numbers, they will be recreated on the remaining machines.

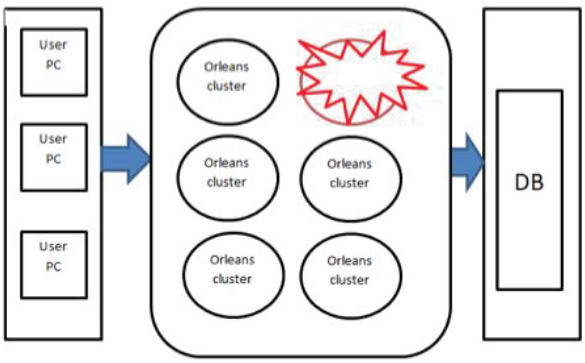

Figure 6.21: The situation of the loss of the computing node.

The framework is completely asynchronous and exchanges data on the basis of TCP / IP protocols between computing nodes in multiplexed mode. Each agent runs in single-threaded mode, which protects it from situations of non-consistent state.

Thus, the framework allows you to store a highly dynamic infrastructure of information system objects in the RAM of all the computing resources involved in the work. Organization of access to these objects is carried out by requesting them by their identification number, which can be either a simple number or a more complex form such as GUIDs and combinations. The organization of storing the state of objects in a persistent storage is abstracted through implementations of various kinds, from relational DBMSs to document-oriented and even user solutions that implement a data read / write interface (**Figure 6.22**).

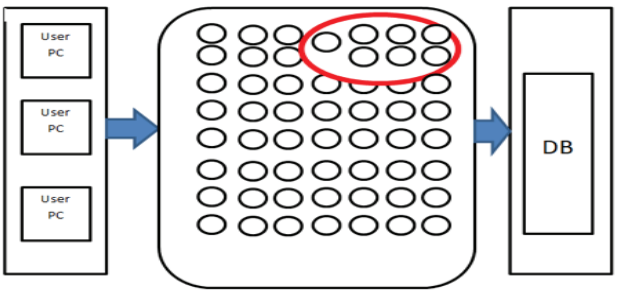

Figure 6.22: Orleans architecture at the highest level.

The architecture of such a solution is based on 2 main types of entities - is it an atomic object or an atomic message queue. The framework allows us to ignore the complexity of the distributed storage of these objects on various servers and concentrate on the business process that we carry out.

Under normal conditions, without using the framework, programmers are faced with the problem of bottlenecks, which are the DBMS (**Figure 6.23**). No matter how productive it is, there always came a moment when the number of write requests was much more than the physical device could handle.

The image shows that the DBMS is becoming a clear bottleneck that can lead to a non-consistent state of the system, since there can be hundreds of thousands of devices, there can be 10 times more requests than the devices themselves (**Figure 6.23**). Obviously, a new solution is needed to solve this problem, as shown in the following image.

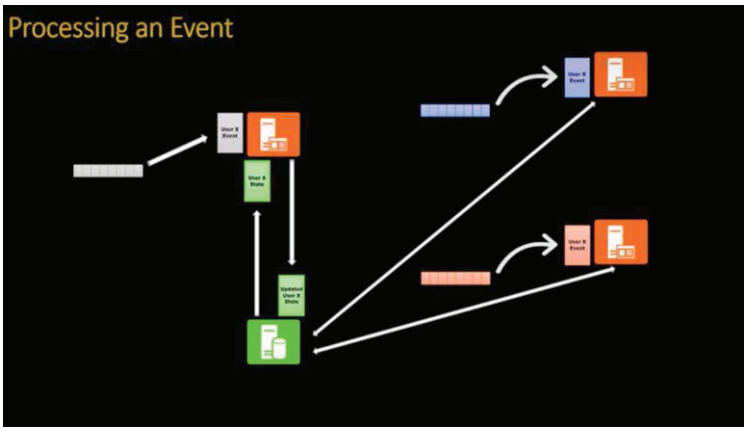

Figure 6.23: The process of collecting data from various devices.

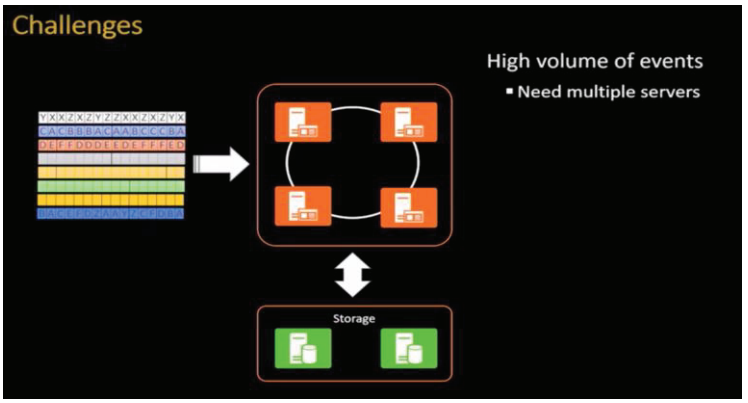

Figure 6.24: Conceptual scheme for solving the problem of system instability.

The framework allows you to operate with the concept of object-oriented programming without the need to blow into the details of the implementation of a particular data warehouse architecture. In this case, the framework is an implementation of both a business model and a data warehouse all rolled into one. Data falling into the guaranteed information infrastructure is in a consistent state at any given time. Reading data and calculating derivatives is carried out using all computing resources that are active on the data point in time. Thus, the system can operate with a single computer serving the requests of several solar collectors, as well as with an unlimited number of solar collectors by connecting additional computing resources and connecting them to the computing cluster. In the case of a reverse rollback (reducing the number of solar collectors in the system), in the system it is enough to simply turn off the redundant machines included in the cluster.

Chapter 7

Management and Software for Double-Circuit Solar Heating Systems with Thermosiphonic Circulation

Authors
Amirgaliyev Y.N, Kunelbayev M, Kalizhanova A.U, Kozbakova A. Kh, Daulbayev S.M, Auelbekov O. A, Kataev N.S, Yedilkhan D, Merembayev T, Ormanov T. A, Sundetov T.

[*]**Corresponding author:** Ministry of Education and Science of the Republic of Kazakhstan Committee of Science Republican State Enterprise Institute of Information and Computational Technologies, E-mail: murat7508@yandex.kz

The use of renewable energy sources contributes to the spread of a continuous increase in energy demand and to the increased participation of environmentally friendly technologies. Photothermal conversion in solar thermal systems is one of the most common ways to use this energy [**141,142**]. The need to provide appropriate operating parameters of the system ensures the use of correctly selected and configured controllers. Solar controllers are manufactured by many companies and firms [**143-146**]. Despite the wide range of solutions available, the controllers are still mostly closed-loop devices and have virtually no expansion options. On the other hand, flexible solutions based on programmable controllers (PLC Programmable

Logic Controller) are applicable only in large systems due to the very high cost of PLCs [**147**]. Recently, however, one can notice a growing demand for fully programmable modular controllers that allow you to integrate several systems into a single operating system. No less important for users is the implementation of a number of additional functions. For example, a control and monitoring system via the Internet [**148**] or the use of a power source with photovoltaic panels [**149**, **150**]. To date, implementations of such systems have relied solely on PLCs, but because of their high cost, they are rarely used in residential installations. Although modularity and extensibility are already offered by several manufacturers of solar controllers, for example, [**151**] However, the software of these devices is still closed. With the proliferation of low-cost microcontroller platforms such as Arduino [**152**], it has become possible to design controllers in a small series and adapt their software to the needs of a particular client. It is also worth noting that such controllers can be easily upgraded when expanding a supported system. Regardless of the design, solar controllers for non-standard, custom-made installations must comply with the requirements defined by the PN-EN 12977 standard [**153**, **154**].

The functionality of the solar thermostat. The main function of each solar controller is to control the solar circuit pump based on the temperature difference between the collector and the hot water tank. Larger systems support collector groups that are located on different parts of the roof. Such systems often support a group of hot water tanks, a pool or underfloor heating. Simple controllers allow only a control signal to be generated for pumps. More sophisticated controllers also allow variable speed pumps to be controlled using a PWM (Pulse Width Modulation) signal, which improves control quality and helps reduce power consumption. The efficiency of the differential thermostat 81 was studied in detail in the 80s and 90s of the twentieth century [**154**]. Several studies, for example [**155**] indicate a significant relationship between energy output and the setting of a differential thermostat. It is shown that the use of a variable controller hysteresis adapted to the current system conditions allows increasing the output of solar energy and, in addition, reducing electricity consumption. However, almost all commercially available solar thermostats provide pump control based on constant hysteresis. The increase in fluid volume must be compensated for by the expansion tank in a well-designed system, but weak design or implementation, as well as a defect in the expansion tank, can damage the system. For this reason, a significant number of users of the solar system decide to invest in an emergency power source [150] or even in a common power system using photovoltaic panels [**151**]. This is all the more justified, since the greatest demand for power associated with the circulation pump at maximum power coincides with the highest power generated by photovoltaic cells. The main controllers provide only the readings of 3-4 temperature sensors in the tanks and collectors of hot water. More complex devices allow the use of up to 5-7 temperature sensors.

Modular Controller for Solar Thermal System

Controllers designed to control solar thermal installations, in particular, must be characterized by a modular structure. This allows you to update the functionality of the controller with further development of the installation. This chapter provides an example of a prototype modular solar controller based on the freely programmable platform Mojo v3 FPGA board [**148**]. The block diagram of the controller is shown in (**Figure 7.1**). The prototype of the controller consists of a central unit that combines all the main control functions, and three main expansion modules: system monitoring, backup power and a weather station.

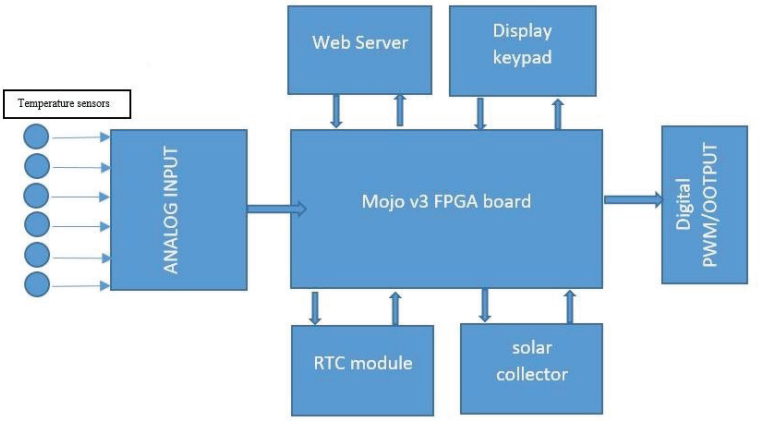

Figure 7.1: The block diagram of the control controller of a dual-circuit solar installation with thermosiphon circulation.

The central unit of the solar controller is based on the Arduino Ethernet platform (**Figure 7.2**), where RJ45 is an Ethernet port; Reset KEY- reset Ethernet shield and Arduino when pressed; SD card - support Micro SD card in FAT16 or FAT32; maximum memory capacity is 2 GB; IC W5200 is a hardware TCP / IP Ethernet controller.

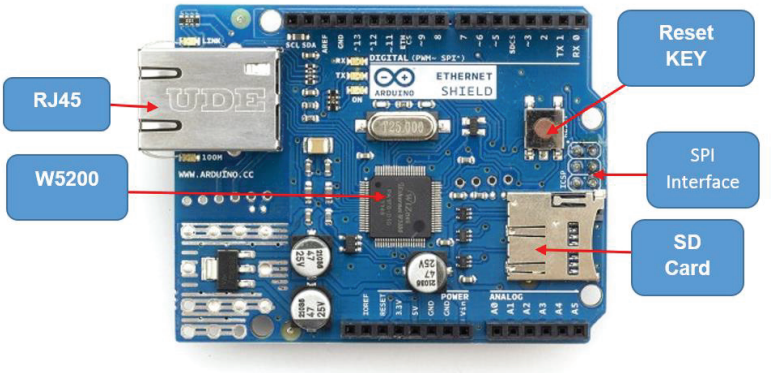

Figure 7.2: Central control unit of a double-circuit solar control system with thermosiphon circulation.

This system uses an Atmel ATmega328 microcontroller operating at a clock frequency of 16 MHz. Equipped with communication interfaces such as SPI, I2C [**156**] and Ethernet, several additional modules can be connected. To provide basic local service, the controller is equipped with a small graphic display (1.8-inch diagonal, resolution 160 × 128 pixels), which communicates with the microcontroller via the SPI bus. In addition to the communication interfaces, the central unit is equipped with 6 analog inputs (for example, for temperature sensors) and 9 available digital inputs / outputs (including 4 PWM for controlling the pump speed). This number of I / O channels allows you to configure the software for a supported installation. The microcontroller is programmed in a language similar to C using the Arduino IDE software development environment.

The presented controller provides a number of monitoring functions for a solar installation. Using the micro-SD card slot built into the Arduino system allows you to implement a data logger that records selected data about the installation. The diagram (**Figure 7.3**) shows a sample of the recorded data of the selected parameters of the solar installation. A large number of measuring channels allows you to add additional temperature sensors at the inlet and outlet of the solar collector, as well as a flow meter.

Experiment. In this study, six digital temperature sensors (Dallas DS18B20) 2,3,4,5,6,7 record the temperature of a flat solar collector with a thermosiphon. Sensors are monitored by a Mojo v3 programmable logistic integrated circuit. Recording the temperature readings stored on the ETHERNET modul 9, sends temperature data and valve states 10 at every 5s intervals. The real-time clock (RTC) 8 records the date and time of the temperature data measurements,

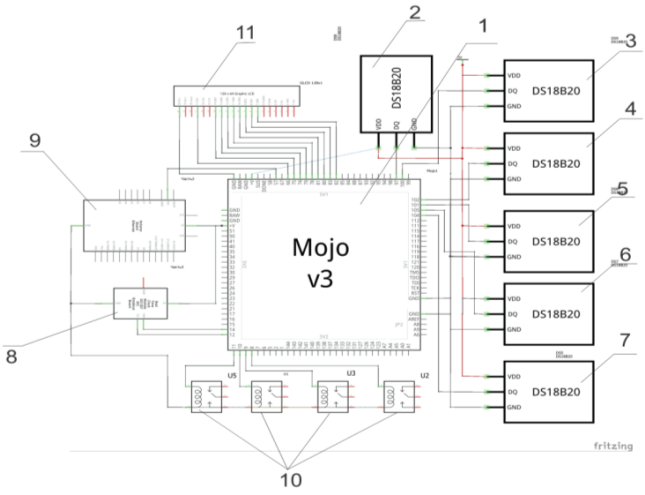

Figure 7.3: Schematic diagram of the connection of Mojo V3 with sensors of the controller control system.

sending them to the Mojo v3 programmable logistic integrated circuit. Six sensors are connected to the Mojo v3 board. with six electric wires, programmed in the VHDL language, which, after processing the temperature data, the date and time received from RTC 8, respectively, save them in XML (extensible markup language) in the ETHERNET module.

The XML language facilitates the processing of this data by automatically or manually interpreting data spreadsheet programs. The temperature data, date, time and valve status of the installation system are displayed on display 11.

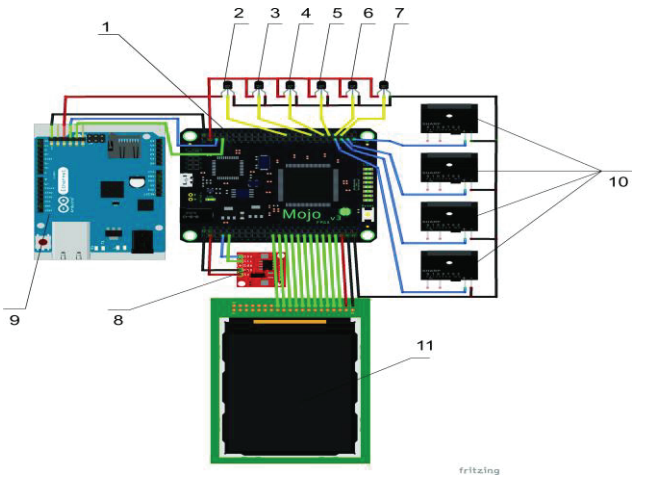

Figure 7.4: Schematic diagram of the controller on the platform Mojo v3.

To create and study a monitoring platform for the thermal control system of a solar installation based on the use of the Mojo v3 platform, the principle of operation of each element from which the network management and monitoring controller will be made is described.

Mojo v3 is a Spartan 6 XC6SLX9 FPGA logic-84 integrated circuit with 84 digital I / O, 8 analog inputs. 8 general-purpose LEDs, 1 reset button, 1 LED to show when the FPGA is configured correctly.

Built-in voltage regulation can withstand 4.8 V - 12 V. And also consists of a microcontroller (ATmega32U4) used to configure FPGA, USB-connection and read analog outputs. A compatible Arduino bootloader is integrated, making it easy to program and microcontroller. On board the flash memory for storing the FPGA configuration file, the Mojo v3 version has a more reliable USB port than v2, minor cosmetic changes and an updated microcontroller with additional memory to add its own code.

(**Figure 7.5**) shows a digital temperature meter DS18B20 whose feature is that the digital temperature meter has a resolution of conversion of 9 to 12 digits and a temperature control alarm function. Monitoring parameters can be set by the user and stored in the non-volatile memory of the sensor. The DS18B20

communicates with the microcontroller via a single-wire communication line using the 1-Wire interface protocol.

Sensor power can be obtained directly from the data line, without using an external source. In this mode, the sensor is powered by energy stored in the stray capacitance.

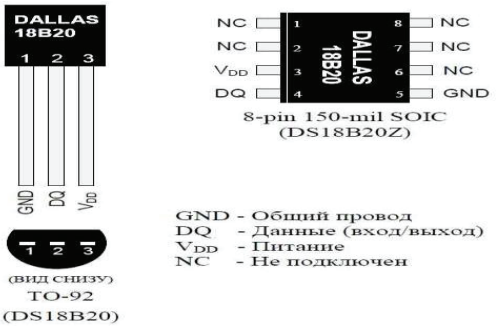

Figure 7.5: DS18B20 Digital Temperature Meter.

The temperature measurement range is from -55 to +125° C. For the range from -10 to +85° C, the error does not exceed 0.5° C. Each DS18B20 chip has a unique 64-bit serial code that allows multiple sensors to connect to one common communication line. Those. through one port of the microcontroller it is possible to exchange data with several sensors distributed over a considerable distance. The mode is extremely convenient for use in environmental control systems, temperature monitoring in buildings, equipment nodes. To expand the functionality of the controller control system, a real-time clock was used - Real Time Clock Module with battery (DS1307) and 16 character LCD displays, which are shown below in (**Figure 7.6**).

Feature of DS1307 module with real time clock. is that the module comes fully assembled and with a programmed current time (you only need to set your time zone before use). Using the equipped lithium battery (CR2032-210mAh) the module can work for at least 5 years without an additional 5V power supply.

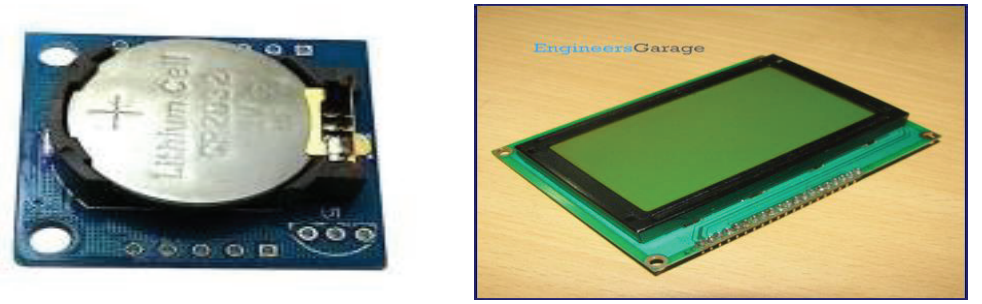

a) Real Time Clock - Real Time Clock Battery Module (DS1307).

b) 16-character LCD displays.

Figure 7.6: DS1307 module with real time clock.

In addition to the real-time clock chip, the module also contains the I2C EEPROM 24C32 chip and an interface for connecting the DS18B20 temperature sensor. The EEPROM non-volatile memory chip allows you to save data received from the sensor locally on the module without the need to constantly pull the microcontroller. The interface to the DS18B20 sensor with a pull-up resistor allows you to add temperature monitoring to the system.

The LCD has a display format of 128x64 pixels and has a yellow-green backlight. Each LCD requires a controller to carry out its internal operations. The LCD uses two KS0108 controllers. Naturally, 16-character LCDs have their limitations in the number of characters displayed. Thus, graphic LCD displays are used to display customized characters and images.

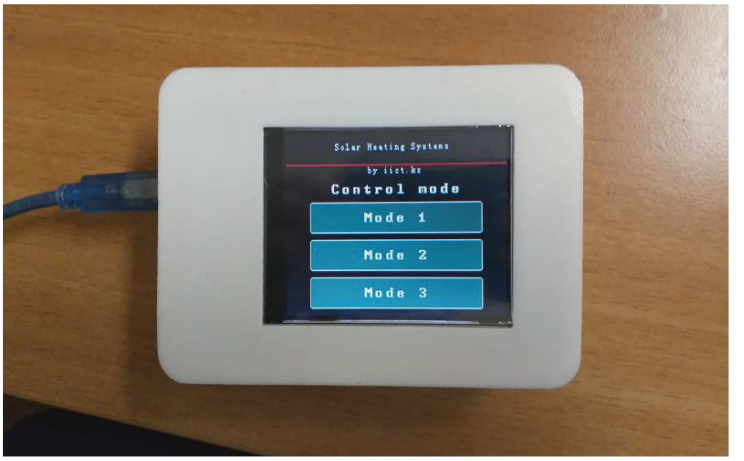

Figure 7.7: Solar control controller.

Dimensions (mm)	120x120x23
Power, (V)	AC110 / AC220
Consumption (W)	< 3
Accuracy of temperature measurement, (° C)	-/+2
Range of measurement of temperature of a collector, (° C)	-10…220
Range of measurement of temperature of a tank, (° C)	0…+110
Maximum power of the pump, (W)	3 шт < 300
Inputs	1 шт pt1000, 2 шт ntc10k
Outputs (relays for pump, valve, heater)	10 A
Operating temperatures (° C)	-10 +50
Класс водозащиты	IP40

Table 7.1: Technical characteristics of the solar control controller.

An optimal algorithm is built into the solar collector control system. At the beginning of the algorithm, the program activates libraries and constants, then the real-time clock module, activation of temperature sensors and activation of communication with the server are connected. If all devices are activated, then communication is established, if not, then activation starts. If the connection is established with the server, then the xml file is saved in the Ethernet module. Then the temperature data of the sensors are read and the temperature data in the Ethernet module is recorded.

Computer and Technical Solutions for Network Management and Monitoring by Double-Circuit Solar Systems with Thermosyphon Circulation

To control a double-circuit solar installation with thermosyphon circulation, a functional Web Server program was developed in (**Figure 7.9**).

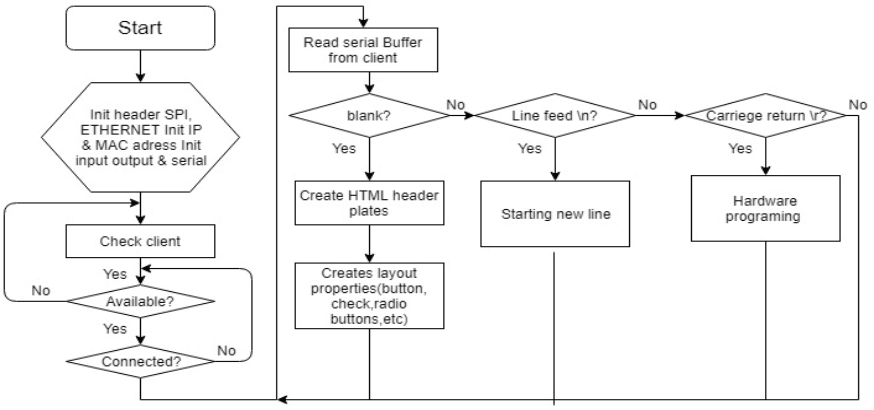

Figure 7.8: Block diagram of a Web Server for a double-circuit solar control system controller with thermosyphon circulation.

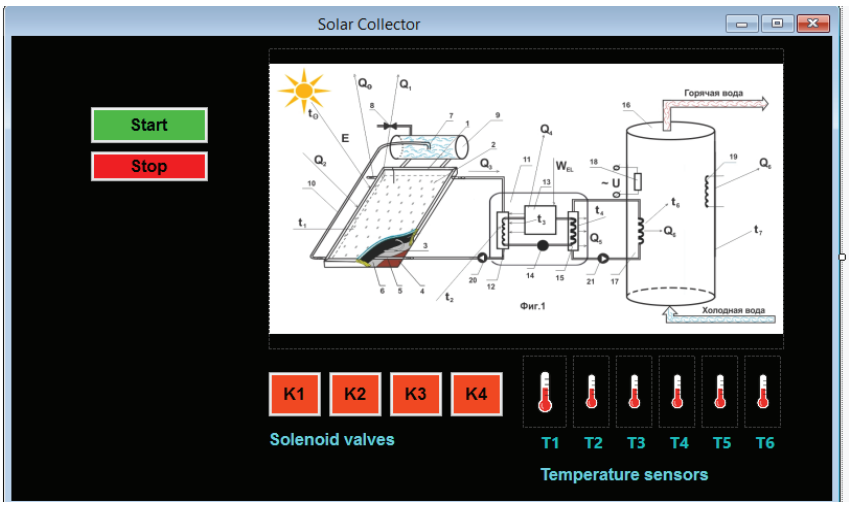

Figure 7.9: Solar controller software control interface.

As you can see from (**Figure 3.9**) of the Web Server, at the start of work, the SPI, Ethernet libraries are initialized, and IP and MAC addresses are also activated. Input, output, and serial data are activated. From the initialization of the data library, the Chess Client module will be connected to the client. If there is a client then the connection is established, if there is no client then it searches for the client again. After the connection, a new HTML file is opened and a layer is created to control the controller, which has six temperature indicators and four valve control buttons and various control elements.

(**Figure 7.10**) shows a dual-circuit solar control system with thermosyphon circulation. The control interface of the solar controller software consists of the system itself, (**Figure 7.1**), four valve status indicators, six temperature sensors for communication with the controller, a start and stop button. Below is the program code in the VHDL language for controlling a dual-circuit solar installation with thermosyphon circulation, which is connected via an Ethernet module with a Web Server. (**Figure 7.11**) shows the code for each button software element, graphic item, and label.

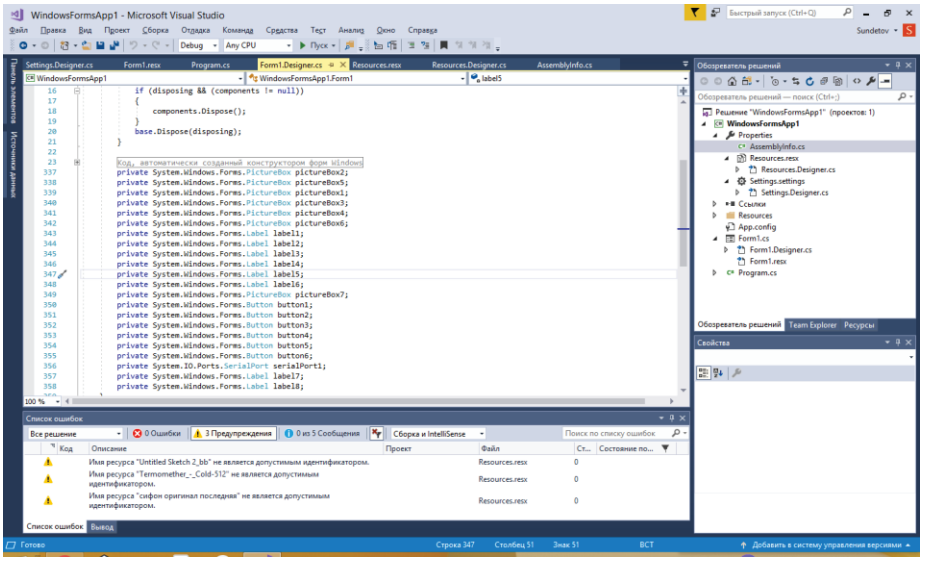

Figure 7.10: Visual studio development environment for declaring elements on a software resource.

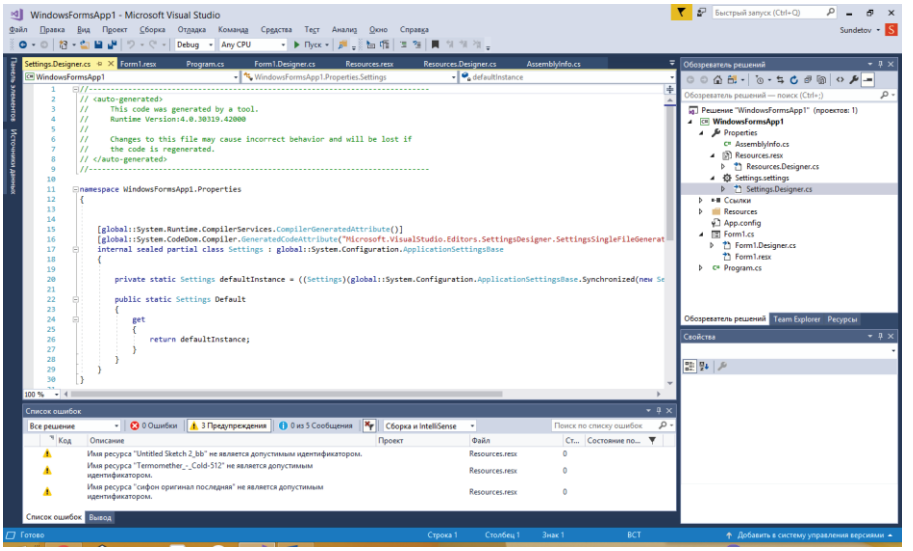

Figure 7.11: Visual studio development environment for configuring software for a bunch of elements of a program resource.

Complete software that shows reads solar data.

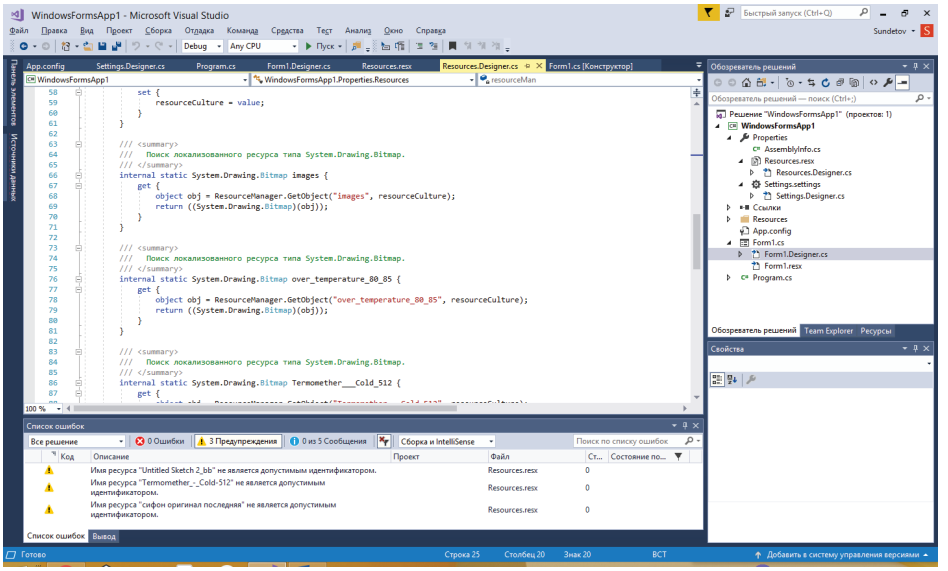

Figure 7.12: Visual studio development environment for bundling software resource elements.

In the NET software, Ethernet_MAC_COL LOCs are local MAC addresses for connecting to the Web Server. NET LED [0] LOC - ports for controlling valves and temperature sensors. NET uart1_sin LOC-ports for data exchange. NET "CLK_100MHZ" TNM_NET = sys_clk_pin - connection speed of the Ethernet module with the Web Server. TIMESPEC TS_sys_clk_pin = PERIOD sys_clk_pin 100000 kHz - period NET "RESET" LOC = "B6" | IOSTANDARD = LVCMOS33 | DRIVE = 8 | SLEW = FAST | PULLDOWN = TRUE - ports for reloading communication with the Web Server.

The operation of the software is based on reading temperature data via Ethernet and visually displays on the LCD display and the Web Server. And also it is possible to control solenoid valves through the Web Server. The software has an additional intelligent program, which depends on the temperature data of the thermosiphon solar installation.

In this work, a new controller for controlling a dual-circuit solar collector with thermosiphon circulation was developed and investigated. To create and study a monitoring platform for the thermal control system of a solar installation based on a double-circuit flat solar collector based on the Mojo v3 platform, the principle of operation of each element from which the network management and monitoring controller is made is described. An algorithm has been developed for a program that activates libraries and constants, then the real-time clock module, activation of temperature sensors and activation of communication with the server are connected. The connection is established with the server, saves the xml file in the Ethernet module, as well as reads the temperature data of the sensors and records the temperature in the Ethernet module. A Web Server block diagram has been created for a dual-circuit solar control system controller with thermosyphon circulation, which initializes the SPI, Ethernet libraries, and also IP and MAC addresses are activated. The operation of the software is based on reading temperature data via Ethernet and visually displays on the LCD display and the Web Server.

Conclusion

As a result of the experiment, the thermal characteristics of a flat solar collector for the production of hot water were investigated. The solar plant is designed for hot water supply (not strict consumers with low temperature potential up to 55° C) for residential buildings, social and cultural facilities and production processes with a single flow rate from 150 to 500 liters of water depending on climatic conditions and geographic latitude of the area. This installation is distinguished by a very low cost of thermal energy and labor costs in the manufacture, through the use of the register of black thin-walled pipes with cellular insulation.

The solar system provides heating of water regardless of the season and weather conditions due to the combined use of solar and electric energy.

Thus, year-round hot water is provided to autonomous production facilities. In winter, it is operated as an electric boiler.

The calculated and experimental energy consumption of uncontrolled heating of water in the solar collector are determined. Comparability of the results was ensured by the observance of the same conditions of experiments and calculations. The graphs have an exponential pattern associated with an increase in heat loss with increasing heating temperature, in the working range from 20^0 C to 60^0 C.

The project presented a simulation model of a double-circuit solar power plant with thermosiphon circulation. The simulation model has the opportunity to observe online the graphs of changes in daily, monthly and annual solar radiation, reserve tank power values, heat output of the heat pump and the current efficiency of the solar collector.

The given simulation model meets two general basic requirements:

- Reflects the logic of the functioning of the system under study in time.
- Provides the possibility of conducting experiments.

In this study, we calculated the calculation of the amount of heat in a single-circuit heliosystem with a thermosiphon circulation. Also calculated the coefficient of capture of solar radiation and the efficiency of the installation. The coefficient of radiation trapping receiver obeys an exponential pattern. The efficiency of solar power plants is estimated by the utilization rate of the installed capacity, which is defined as the ratio of the plant performance at a given radiation mode over time T to the performance over the same period of time when the plant is running with full design capacity.

The optimal angle of slope, at which the daily intake of solar radiation, averaged over the entire non-heating season, is maximum, is in April, June, July, August (summer period) - 30, i.e. 2˚ higher than the generally accepted recommended. For the transition period - for March, September 45˚, also 2˚ higher if recommended to be taken as year-round.

S = Ψ =43˚. For the winter period - February, October, November, the optimum angle of inclination of the solar collector is 55˚, i.e. 3˚ less than the generally accepted recommended (winter period S = 58˚ for Almaty).

The theoretical background of energy-saving electric heating of water in the solar collector-battery has been carried out. the temperature pattern in time changed almost linearly.

The calculated and experimental energy consumption of uncontrolled (at a constant power of the heating element) of water heating in the solar collector were determined. Comparability of the results was ensured by the observance of the same conditions of experiments and calculations. In the process of

controlled heating, a linear increase in temperature from 20 to 60° C was ensured, by regulating the voltage of the heating element with a power of 1.5 kW from $U_о$=165W до $U_н$=220W. In this case, the energy intensity of the process was 13.1 kW, i.e. was less by 1.7 kWh or 11.5% than with uncontrolled heating.

Calculated calculation of temperature and flux density of solar radiation over time. Also calculated the efficiency of the installation and the efficiency of the installation design. As can be seen from the graphs, the temperature of heating water in a solar collector with a thermosyphon has an exponential function in time, which says that in summer the temperature of the thermosyphon tank heats up faster than in winter. In a series of experiments, the dependences of the flux density of solar radiation on time, which reached up to 800 W / m2, were obtained, and this suggests that the experimental design model of solar power plant operates in the normal test mode.

Analysis and optimization of solar energy exergy was carried out on a flat collector with a modified cavity receiver, taking into account the content of incident solar radiation. Using the heat balance equation, the calculated trapping coefficient was obtained depending on the time τ, and the radiation trapping coefficient depending on the angle of incidence of the rays on the surface of the flat heat sink from the zenith point. Increasing the efficiency of exergies with increasing temperature on the receiver to the optimum temperature is reached, and then begins to decrease.

Based on the use of the f-chart method, a system was developed for liquid solar heating and an estimate of the share of the total heat load (load on household water and heating) provided by solar energy for a family of six in Almaty (Kazakhstan). From the research done, the larger the collector area, the greater the annual share of the load of solar energy. It can be seen from the experimental data that the total solar radiation in the summer months is higher and lower in the winter months, and it was also calculated using the f-chart method that the peak value of the heat load occurs in January, while the lowest heat load is observed in the summer months of the year. This indicates that the change in heat load is in phase with the need for heat load. Due to the influence of the collector tilt angles, the temperature increases from the minimum value in March and reaches its maximum value in July. It was found that for the city of Almaty (Kazakhstan), the optimal annual inclination angle of the collector configuration, which gives the maximum share of the solar load, is about 45°.

An exergy analysis of a flat solar solar collector with thermosiphon circulation is based on the calculation of the heat loss coefficient, collector heat transfer coefficient and plate exposure coefficient. However, the accuracy of the calculation will lead to better accuracy. In this work, it was proved that the

maximum level of exergy can be achieved in the temperature range, but the efficiency of the heat pump decreases, while the ambient temperature has a positive effect on thermal efficiency, while it negatively affects the exergy efficiency. It was also proved that with a circulating solar water system, exergy efficiency of about 4% can be expected.

The entropy calculation methodology is used to estimate the heat loss in solar collectors. This technique identified critical places in a dual-circuit heliosystem with thermosiphon circulation. The main conclusions were drawn in the project, which can be listed as follows. When applying the 2nd law of thermodynamics, an accurate method is provided for estimating heat losses in flat solar collectors. Thermal conductivity and convection in the near-wall zones are the main cause of heat loss in flat solar collectors. Thermal losses of the solar collector can be reduced by choosing the slope of the collector with minimal generation of entropy. As can be seen from the experimental work, entropy generation occurs mainly due to these heat transfer modes. The total entropy generation rate reaches a minimum when the collector has an inclination angle of 60 degrees.

The framework allows you to operate with the concept of object-oriented programming without the need to blow into the details of the implementation of a particular data warehouse architecture. In this case, the framework is an implementation of both a business model and a data warehouse all rolled into one. Data falling into the guaranteed information infrastructure is in a consistent state at any given time. Reading data and calculating derivatives is carried out using all computing resources that are active on the data point in time. Thus, the system can operate with a single computer serving the requests of several solar collectors, as well as with an unlimited number of solar collectors by connecting additional computing resources and connecting them to the computing cluster. In the case of a reverse rollback (reducing the number of solar collectors in the system), in the system it is enough to simply turn off the redundant machines included in the cluster.

sssdual-circuit solar collector with thermosiphon circulation. To create and study a monitoring platform for the thermal control system of a solar installation based on a double-circuit flat solar collector based on the Mojo v3 platform, the principle of operation of each element from which the network management and monitoring controller is made is described. An algorithm has been developed for a program that activates libraries and constants, then the real-time clock module, activation of temperature sensors and activation of communication with the server are connected. The connection is established with the server, saves the xml file in the Ethernet module, as well as reads the temperature data of the sensors and records the temperature in the Ethernet module. A Web Server block diagram has been created for a dual-circuit solar control system controller with thermosyphon circulation, which initializes

the SPI, Ethernet libraries, and also IP and MAC addresses are activated. The operation of the software is based on reading temperature data via Ethernet and visually displays on the LCD display and the Web Server.

References

1. Yi ML, Kung MC, Keh CC, Tsong SL (2012). Performance of Thermosyphon. Solar Water Heaters in Series Energies 5: 3266-3278.
2. Myeong JK (2015).Multi-Objective Optimization Design for Indirect Forced-Circulation Solar Water Heating System Using NSGA-II. Energies 8: 13137-13161.
3. Xu J, Ming L, Weidong L, Tufeng Zh, Yunfeng W, et al (2015). Effect of Installation of Solar Collector on Performance of Balcony Split Type Solar Water Heaters. International Journal of Photoenergy 6: 1-9.
4. Lacour A, Aidan D (2013).Thermal performance analysis of a solar water heating system with heat pipe evacuated tube collector using data from a field trial. Solar Energy 90: 17-28.
5. Ruchi Sh, Sumathy K, Phillip E, Jiawei G (2013). Recent advances in the solar waterheating systems: A review. Renewable and Sustainable Energy Reviews 19: 173-190.
6. Siddiqui MU, Said SAM (2015). A review of solar powered absorption systems .Renewable and Sustainable Energy Reviews 42: 93-115.
7. Kalogirou SA (2004). Solar thermal collectors and applications. Progress in Energy and Combustion Science 30: 231-295.
8. Chow TT, Fong KF, Chan A, Lin Z (2006). Potential application of a centralized solar water-heating system for a high-rise residential building in Hong Kong. Applied Energy 83:42-54.
9. Park SR, Pandey AK, Tyagi VV, Tyag SK (2014) Energy and exergy analysis of typical renewable energy systems. Renewable and Sustainable Energy Reviews.30: 105-123.
10. Hussein HMS (2003).Optimization of a natural circulation two phase closed thermosyphon flat plate solar water heater. Energy Conversion and Management 44: 2341-2352.
11. Khairnasov SM, Naumova AM (2016). Heat pipes application to solar energy systems. Applied Solar Energy 52: 47-60.
12. Maldonadoa RD, Huertab E, Coronab JE, Cehb O, Leone AI, et al (2014). Design and construction of a solar flat collector for social housing in México. Energy Procedia 57: 2159-2166.
13. Carlos Eduardo CN, Magno LV, Fernando T, Gilson D (2016). Software for designing solar water heating systems. Renewable and Sustainable Energy Reviews 58: 361-375.
14. Kumar S, Dubey A, Tiwari GN (2014). A solar still augmented with an evacuated tube collector in forced mode. Desalination 374: 15-24.
15. Karatayeva M, Michele LC (2014). Current Energy Resources in Kazakhstan and the Future Potential of Renewables: A Review. Energy Procedia 59: 97-104.

16. Teleuyev GB, Akulich OV, Kadyrov MA, Ponomarev AA, Hasanov EL, et al (2017). Problems of Legal Regulation for Use and Development of Renewable Energy Sources in the Republic of Kazakhstan. International. Journal of Energy Economics and Policy 7: 296-301.

17. Nurlankyzy S, Xiong Y, Mengliang L, Ke W (2016). Investigation on Solar Energy Industry Development Model in Kazakhstan. Open Journal of Business and Management 4: 393-400.

18. Ravil IM, Ishmanov A, Andreev VA, Alikhodzhayev I, Muhamedijeva J, et al (2015). Technological preconditions of monitoring of renewable energy sources of the Republic of Kazakhstan Twelve. International Conference on Electronics Computer and Computation (ICECCO) 14287317.

19. Salman A, Nadeem A, Akhanova G, Houghton T, Muhammad S F, et al (2017). Multi-criteria evaluation of renewable and nuclear resources for electricity generation in Kazakhstan. Energy 141: 1880-1891.

20. Tomas M, Vladimir Z, Juliane M (2009). Detailed modeling of solar flat-plate collectors with design tool kolektor 2.2, building simulation. In Eleventh International IBPSA Conference, Glasgow, Scotland 2017: 2289-2296.

21. Duffie JA, Beckman WA (1980). Solar Engineering of Thermal Processes, 2nd ed.; John Wiley & Sons, Inc.New York 23: 73-74.

22. Koyuncu T (2006). Performance of various design of solar air heaters for crop drying applications. Renewable Energy 31: 1073-1088.

23. Kicsiny R (2016). Improved multiple linear regression based models for solar collectors Renewable Energy 91: 224-232.

24. Gao W, Lin W, Liu T, Xia C (2007). Analytical and experimental studies on the thermal performance of cross-corrugated and flat plate solar air heaters. Applied Energy 84: 425-441.

25. Alvarez A, Cebaza O, Muñiz MC, Varela LM (2010). Experimental and numerical investigation of a flat-plate solar collector. Energy 35: 3707-3716.

26. Buzás J, Farkas I, Biró A (1998). Modelling and simulation of a solar thermal system. Mathematics and Computers in Simulation 48: 33-46.

27. Chow TT, He W, Ji J (2006). Hybrid photovoltaicthermosyphon water heating system for residential application. Solar Energy 80: 298-306.

28. Dormand JR, Prince PJ (1980). A family of embedded Runge-Kutta formulae. Journal of Computational and Applied Mathematics 6: 19-26.

29. Kahrobaian A, Malekmohammadi H (2008). Exergy Optimization Applied to Linear Parabolic Solar Collectors. Journal of Faculty of Engineering 42: 131-144.

30. Zhai RR, Zhu Y, Yang YP, Tan KY, Eric H, et al (2013). Exergetic and Parametric Study of a Solar Aided Coal-Fired Power Plant. Entropy 15: 1014-1034.

31. Chang YP (2010). Optimal the tilt angles for photovoltaic modules in Taiwan. International Journal of Electrical Power and Energy Systems 32: 956-964.

32. Kern J, Harris I (1975). On the optimum tilt of a solar collector. Solar Energy. 17: 97-102.

33. Lewis G (1987). Optimum tilt of solar collector. Solar Wind Energy 4: 407-410.

34. El-Kassaby MM, Hassab MH (1994). Investigation of a variable tilt angle Australian type solar collector. Renewable Energy 4: 327-332.

35. Chiou JP, El-Naggar MM (1986). Optimum slope for solar insolation on a flat surface titled toward the equator in heating season. Solar Energy 36: 471-478.

36. Тайсаева В.Т, Сарапов А.А. Расчет прихода солнечной радиации на наклонную поверхность Электрификация технологических процессов сельскохозяйственного производства . Сборник науч.трудов. - Новосибирск, 1988. - С. 23-31.

37. Omarov RA, Umbetov ES. A study of the angle of inclination of the solar collector Sib. Results of the study 5: 99-103.

38. Scientific and applied reference book on the climate of the USSR. - L.: Hydrometeoizdat, 1989-639.

39. Dutta GK, Saha SK (1990). Energy analysis of solar thermal collectors Renew. Energ. Environ 33:283-287.

40. Tyagi SK, Wang SW, Singhal MK, Kaushik SC, Park SR, et al (2007). Exergy analysis and Parametric study of concentrating type solar collectors. International Journal of Thermal Sciences 46: 1304-1310.

41. Liu G, Cengel YA, Turner RH (1995). Exergy analysis of a solar heating system. Journal of Solar Energy 117: 249-251.

42. Torres-Reyes E, Cervantes DGJG, Ibarra-Salazar BA, Picon-Nunez MA (2001). A Design method of flat-plate solar collectors based on minimum entropy generation. Exergy 1: 46-52.

43. Bejan A, Keary DW, Kreith F (1981). Second law analysis and synthesis of solar collector systems. Journal of Solar Energy 103: 23-28.

44. Lavan Z, Thompson J (1977). Experimental Study of Thermally Stratified Hot Water Storage Tanks. Solar Energy 19: 519-524.

45. Wood RJ, Al-Muslah SM. O Callaghan PW, Probert SD (1981). Thermally Stratified Hot Water Storage Systems. Applied Energy 9: 231- 242.

46. Haller MY, Cruickshank CA, Streicher W, Harrison SJ, Andersen E, et al (2009). Methods to Determine Stratification Efficiency of Thermal Energy Storage Processes-Review and Theoretical Comparison. Solar Energy 83: 1847-1860.

47. Sharp MK, Loehrke RI (1979). Stratified Thermal Storage in Residential Solar Energy. Applications Energy 3: 106-113.

48. Wuestling MD, Klein SA, Duffie JA (1985). Promising Control Alternatives for Solar Water Heating Systems. Journal of Solar Energy Engineering 107: 215-221.

49. Fanney AH, Klein SA (1988). Thermal Performance Comparisons for Solar Hot Water Systems Subjected to Various Collector and Heat Exchanger Flow Rates. Solar Energy 40: 1-11.

50. Hollands KGT, Lightstone MFA (1989). Review of Low-Flow Stratified-Tank Solar Water Heating Systems. Solar Energy 97-105.

51. Kleinbach EM, Beckman WA, Klein SA (1993). Performance Study of One-Dimensional Models for Stratified Thermal Storage Tanks. Solar Energy 50: 155-166.

52. Cristofari C, Notton G, Poggi P, Louche A (2003). Influence of the Flow Rate and the Tank Stratification Degree on the Performances of a Solar Flat-Plate Collector International. Journal of Thermal Sciences 42: 455-469.

53. Eamesi PC, Norton B (1998). The Effect of Tank Geometry on Thermally Stratified Sensible Heat Storage Subject to Low Reynolds Number Flows. International Journal of Heat and Mass Transfer. 41: 2131-2142.

54. Nelson JEB, Balakrishnan AR, Murthy SS (1999). Experiments on stratified chilled-water tanks : Experiments with stratified chilled water storage tanks. International Journal of Refrigeration 22: 216-234.

55. Hobbi A, Siddiqui K (2009). Optimal Design of a Forced Circulation Solar Water Heating System for a Residential Unit in Cold Climate Using TRNSYS. Solar Energy: 700-714.

56. Lundh M, Zass K, Wilhelms C, Vajen K, Jordan U (2010). Influence of Store Dimensions and Auxiliary Volume Configuration on the Performance of Medium-Sized Solar Combisystems. Solar Energy 84: 1095-1102.

57. Shariah AM, Ecevit A (1995). Effect of Hot Water Load Temperature on the Performance of a Thermosyphon Solar Water Heater with Auxiliary Electric Heater Energy. Conversion and Management 36: 289-296.

58. Bojić M, Kalogirou S, Petronijevic K (2002). Simulation of a Solar Domestic Water Heating System Using a Time Marching Model. Renewable Energy 27: 441-452.

59. Rodríguez-Hidalgo MC (2012) Domestic Hot Water Consumption vs solar Thermal Energy Storage: The Optimum Size of the Storage Tank. Applied Energy 97: 897-906.

60. Kim YD, Thu K, Bhatia HK, Charanjit SB, Kim CN, et al (2012). Thermal Analysis and Performance Optimization of a Solar Hot Water Plant with Economic Evaluation. Solar Energy 86: 1378-1395.

61. Papanicolaou E, Belessiotis V (2009). Transient Development of Flow and Temperature Fields in an Underground Thermal Storage Tank under Various Charging Modes. Solar Energy 83: 1161-1176.

62. Garg HP, Chakravertty S (1988). Thermal analysis of an evacuated tube collector module. Solar and Wind Technology 5: 525-531.

63. Kumar R, Adhikari RS, Garg HP, Kumar A (2001). Thermal performance of a solar pressure cooker based on evacuated tube solar collector. Applied Thermal Engineering 21: 1699-1706.

64. Morrison GL, Budihardjo I, Behnia M (2004). Water-in-glass evacuated tube solar water heaters. Solar Energy 76: 135-140.

65. Shah LJ, Furbo S (2004). Vertical evacuated tubular-collectors utilizing solar radiation from all directions. Applied Energy 78: 371-395.

66. Morrison GL, Budihardjo I, Behnia M (2005). Measurement and simulation of flow rate in a water-in-glass evacuated tube solar water heater. Solar Energy 78: 257-267.

67. Amirgaliyev Ye, Kunelbayev M, Amirgaliyev B, Kalizhanova A, Kozbakova A et al (2019). F-diagram research method for double circuit solar system with thermosyphon circulation. Book Thermodynamics and Energy Engineering 1-13.

68. Wójcik W, Kalimoldayev M, Amirgaliyev Y, Kunelbayev M, Kalizhanova A, et al (2019). Exergy analysis of double-circuit flat solar collector with thermosyphon circulation. Environmental Science 35-39.

69. Amirgaliyev Y, Kunelbayev M, Auelbekov O, Katayev N, Kalizhanova A, et al (2019). Methodology of computing the entropy generation and researching the thermal characteristics for thermosiphon flat solar collector. IEE 5th International Conference on Power Generation Systems and Renewable Energy Technologies (PGSRET). Turkey 455-462.

70. https://www.iea-shc.org/Data/Sites/1/publications/Solar-Heat-Worldwide-2019.pdf

71. Suresh NS, Rao BS (2017). Solar energy for process heating: a case study of select Indian industries. Journal of Cleaner Production 439-451.

72. Hassanzadeh A (2015). Experimental Study on Increasing the Electrical Efficiency of Photovoltaic Panel with Decreasing Rear Surface Temperature. Sharif University of Technology.

73. Abdelhamid M, Widyolar BK, Jiang L, Winston R, Yablonovitch E, et al (2016). Novel double-stage high-concentrated solar hybrid photovoltaic/thermal (PV/T) collector with nonimaging optics and GaAs solar cells reflector. Applied Energy182: 68-79.

74. Fath HES, Elsherbiny SM, Hassan AA, Rommel M, Wieghaus M, et al (2008). PV and thermally driven small-scale, stand-alone solar desalination systems with very low maintenance needs. Desalination 58-69.

75. Shukla R, Sumathy K, Erickson P, Gong J (2013). Recent advances in the solar water heating systems: a review. Renewable and Sustain Energy Reviews: 352-365.

76. Guo H, Ali HM, Hassanzadeh A (2016). Simulation study of flat-sheet air gap membrane distillation modules coupled with an evaporative crystallizer for zero liquid discharge water desalination. Applied Thermal Engineering 108: 486-501.

77. Jose PD (1957). The flux through the focal spot of a solar furnace. Solar Energy 1: 19-22.

78. Evans DL. On the performance of cylindrical parabolic solar concentrators with flat absorbers. Solar Energy 1977: 379-385.

79. Daly JC (1979). Solar concentrator flux distributions using backward ray tracing. Applied Optics 18: 2696-2700.

80. Nicolas RO (1987). Optical analysis of cylindrical-parabolic concentrators: validity limits for models of solar disk intensity. Applied Optics 26: 3866-3870.

81. Jeter M (1987). Analytical determination of the optical performance of practical parabolic trough collectors from design data. Solar Energy: 11-21.

82. Kaushika ND (1993). Viability aspects of paraboloidal dish solar collector systems. Renew Energy 3: 90-98.

83. Kalogirou, S (1996). Artificial neural network for predicting the local concentration ratio of parabolic trough collectors. International Proceedings Eurosun' 96, Freinberg. Germany 470-475.

84. Gombert A, Glaubitt W, Rose K, Dreibholz J ,Blasi B, et al (2000). Antireflective transparent covers for solar devices. Solar Energy 68: 357-360.

85. Eck M, Steinmann WD (2005). Modelling and design of direct solar steam generating collector fields. Journal of Solar Energy Engineering 127: 371-380.

86. Grena R (2010). Optical simulation of a parabolic solar trough collector. International Journal of Sustainable Energy 29: 19-36.

87. Yang B, Zhao J, Xu T, Zhu Q (2010). Calculation of the concentrated flux density distribution in parabolic trough solar concentrators by Monte Carlo ray-trace method. Symposium on Photonics and Optoelectronics 208-216.

88. Kumar KR, Reddy KS (2010). Determination of concentrated flux intensity distribution for solar parabolic trough concentrator. In: Proceedings of 9th International Conference on Sustainable Energy Technologies. Shanghai, China 205.

89. He YL, Xiao J, Cheng ZD, Tao YB (2011). A MCRT and FVM coupled simulation method for energy conversion process in parabolic trough solar collector. Renew Energy 36: 976-985.

90. Amirgaliyev YN, Kunelbayev M, Wójcik W, Kozbakova AK, Irzhanova AA, et al (2018). Solar-driven resources of the Republic of Kazakhstan. Medical Science 3: 18-27.

91. Nina GJ and George C (2010). Human skin pigmentation as an adaptation to UV radiation. Proceedings of the National Academy of Sciences 107: 8962-8968.

92. Kultan J, Baitassov T, Ishankulov M, Rivkina N (2013). Climatic conditions of Astana For the development of alternative energy sources 4 International Conference Renewable Energy Sources. Tatranské Matliare, Slovak Republic: 200-209.

93. Evangelos B, Christos T (2018). Analytical Expression of Parabolic Trough Solar Collector Performance. Designs 2: 1-17.

94. Duffie JA, Beckman WA (2013). Solar Engineering of Thermal Processes. Solar Energy and Photovoltaics 504-506.

95. Beckman WA, Klein SA, Duffie JA (1977). Solar Heating Design by the f-chart method. Interscience 190-193.

96. Khalid AJ, Qussai JAG (2003). Development of design charts for solar cooling systems Part II: Application of the cooling f-chart. Energy Conversion and Management: 341-355.

97. Ibrahim AM (1987). Water Resource development in Riyadh, Saudi Arabia. Desalination 193-202.

98. Jafarkazemi F, Ahmadifard E (2013). Energetic And Exergetic evaluation of flat plate solar collectors Renew. Energy 55-63.

99. Marletta L (2013). Air conditioning systems from a 2nd law perspective. Entropy 859-877.

100. Mohammad R,Yazdi MRM, Mehdi A, Marc AR (2015). Exergy, economic and environmental analyses of gas turbine inlet air cooling with a heat pump using a novel system configuration. Sustainability 7: 14259-14286.

101. Duffie JA, Beckman WA (1974). Solar engineering of thermal process. Solar Energy and Photovoltaics 98-105.

102. Duffie JA, Beckman WA (1991). Solar engineering of thermal process. Solar Energy & Photovoltaics 116-121.

103. Goswami DY, Kreith F, Kreider JF (2000). Principles of solar engineering. 2nd ed USA: Taylor & Francis PA: 92-99.

104. Szargut J, Morris DR, Stewart FR (1998). Exergy analysis of thermal, chemical, and metallurgical processes. OSTI GOV collections 20-26.

105. Ozgener O. Design, test and performance evaluation of a solar-assisted ground-source heat pump system for greenhouse heating using energy, exergy and exergoeconomic analysis methods In Solar Energy Science Division, Graduate School of Natural and Applied Sciences, Ege University. Izmir, Turkey, 2005 105.

106. Amirgaliyev YN, Kunelbayev M, Wojcik W, Kalizhanova AU, Auelbekov OA, et al (2018). Solar-driven resources of the Republic of Kazakhstan. News of The National Academy Of Sciences Of The Republic Of Kazakhstan Series Of Geology And Technical Sciences 13: 18-27.

107. Kalogirou SA (2004). Solar thermal collectors and applications. Prog Energ Combust 231-235.

108. Bejan A (1996). Entropy generation minimization: the method of thermodynamic optimization of finite-size systems and finite-time processes. Boca Raton, Fla.: CRC Press:135-140.

109. Herwig H, Kock F (2007). Direct and indirect methods of calculating entropy generation rates in turbulent convective heat transfer problems. Heat and Mass Transfer 15-24.

110. Amirgaliyev Y, Kunelbayev M, Kalizhanova A, Auelbekov O, Katayev N, et al (2019). Theoretical And Mathematical Analysis Of Double-Circuit Solar Station With Thermo Siphon Circulation. Journal of Polytechnic-Politeknik 22: 485-493.

111. Agarwal VK, Larson DC (1981). Calculation of the top loss coefficient of a flat-plate collector. Solar Energy 27: 69-71.

112. Amirgaliyev Y, Kunelbayev M, Auelbekov O, Katayev N, Kalizhanova A, et al (2019). Methodology of computing the entropy generation and researching the thermal characteristics for thermosiphon flat solar collector. 5th International Conference on Power Generation Systems and Renewable Energy Technologies (PGSRET) 455-462.

113. Yoo JH. Evaluation of Solar Hot Water Heating System Applications to High-rise Multi-family Housing Complex based on three Years of System Operation. Energy and Buildings 101: 54-63.

114. Chow TT, Fong KF, Chan ALS, Lin Z (2006). Potential application of a centralized solar water-heating system for a high-rise residential building in Hong Kong. Applied Energy 83: 42-54.

115. Badescu V. Simulation Analysis for the Active Solar Heating System of a Passive House. Applied Thermal Engineering 25: 2754-2763.

116. Siddiqui MU, Said SAM. A review of solar powered absorption systems. Renewable and Sustainable Energy Reviews 42: 93-115.

117. Kalogirou SA. Solar thermal collectors and applications. Progress in Energy and Combustion Science 30: 231-295.

118. Maldonadoa RD, Huertab E, Coronab JE, Cehb O, Leóne AI, et al. Design and construction of a solar flat collector for social housing in México. Energy Procedia 57: 2159-2166.

119. Nogueira C, Vidotto M, Toniazzo F, Debastiani G. Software for designing solar water heating systems. Renewable and Sustainable Energy Reviews 58: 361-375.

120. Farahat S, Sarhaddi F, Ajam H. Exergetic optimization of flat plate solar collectors. Renewable Energy 1169-1174.

121. Luminosu I, Fara L (2005). Determination of the optimal operation mode of a flat solar collector by exergetic analysis and numerical simulation. Energy 30: 731-747.

122. Park SR, Pandey AK, Tyagi VV, Tyagi SK (2014). Energy and exergy analysis of typical renewable energy systems. Renewable and Sustainable Energy Reviews 30: 105-123.

123. Amirgaliyev YN, Kunelbayev M, Wojcik W, Kalizhanova AU, Auelbekov OA, et al (2018). Solar-driven resources of the Republic of Kazakhstan. Series of Geology and Technical Sciences 3: 18-27.

124. Morini GL, Piva S (2007). The simulation of transients in thermal plant Part I: Mathematical model. Applied Thermal Engineering 27: 2138-2144.

125. Amirgaliyev Y, Merembayev T, Kunelabyev M. Dynamic Simulation of a Solar Hot Water Heating System for Kazakhstan Climate Conditions. 2018 14th International Conference on Electronics Computer and Computation (ICECCO) 206-212.

126. Ping Li (2012). Robust logitboost and adaptive base class (abc) logitboost. Computer Science, Mathematics 9020623.

127. Richardson M, Dominowska E, Ragno E (2007). Predicting clicks: estimating the click-through rate for new ads. In Proceedings of the 16th international conference on World Wide Web 521-530.

128. Christopher JCB (2010). From ranknet to lambdarank to lambdamart An overview. Learning 11: 81.

129. United States Department of Energy: 2012 renewable energy data book. http:www.nrel.gov/docs/fy14osti/60197.pdf.

130. Amirgaliyev Y, Yunussov R, Mamyrbayev O (2016). Optimization of people evacuation plans on the basis of wireless sensor networks. Research Article Open Access 206-213.

131. Wilson J, Redmond E. Seven Databases in Seven Weeks. A Guide to Modern Databases and the NoSQL Movement 1st Edition, 2012.

132. Andreassen O, Marazita F, Miskowiec M. Upgrade of the CERN RADE framework architecture using RabbitMQ and MQTT. Proceedings, 16th International Conference on Accelerator and Large Experimental Physics Control Systems.

133. Amirgaliyev Y, Merembayev T, Kunelbayev M (2018). Dynamic simulation of a solar hot water heating system for Kazakhstan climate conditions. 14th International Conference on Electronics Computer and Computation: 206-212.

134. Burckhardt S. Coppieters T (2018). Reactive Caching for Composed Services: Polling at the Speed of Push. Proceedings of the ACM on Programming Languages 2: 38.

135. Bernstein P (2018). Actor oriented Database Systems. 34th International Conference on Data Engineering 121-125.

136. Bernstein PA, Burckhardt S, Bykov S, Crooks N. Faleiro JM, et al (2017). Geo-Distribution of Actor-Based Services. Proceedings of the ACM on Programming Languages 56-62.

137. Rabiee A (2018). Analyzing Parameter Sets For Apache Kafka and RabbitMQ On A Cloud Platform 26-35.

138. Bykov S, Geller A, Kliot G, Larus JR, Pandya R, et al (2011). Orleans: cloud computing for everyone. Proceedings 16: 1-16.

139. Bernstein PA, Bykov S, Geller A, Kliot G, Thelin J, et al (2014). Orleans: Distributed Virtual Actors for Programmability and Scalability. Journal of Thelin 63139052.

140. Bykov S, Geller A, Kliot G, Larus JR, Pandya R, et al (2010). Orleans: A Framework for Cloud Computing. Journal of Thelin 15746395: 110-116.

141. Kalogirou SA (2004). Solar thermal collectors and applications. Progress in Energy and Combustion Science 30: 231-295.

142. Wang Z, Yang W, Qiu F, Zhang X, Zhao X, et al (2015). Solar water heating: From theory, application, marketing and research. Renewable and Sustainable Energy Reviews 41: 68-84.

143. http:www.compit.pl/katalog/kategoria_12_regulatory-ukladow-solarnych.html

144. http:www.geco.pl/prod.php?id=169&lang=pl

145. http:www.steca.com/index.php?Solar_Electronics_by_Steca

146. http:www.caleffi.com/usa/en-us/catalogue/solar-1

147. Nagaraju J, Garud SS, Ashok Kumar K, Ramakrishna RM (1999) 1 MWth INDUSTRIAL SOLAR HOT WATER SYSTEM AND ITS PERFORMANCE. Solar Energy 66: 491-497.

148. Stettler S, Gut W, Koch F, Roch R, Salathe A, et al (2014). Web-based functionality check for solar heating systems. Energy Procedia 48: 674-680.

149. Porzuczek J (2014). A novel approach for the design of the modular controllers for solar thermal systems. Technical Transactions 24: 665-670.

150. Grassie T, MacGregor K, Muneer T, Kubie J (2002). Design of a PV driven low flow solar domestic hot water system and modeling of the system collector outlet temperature. Energy Conversion and Management 43: 1063-1078.

151. PN-EN 12977-5: 2012, Słoneczne systemy grzewcze i ich elementy Systemy wykonywane na zamówienie, Część 5: Metody badania wydajności wyposażenia regulacyjnego.

152. Peter M, Druck P (2008). Testing of controllers for thermal solar systems. Solar Energy 82: 676-685.

153. Muralidhar GK, Nagaraju J, Mohan S (1991). Differential temperature controller: An energy conservative device for solar water heating system Energy Conversion and Management 31: 61-63.

154. Kicsiny R, Farkas I (2012). Improved differential control for solar heating systems. Solar Energy 86: 3489-3498.

155. Mielczarek W. Szeregowe interfejsy cyfrowe. Helions 1993.

156. http:www.label.pl/po/rek900.mx.html.

About the Authors

Yedilkhan Amirgaliyev, Chief Researcher, Doctor of Technical Sciences, Professor. Head of the laboratory. The Science Committee of the Ministry of Education and Science of the Republic of Kazakhstan. The author of more than 300 scientific papers and several patents, authors certificates on Software. Research interests: Artificial Intelligence and Robotics, Pattern Recognition, Digital Technologies in Green Energy.

Murat Kunelbayev, Chief Researcher of the Laboratory of Artificial Intelligence and Robotics, Institute of Information and Computational Technologies of Committee of Science MES RK. The author of more than 100 scientific papers and more than 18 patents, authors certificates on Software. Research interests: Artificial Intelligence and Robotics, Green Energy, Thermophysics and Thermodynamics.

ISBN: 978-1-63278-898-6

978-1-63278-898-6